ＩＳＳＮ１３４６－７８４０

港湾空港技術研究所資料

TECHNICAL NOTE

OF

THE PORT AND AIRPORT RESEARCH INSTITUTE

No.1320 June 2016

Sediment Transport and Near-Bed Dynamics by Currents and Waves in Muddy Environments of Inner Bay

中川　康之

国立研究開発法人　海上・港湾・航空技術研究所

National Institute of Maritime,
Port and Aviation Technology, Japan

CONTENTS

Synopsis ····· 3

1. Introduction ····· 5
1.1 Background of the study ····· 5
1.2 Aim of the study and setup of the thesis ····· 6
References for Chapter 1 ····· 7

2. Characteristics of muddy bed structure ····· 8
2.1 Introduction ····· 8
2.2 Specific features of muddy bed structures ····· 8
2.3 Measurement of mud-water interface in Ariake Bay ····· 9
2.3.1 Site description ····· 9
2.3.2 Field survey for mud density measurement ····· 10
2.3.3 Measurement results in Ariake Bay ····· 11
2.4 Sediment properties of muddy bed of study site in Tokyo Bay ····· 13
2.4.1 Site description ····· 13
2.4.2 Methods ····· 14
2.4.3 Measurement results and discussions ····· 15
2.5 Conclusions ····· 18
References for Chapter 2 ····· 19

3. Fine sediment dynamics under tide-dominated condition ····· 20
3.1 Introduction ····· 20
3.2 Field observations ····· 21
3.3 Estimation of suspended sediment concentration profiles with ADCP's backscatter data ····· 21
3.3.1 Relationship between SSC and backscatter intensity ····· 21
3.3.2 Estimated result of SSC by ADCP backscatter data ····· 22
3.4 Estimation of erosion rate parameter from field data ····· 24
3.4.1 Erosion rate formula for muddy bed ····· 24
3.4.2 Parameter acquisition procedure ····· 24
3.5 Simulation of temporal variation of total suspended load ····· 25
3.5.1 A one-point TSL model ····· 25
3.5.2 Simulation of temporal variation of total suspended load ····· 26
3.6 Conclusions ····· 27
References for Chapter 3 ····· 28

4. Data analysis and modeling of mud transport during storm event in Tokyo bay ····· 30
4.1 Introduction ····· 30
4.2 Site description ····· 30
4.3 Instrumentation ····· 30
4.4 Data analysis ····· 31
4.4.1 Estimation of bed shear stresses ····· 31
4.4.2 Erosion flux and bed elevation measurements ····· 32

4.5 Observed data in the storm and flood event ····· 33
4.6 Estimation of near-bed sediment fluxes ····· 34
4.6.1 Vertical fluxes ····· 34
4.6.2 Fluid mud flow ····· 35
4.7 Results ····· 36
4.7.1 Erosion flux estimation ····· 36
4.7.2 Sediment budget analysis near bed surface ····· 36
4.7.3 Derivation of fluid mud flux formula ····· 37
4.8 Conclusions ····· 38
References for Chapter 4 ····· 39

5. Effect of wind wave disturbance on temporal variation of near-bottom dissolved oxygen in inner Tokyo bay ····· 42
5.1 Introduction ····· 42
5.2 Monitoring site and instrumentations ····· 42
5.3 Measurement results and discussion ····· 43
5.3.1 Salinity, temperature and DO concentration variations in summer of 2010 ····· 43
5.3.2 DO concentration and wind events ····· 44
5.3.3 DO concentration and wind waves ····· 45
5.3.4 Near-bed processes of wave induced disturbance and DO concentration ····· 47
5.4 Conclusions ····· 49
References for Chapter 5 ····· 49

6. Application of fluid mud model with stochastic approach of bottom shear stress estimation to storm event simulation ····· 50
6.1 Introduction ····· 50
6.2 Stochastic approach for estimation of wave induced bottom shear stress Monitoring site and instrumentations ····· 51
6.2.1 Characterization of wave induced instantaneous velocity ····· 51
6.2.2 PDFs of instantaneous orbital velocity and bottom shear stress ····· 52
6.3 Stochastic formula for sediment transport rate ····· 54
6.3.1 Excess bottom shear stress ····· 54
6.3.2 Estimation of fluid mud transport rates ····· 55
6.4 Application of the model to simulation of observed storm event Conclusions ····· 57
6.4.1 Simulation of current and wave field during storm event ····· 57
6.4.2 Simulation results of fluid mud transport ····· 58
6.5 Conclusions ····· 60
References for Chapter 6 ····· 61

7. Summary and conclusions ····· 63

Acknowledgements ····· 64

内湾域における波と流れによる底泥輸送および海底環境の動態に関する研究

中川　康之*

要　旨

内湾域沿岸部における効率的な海域利用や，適切な水域環境の保全を行っていくためには，海域特性の把握をふまえた環境変動の予測技術の向上が必要とされている．本研究で対象とする東京湾および有明海における底質環境の特徴として，シルト・粘土分を主体とする泥質物が湾内の広い範囲に堆積し，地形変化をはじめとする水域環境の動態を評価するうえでは，底泥の堆積特性や外力条件に応じた挙動特性の把握が重要となる．本研究では，これらの海域を対象とした現地観測を通じて，現地底泥の堆積分布のモニタリング手法の構築と，潮汐流や波浪外力による底泥移動や底層の水質変動に関する実態の把握，さらに現地観測を通じて明らかとなった底泥の堆積および挙動特性を反映させた底泥輸送のモデル化を試みた．

堆積特性の把握においては，現地底泥のコアサンプル採取・分析や現地式密度計を新たに導入した底泥湿潤密度の現場計測を行い，底泥移動を評価するうえで重要となる底泥極表層における含水比等の鉛直分布構造について，各観測海域での特徴を明らかとした．特に東京湾深場においては，含水比 300%以上の流動性の高い軟泥が 20cm 程度堆積していることが確認された．一方，超音波式流速計を用いた流動場の計測と，懸濁物濃度や溶存酸素濃度等の同時計測による底面境界観測システムを導入した長期連続観測により，潮汐流や波浪等の作用外力に対する底泥移動や水質変動に関する応答特性の解明を試みた．各観測海域での物質輸送の評価に重要となる外力条件の特徴を配慮し，有明海では潮汐流による底泥の巻き上げに伴う SS(浮遊懸濁物)の輸送現象を，また東京湾奥部では高波浪時の波浪擾乱に伴う底泥挙動や水質変動に注目したデータ解析を行った．潮汐流による SS 輸送現象に対しては，全水深を通じた SS 濃度の流速変動に対応する変動量の解析を基に，巻き上げ限界や巻き上げ速度等のモデル・パラメータの最適化を行い，懸濁物輸送量を適切にシミュレートする SS 輸送モデルを構築した．また，平常時には静穏な環境にある東京湾奥部においては，強風時に生じる風波擾乱の発達程度に応じて，底泥の顕著な移動や貧酸素期における DO(溶存酸素)濃度の回復が生じることを示し，波浪外力が海底環境に及ぼす影響の実態を明らかとした．

東京湾における記録的な高波浪イベント時の観測データからは，海底面直近での底泥輸送量の収支解析を通じて，一般的な底泥輸送モデルで考慮されている巻き上げ・沈降過程以外にも，泥層内で生じる泥の水平輸送過程が重要であることを示し，さらに泥層内の鉛直構造を反映させた泥輸送モデルを新たに導出した．また，本モデルの実海域シミュレーションへの応用を通じて，波浪外力の時間変動の確率的評価を導入することにより，底泥輸送量の再現性が向上することを明らかとした．

キーワード：内湾，底泥，潮汐流，波浪，底質輸送，海底環境

* 沿岸環境領域長（兼沿岸土砂管理研究グループ長）
〒239-0826 横須賀市長瀬3-1-1 国立研究開発法人 海上・港湾・航空技術研究所 港湾空港技術研究所
電話：046-844-5051　Fax：046-844-1274　　e-mail:nakagawa@pari.go.jp

Sediment Transport and Near-Bed Dynamics by Currents and Waves in Muddy Environments of Inner Bay

Yasuyuki NAKAGAWA*

Synopsis

Understanding of dynamics of coastal morphology and sedimentary environment is critical topics for sustainable use and management of coastal and estuarine area. The target area of the present study, the Ariake Bay and the Tokyo Bay, are typical embayment in Japan, where mud or fraction of silt and clay is dominant in the bottom sediments, and the process of fine sediment transport is an important factor for their water environment in the area. Several field monitoring were carried out in the present study for capturing characteristics of spatial distribution of muddy sediment and near-bottom processes including transport process of mud and water quality changes under the forces of waves and currents. Furthermore, the knowledge obtained through the field monitoring were applied for modelling of fluid mud transport processes.

For the capturing sediment characteristics, besides the acquisition of key parameters of sediment strength such as bulk density and water content from sediment cores, an in-situ device was also newly introduced for direct measure of bulk density of bottom mud. In the Tokyo Bay site, thickness of fluid mud layer is relatively higher in the offshore from the river mouth area with the thickness of over 20 cm. Through the deployments of long-term monitoring in the fields, where several acoustic velocimeters and synchronized measurements of water qualities including turbidity, dissolved oxygen and so on, the present study examines sediment dynamics and water quality change due to waves and currents. Considering dominant forces in the study sites, suspended sediment transport processes due to tidal current is examined and modeled with the data from the Ariake Bay. On the other hand, sediment transport and water quality changes near the bed due to wind waves are focused on for the study of the Tokyo Bay.

Dynamical processes during an extreme storm events due to a passage of typhoon were successfully captured in the monitoring campaign of the Tokyo Bay and the data analyses revealed the importance of fluid mud transport in the near surface mud layer. Model for the fluid mud transport is newly derived and applied for numerical simulations of mud transport process under the storm condition. Through the validation process of the model, it appears that stochastic approach is effective for the evaluation of wave forces on the fluid mud transport simulation.

Key Words: Embayment, Mud, Tidal current, Wind wave, Sediment transport process, Near-bed environment

* Director of Coastal and Estuarine Environment Department
3-1-1 Nagase, Yokosuka, 239-0826 Japan
Phone : +81-46-844-5051 Fax : +81-46-844-1274 e-mail:nakagawa@pari.go.jp

1. Introduction

1.1 Background of this study

Muddy sediments consists of silt and clay particles are mainly supplied through rivers discharge and commonly deposited in estuaries and coastal embayments during calm conditions of external forces on the bed such as currents and waves. After the deposition of the muds, however, they may be resuspended and transported depending upon the extent of current and wave forces. Since the dynamical muddy sediment transport processes cause changes not only in topography but also in sedimentary and water quality environments, understanding of the sedimentary process is crucial for effective uses and sound managements of the coastal and estuarine area.

From an economical view point, the prediction of sediment movement is critical for the estimation of maintenance dredging cost for port and harbor operations because the sediment movement often results in shoaling or siltation of navigation channels and harbor basins. The siltation problems are especially sever at ports and harbors locating near river mouth and extensive trials for minimizing siltation have been experienced in many countries (PIANC・2008). In Japan, several studies on muddy sediment have been carried out extensively in 1980's to solve engineering problems for the port development at the shallow muddy coast of surrounded by the intertidal mud flat in the Ariake Bay (Port and Harbour Research Institute, 1990). In recent years, while the deeper navigation channels are required due to increases in vessels draught, placement of dredged materials in open water is strictly prohibited under the international regulation. Hence, there are compelling reasons to execute the study of fine sediment dynamics that can be applied for minimize the maintenance dredged volumes.

To provide a better understandings of mud behaviors is necessary also for assessing coastal and estuarine environments by elucidating several specific characteristics of the fine sediments. Muddy sediments are often include organic materials and contaminants because pollutants are likely absorbed on to silt and clay particles. Water quality is also highly related to the sediment condition and hypoxia is sometimes caused by decomposition of organic matters in the fine sediment. Resuspension of the mud results in high turbidity with attenuation of light through the water column causing wither of submerged aquatic vegetation.

Many studies have examined the mud behaviors in fields such as the dynamics of wave induced resuspension in an estuarine environment (Sanford, 1994, Shiraishi et al., 2000) and the fluid mud behaviors in areas of continental shelves (Vinson and Mehta, 2003, Traykovski et al. 2007). Difficulty of grasping the movement of the mud in the field is due to infrequent but intense nature of the mud transport dynamics, which are under site specific and intermittent conditions of driving forces such as river flood and storm waves. Hence, field monitoring is still a powerful tool to elucidate unknown processes of mud behaviors in site, where it is required to properly choose in-situ instrumentation layouts for optimal acquisition of target data.

Several types of numerical models have been developed for simulating the sediment transport processes in coastal and estuarine area. The models classified as so called process-based models typically consist of any 3-D hydrodynamic model and sediment modules (e.g. Amoudry and Souza, 2011). Sediment modules implement different formulations depending on the sediment types of mud (cohesive) and sand (non-cohesive), respectively. For muds, which is the focus of the present study, the formulations for erosion with the power low (e.g. Ariathurai and Krone, 1976) are conventionally used, where considering erosion rate parameter and critical shear stress for erosion. These parameters are highly site specific and depend on several sediment properties such as particle size, water content or consolidating state of muds, which is sometime of vertical structure also. We need any efficient method for acquisition of the sediment parameters that reflecting the state of mud deposition in field for applying the numerical model.

Furthermore, formation of fluid mud layer near the bed is also specific characteristics in muddy environments and leads to more complicated situation to be modeled since the fluid mud behaves as Non-Newtonian fluid depending on the concentration (Mehta, 1991). Two layer approach is one of typical ways to incorporate the

fluid mud layer in numerical models, considering mass and momentum conservation equations for the non-Newtonian fluid (e.g. Odd and Cooper, 1989, Tsuruya et al. 1994). This approach has been still utilized (e.g. Deltaress, 2014), where density in the fluid mud layer is assumed as constant for simplicity. Because the vertical structure of density or concentration profile in the fluid mud layer is critical to determine the horizontal sediment flux, it is a challenge to properly incorporate the vertical structure of the fluid mud density in the model.

1.2 Aim of this study and set-up of this thesis

The aim of the study is to enhance our understanding and modeling of mud behavior and near-bed dynamics under current and wave forces. The set-up of the thesis is depicted in Figure 1.1.

Chapter 2 presents observation results of vertical structure of muddy sediment concentration in fields of typical Japanese embayments. This chapter also discuss comparison of several methods for measurement of muddy bed characteristics depending on the water content.

From Chapter 3 through Chapter 5, several analysis of field measured data are carried out to elucidate specific phenomena of muddy sediment transport processes and near bed dynamics due to waves and currents. The target phenomena that these chapter deal with are summarized in Table 1.1. Chapter 3 describes dynamics of suspended fine sediments under the tide dominated condition at a monitoring site with the water depth of around 8 m in a meso-tidal environment. Temporal change in suspended sediment concentration profile is calculated using acoustic back scatter signals through the water column and they are applied for estimation pick up rate of the bottom sediment with 1DV analysis.

On the other hand, wave dominated resuspension phenomena in a bay at intermediate water depth, around 25 m, is demonstrated in Chapter 4. Field monitored data are shown to reveal fine sediment transport processes under an extreme storm event during a passage of typhoon. Considering the characteristics of muddy bed structure represented in Chapter 2, fluid mud transport model is newly derived in the chapter.

Chapter 5 is dedicated to near-bed dynamics from another view point and discussed effect of wave disturbance on temporal change in near-bed water quality or dissolved oxygen concentration. Field data shows the key role of high wind wave events in recovery of concentration of dissolved oxygen near the bed from hypoxia state.

In Chapter 6, the fluid mud transport model derived in Chapter 4 is applied to simulate mud transport dynamics during the observed storm events around the monitoring site coupling with 3D hydrodynamic and wave models. In the simulation, bottom shear stress due to current and waves are newly modeled as stochastic approach considering irregularity of the wind wave instantaneous velocity above the bed.

Finally, in Chapter 7 the previous chapters are summarized and over all conclusions and future works are presented.

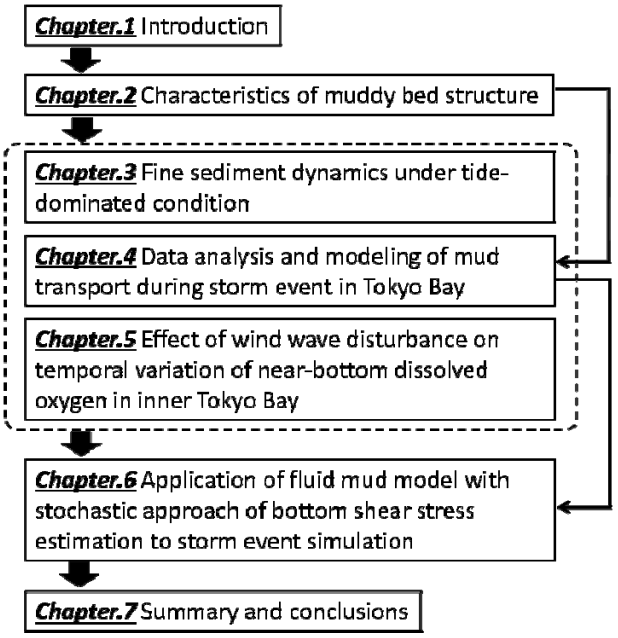

Figure 1.1 Set-up of the thesis

Table 1.1 Target phenomena of field monitoring for sediment transport and near bed dynamics discussed in Chapter 3, 4 and 5

Chapter #	Water depth at monitoring site	Target depth of concern	Forcing factors	Target phenomena
3	8 -12m	Through the all water column	Tidal current	Suspended sediment dynamics
4	25 m	Near bed and in mud layer	Current and Storm waves	Suspended and Fluid mud dynamics
5	15 m	Near bed water column	Waves	Water quality (DO concentration) change

RFERENCES for Chapter 1

Amoudry, L. O. and A. Souza (2011): Derterministic coastal mor-phological and sediment transport modeling: Areview and discussion, Reviews of Geophysics, 49, pp.RG2002-2011.

Ariathurai, R. and R.B. Krone (1976): Finite element model for cohesive sediment transport, Journal of Hydraulics Division, ASCE, ol.102, No.3, pp.323-338.

Deltares (2014): Delft3D-FLOW user manual, ver:3.15.34158, 684p.

PIANC (2008): Minimising harbour siltation, PIANC Report No.102, 75p.

Mehta, A. (1991): Understanding fluid mud in a dynamic environment, Geo-Marine Letters, Vol. 11, pp.113-118.

Odd, N.V.M. and A.J. Cooper (1989): A two-dimensional model of the movement of fluid mud in a high energy turbid estuary, Journal of Coastal Research, Vol.5, pp.185–193.

Port and Harbour Research Institute (1990): Engineering guide book for siltation countermeasures, 257p. (in Japanese)

Sanford, L.P. (1994): Wave-forced resuspension of upper Chesapeake May muds, Estuaries, Vol.17, No.1B, pp.148-165.

Shiraisi, S., M. Iijima, K. Nagano and K. Nakatsuji (2000): Resuspension of muddy sediment by tidal current and waves off Kansai International Airport, Proc. of Coastal Engineering, Vol. 47, pp.1076-1080. (in Japanese)

Traykovski, P., P. L. Wiberg, and W. R.Geyer (2007): Observations and modeling of wave-supported sediment gravity flows on the Po prodelta and comparison to prior observations from the Eel shelf, Continental Shelf Research, Vol.27, pp.375-399.

Tsuruya, H., K. Murakami, I. Irie, H. Sasajima and M. Itoi (1994): 3-D numerical model for siltation estimate considering fluid mud dynamics, Proc. of Coastal Engineering, Vol. 41, pp.1011-1015. (in Japanese)

Vinzon, S. B. and Mehta, A. J., (2003): Lutoclines in high concentration estuaries: Some observations at the mouth of the Amazon, Journal of Coastal Research, Vol.19, No.2, pp.243-253.

2 CHARACTERISTICS OF MUDDY BED STRUCTURE

2.1 Introduction

Fine sediments including silt and clay often accumulates and deposits on the sea bed in enclosed bay and estuarine seas. Such fine materials sometimes form very soft mud layer with high water content near the surface of bottom sediments and it may make difficult to identify the interface between the settled bottom sediments and sea waters with an intermediate layer so called fluid mud layer. The existence of the fluid mud layer may cause the difficulty in defining the sea bed level and it has been one of the critical problems for the maintenance of navigation channels in port and harbor facilities. From the environmental viewpoints, the understanding of existence and movement of soft mud layer on the sea bottom is crucial for the estimation of the fate of various substances which are detached with fine sediments and harmful to water environments.

Since erodibility of mud deposits depends on sediment parameters such as water content or bulk density (e.g. Whitehouse et al., 2000), spatial structure of the muddy sediment including vertical profile as mentioned above should be taken into consideration for analysis of sediment dynamics (e.g. Sanford and Maa, 2001). However, spatial distribution and structure of sediment in field are determined by site specific conditions of sediment supply and forcing factors such as wave and current. Therefore, better understanding of sediment characteristics in field is required for modeling of sediment dynamics with more reliability.

In the present chapter, after reviewing general aspects of muddy sediment characteristics, some field measured data taken at the target field of the present study in the Ariake Bay and the Tokyo Bay are demonstrated to present actual situations of vertical structures of near bed surface at the typical muddy environments. Besides conventional sediment analysis method with taking core samples in the field, the present study apply other measurement methods including an in-situ bulk density measurement device and a vane strength meter etc. Through the data analysis, the existences of fluid mud layer in the fields are confirmed and their thickness are quantified considering the vertical structures.

2.2 Specific features of muddy bed structures

One of the prominent properties of fine bottom sediment is the dependency of their dynamic behaviors on the water contents or sediment concentration as summarized in Figure 2.1. The concentration or dry density of mud, C, is ranging from the order of $<\sim 10^{1}$

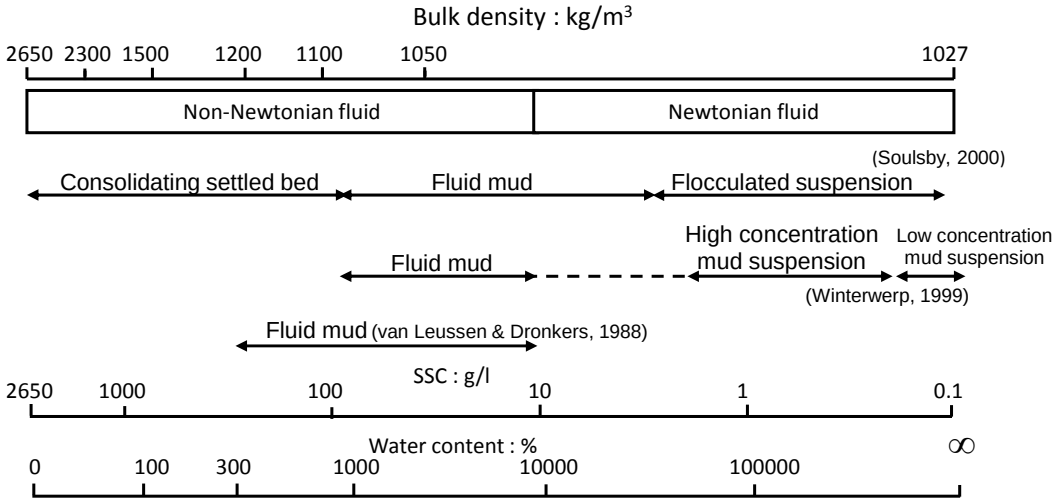

Figure 2.1 Classification of mud states depending on sediment concentration

g/l as suspension state through the order of > 10^3 g/l as consolidated state. Suspension with high concentration around 10^1 g/l can affect the turbulent flow field and may damping the turbulent energy in the overlying sea water (e.g. Winterwerp, 1999), though it is treated as Newtonian fluid. Between the two these states, there is a transient state or so called fluid mud with the concentration of the order of a few 10^1 to 10^2 g/l, though there are several definition for the range of concentration, where the mud behaves as laminar-flow and non-Newtonian fluid. Behavior of the fluid mud is sometime crucial process for causing siltation of navigational channels and harbor basins (e.g. PIANC, 2008) and also for determining distribution of muddy sediments around the continental shelf during flood dispersals (e.g. Kineke et al., 1996, Traykovsky et al., 2000). The process of fluid mud formation is not clear enough for setting up universal model of them and may sometimes be infrequent phenomena only during high concentration event. The feature of fluid mud is required to be captured by field monitoring.

Schematic profile of fine sediment concentration from the water column through the settled bed is depicted by Ross and Mehta (1989) as in Figure 2.2 showing appearances of several mud states as mentioned above depending on the sediment concentration. Availability of information on the vertical profile of sediment concentration may be critical for estimating transport rates of sediment under forces such as current and waves. In order to gain the profile, both suspended and bottom sediments are taken by any water sampler for suspension and by any sediment core sampler for accumulated sediments, respectively. As another method to directly measure the profile of density, there are several in situ devices including tuning folk type densimeter and gamma ray type system (e.g. Nichols, 1985, and PIANC, 2008). In the following sections, characteristics of vertical structures of muddy environment are examined with some field data taken by the techniques combining several methods.

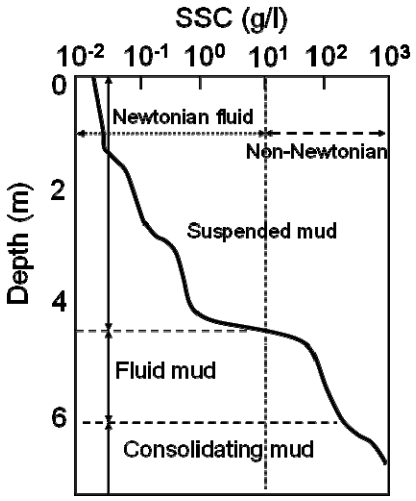

Figure 2.2 Schematic vertical profile of fine sediment concentration (after Ross and Mehta, 1989)

2.3 Measurement of mud-water interface in Ariake Bay

2.3.1 Site description

The Ariake Bay is one of the largest estuaries in Japan on the western coast of Kyushu Island (Figure 2.3), with a surface area of 1,700 km^2 and an averaged depth of 20 meters. Tidal effects are prominent all over

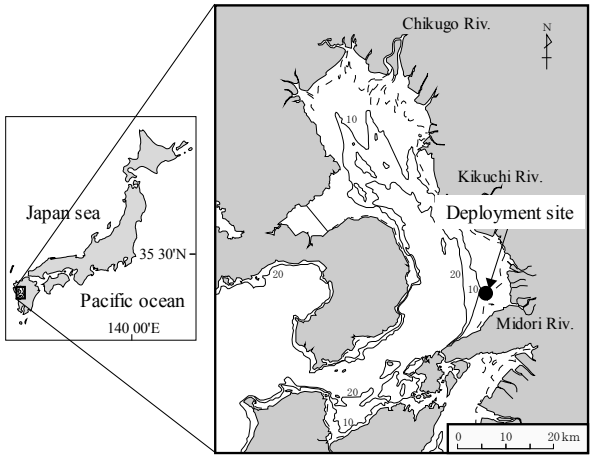

Figure 2.3 Location of Ariake bay and Port of Kumamoto

the estuary and the range at spring tide varies from 4 m at the mouth and increases to more than 6 m towards the upper estuary. Annual mean rate of freshwater supply is around 250 m^3/s flowing through main rivers including Chikugo River into the north-east and Kikuchi and Midori Rivers into east coast of the Bay, where intertidal mudflats are developed. The overall spatial distribution of surficial bottom sediments varies depending on the specific location in the Bay and fine materials (less than 75 μm) are dominant off the north-west and middle-east coast of the bay as shown in Figure 2.4.

The study site of the present study is off shore area at the middle-east coast of the bay near the Kumamoto city, where muddy sediments are dominant and inter tidal mud flats are formed at the river mouth of the Shira River and the Midori River as mentioned above. Tidal range is around 4 m during spring tide period in the area and semi diurnal component is dominant with the flood tide of onshore-ward current and the ebb tide of offshore-ward current. In the embayment of the test site, a dredged navigational channel accesses to the harbor basin of the port of Kumamoto which is located offshore of the intertidal mud flat area as shown in Figure 2.5. As shown in the figure, four stations are selected to take sediment samples and measuring in-situ bulk density profiles. The Stn. a and b are located at the north and south side of the navigation channel of the Kumamoto Port with the water depth of less than 4 m. Of the stations on the navigation channel, St.c is located inside the dredged area with the water depth of -7.7 m. St.d is also on the navigation channel but the location is not dredged with the natural water depth of -8.6 m.

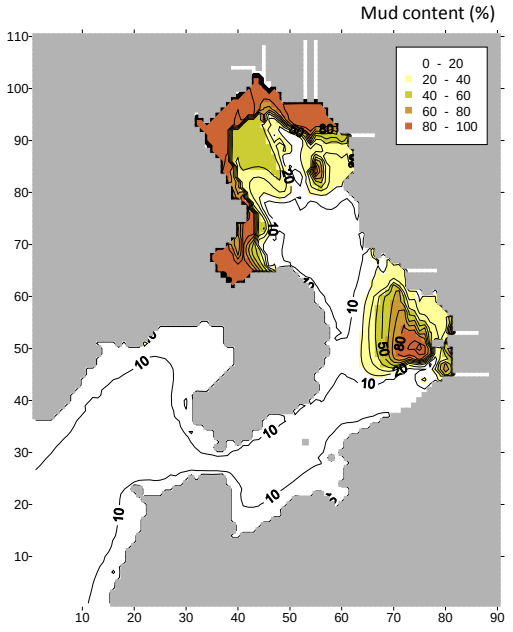

Figure 2.4 Distribution of mud content in Ariake bay

2.3.2 Field survey for mud density measurement

Field survey was carried out on December 11 and 12 in 2002 at the monitoring stations around the Kumamoto Port. At these points, sediment samples were taken with core samplers with the diameter of 43 mm. The sediment core samples were sliced with the thickness of 10 cm and analyzed for sediment properties such as bulk density, particle size distribution, dry density, etc. Soundings were also carried out by an acoustic sounding with the frequency of 200 kHz and a lead line also. The weight of lead used for the sounding is 6.2 kg and the area of base is 20.25 cm^2. In addition to the taking core samples and the measurement of bed level with the conventional techniques, an in-situ densimeter was also applied to measure bulk density of

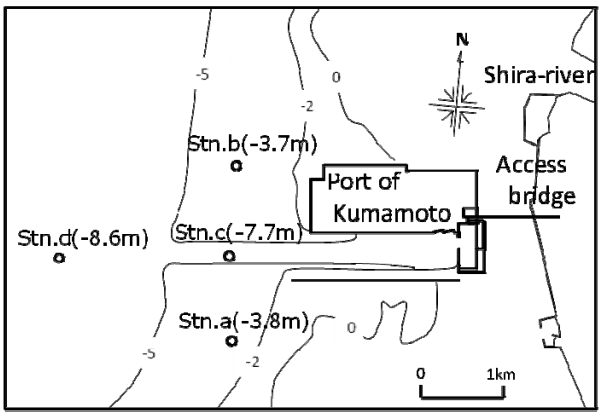

Figure 2.5 Study site and sampling locations around the port. (Bed elevations below the datum line; D.L., are indicated in brackets)

sediment. All these sampling and measurements were carried out at each station, where a research boat was moored as illustrated in Figure 2.6.

The density measurement device used in the present study is one of the tuning folk type densimeter, a product of HR-Walingford (Hydramotion Co. presently) and model XL-4 (Figure 2.7), with the mono folk type sensor of 10 cm length and 1.5 cm diameter. The measurement system detects the vibration frequency of the sensor that varies with the density of the surrounding medium. Total weight of the sensor unit is 5 kg in the air and 4 kg in the water. It is connected through a cable with a PC and both measured depth and density data are logged at the same sampling rate of 1 Hz. The measurement range of density is 0.9-1.5 g/cm^3 and the resolution is 0.001 g/cm^3. For the measurement at the site, the sensor was suspended from the boat and taken down at 10 cm pitch near the bottom level, considering the previous measurement results of the soundings. The density can be measured until the sensor is buried in the consolidated mud layer.

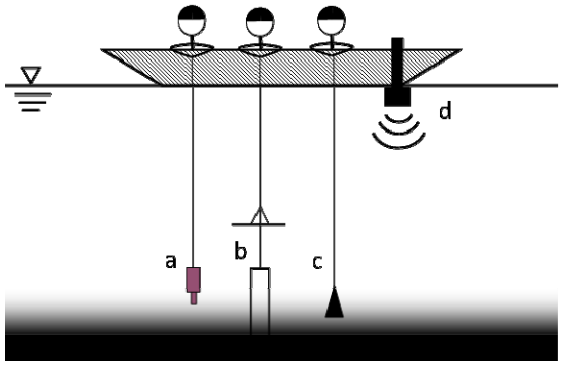

Figure 2.6 Schematic of field measurement of mud bed structure (a: In-situ densimeter, b: Sediment core sampling, c: Lead method, d: Acoustic sounding with 210kHz)

Figure 2.7 Sensor of in-situ mud density measurement

2.3.3 Measurement results in Ariake Bay

(1) Surface sediment properties

Physical characteristics of the bottom surface sediments at the field in the Kumamoto bay are shown

Table 2.1 Surface sediment properties at the monitoring stations

	Stn.a	Stn.b	Stn.c	Stn.d
D50(μm)	24.9	2.5	2.0	<1.0
% of Sand(>75μm)	24.8	4.7	3.6	2.6
% of Silt(5<d<75μm)	46.5	37.3	33.3	30.0
% of Clay(d<5μm)	28.7	58.0	63.1	67.4
Density of Perticles (g/cm^3)	2.697	2.682	2.662	2.674
Water content (%)	81.4	159.6	222.6	179.8
Bulk Density(g/cm^3)	1.513	1.357	1.180	1.114

in Table. 2.1. Most the surface sediments at the stations consists of fine sediments with the median grain size of less than 2.5 μm and with the mud content of over 97 %, except the St.a where sand fraction is relatively high or mud content (sum of silt and clay fractions in weight) is less than 80 %. The higher mud content correlates with the higher water content, which is defined as following.

$$W_c = 100 \times \frac{w_w}{w_s} \tag{2.1}$$

where w_w: mass of water and w_s: mass of sediment grains. The highest value of the water content in the monitoring stations is over 220 % at St.c. The dry density of the sediment particles are almost same values around 2.6 g/cm^3. However, the bulk density is ranging from 1.11 through 1.51 g/cm^3 and it decreases less than 1.2 g/cm^3 in the high water content environment, which is classified as the fluid mud at St.c and d.

As the spatial feature of sediment properties in the study area, the south part of the navigation channel shows the relatively higher sand contents as shown in the result of St.b in contrast to the muddy environment at St.a in the north side of the channel. Though the mud content is high at St.a, fluid mud is not observed and it is considered to be because of current and wave disturbance for near surface sediment in the shallow area. On the other hand, the higher water content and fluid mud are observed at the relatively deeper stations of St.c and St.d. It should be noted that Stn.c is located in the navigation channel dredged up to -7.7 m from the original depth of less than 4 m. This fact indicates that the dredged channel accumulates fine particles with so high concentration that fluid mud layer may be formed.

(2) Vertical structure of fluid mud layer

Bulk density distribution in the bottom sediment layer can be obtained by analysis of sediment core

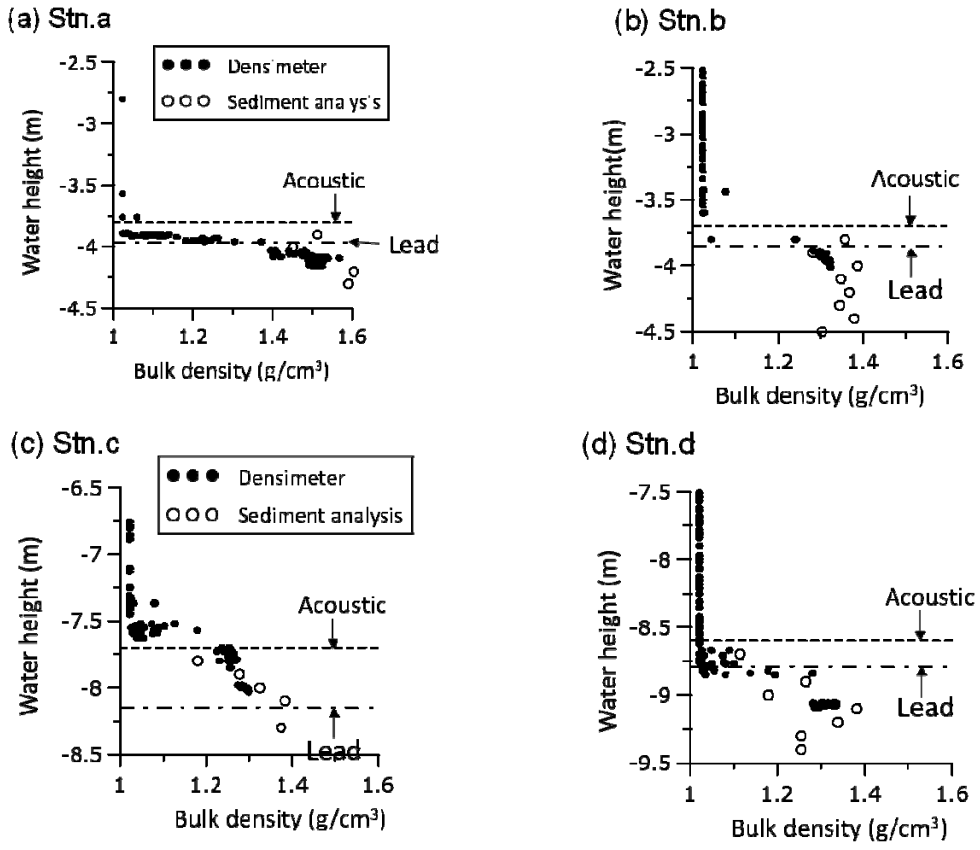

Figure 2.8 Measured density profiles by sediment core analysis and in-situ densimeter. (The vertical scale is relative to D. L.) at Stn.a (a), Stn.b (b), Stn.c (c) and Stn.d (d) .

samples. The analyzed data for the core samples taken from the Kumamoto Bay are plotted by the circles in Figure 2.8. The figure also shows the measured bulk density profiles with the in-situ device plotted by dots from water column through the near bottom sediment. The bottom level detected by the acoustic device and the lead method are also indicated by the dotted lines for the acoustic and dashed lines for the lead line results, respectively.

At the Stn.a with the relatively higher sand content, the bulk densities near the bottom surface are over 1.4 g/cm^3 all through the sliced layers of sediment core sample showing rigid sediment condition. The density profile measured by the in-situ densimeter shows rapid increase in the bulk density at the interface between the sea water with the density of around 1.02 g/cm^3 and the consolidated sediment with the density of over 1.4 g/cm^3. In case of muddy sediment with relatively lower water content at Stn.b, the densities obtained by the core sample analysis shows almost uniformly distribute in vertical around 1.3-1.4 g/m^3, which is categorized as consolidating mud. The in-situ bulk density measurement result shows rapid increase at the interface between the sea water and the mud layer. The difference between the detected bed levels by the acoustic device and the lead method is around 15 cm both for Stn.a and Stn.b.

In the cases of the mud with higher water content at Stn.c and Stn.d, the vertical structures are different from the above two stations and they shows gradual increase on bulk density into the depth as shown in Figure 2.8 (c) and (d). The measured profile of the bulk density by the in-situ densimeter for these stations shows the transition layer with the thickness of around 10 to 20 cm where the bulk density is between 1.02 and 1.2 g/cm^3. These detection of the density range with the thickness around 10 to 20 cm means the existence of fluid mud layer at these layers. Depending on the thickness of the fluid mud layer, the difference between the bed levels of the acoustic bottom and the lead line detection and it becomes as much as 50 cm in the most high water content mud case at Stn.c. This is considered to be caused by the settling and accumulation of fine sediments in the dredged navigation channel. Vertical profile of the bulk density with the in-situ device were measured several times at measurement point in the navigation channel and they are almost same profile as shown in Figure 2.8.

2.4 Sediment properties of muddy bed of study site in Tokyo Bay

2.4.1 Site description

Another study site is located at the Tama River mouth in the Tokyo Bay, Japan (Figure 2.9). The surface area of the bay is approximately 1,500 km^2 and averaged depth is around 15 m experiencing semi-diurnal, meso-tidal condition with a maximum spring tidal range of around 2 m in the upper bay area. The tributary of the bay has a high population of almost 30 million people and the coastal area has been has been highly developed artificially for industrial uses. Several river flowing into the bay mainly at the north eastern shore of the bay, including the Ara River, the Edo River and the Tama River, etc. One of the major concerns for the environment in the bay area is the

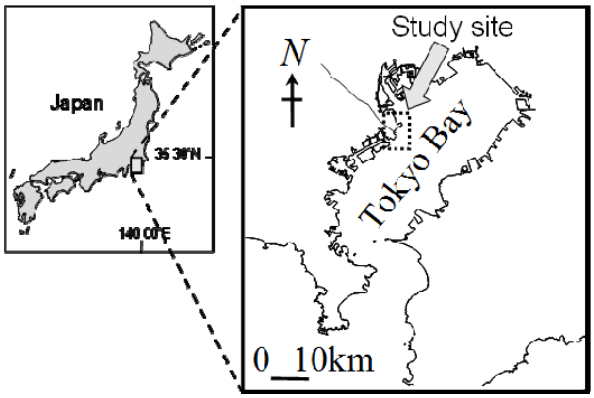

Figure 2.9 Map of the Tokyo Bay and location of the study site

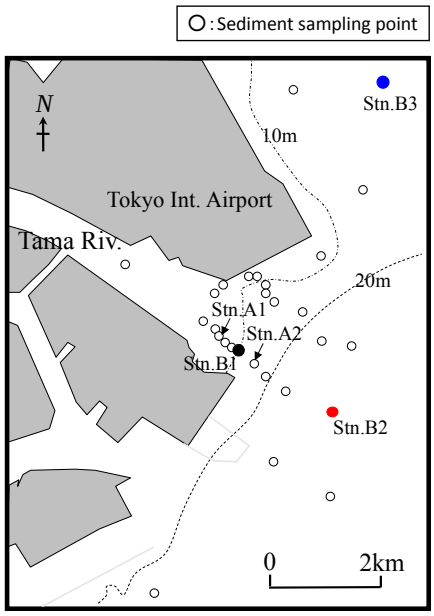

Figure 2.10 Core Sampling points in the study area

deterioration of water and sediment qualities having negative impact on benthic organisms (e.g. Kodama and Horiguchi 2010).

The site of the present study is off the mouth of the Tama River, which discharges into the north-western shore of the inner Bay with the total drainage basin area of 6,000 km^2. The Tama River has basin area of 1,240 km^2 (the second largest of the bay) and carries around 20 m^3 /s at typical background flow rates and 200-1,000 m^3 /s during flood events. The topography of the river mouth area has been highly developed artificially for industrial uses and a runway for the Tokyo International Airport has been newly extended in the water area for recent years. A monitoring project was running at this site since 2007 in order to grasp the environmental evolution of physical, chemical, and ecological aspects. The present study, as a part of the monitoring project, focused on the sedimentary processes and carried out analyses of sediment core samples to get information on sediment properties and to monitor changes in sediment characteristics in the area.

2.4.2 Methods

Core samples were taken at the 25 points indicated in Figure 2.10 around the Tama river mouth from May 30 through June 10, 2006. Undisturbed sediments were taken by divers using core samplers with the diameter of 10.5 cm and the sediments in the depth of 30 cm from the surface were sliced into 4 layers of 0-1 cm, 1-5 cm, 5-15 cm and 15-30cm, respectively. These sliced sediment samples were applied for the analyses of sediment size, water content, ignition loss etc.

The exposed sediment out of the core sampler was sliced off at the prescribed depth by pushing up the sediment at the bottom end. During the slicing procedures, all these exposed mud states were classified visually as “fluidized mud” or “consolidating mud” according to the condition when sediments were pushed out of the core sampler at the top as shown in Figure 2.11. A handy vane which is an improved torque meter (e.g. Sassa and Watabe, 2007) was also applied for the

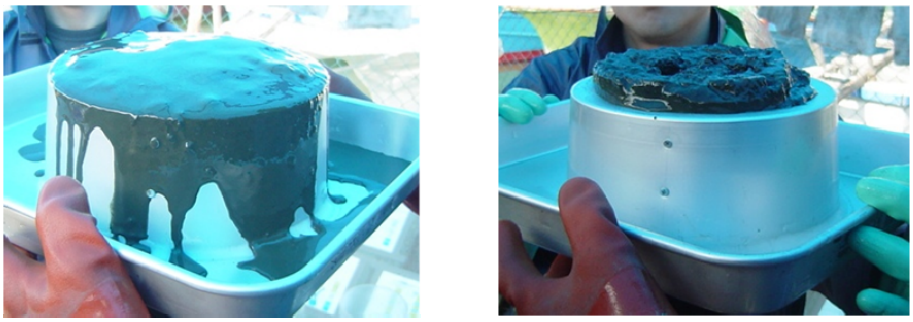

(a) fluid mud　　(b) Consolidating mud

Figure 2.11 Picture of fluid mud categorized by the visual classification

measurement of sediment strength. The size of each vane blade used here is 7.5 mm in the width, 30 mm in the height, and the strength measured every 20 mm pitch in the depth.

For determining the stratified fluid mud layer in the muddy environment, acoustic device such as a sub-bottom profiler can be utilized for capturing the vertical structures of bottom sediments. In order to detect the near-surface fluid mud layer and the consolidating mud layer in the deeper layer, multi-frequency system is often applied and the higher frequency acoustic signal around 200 kHz reflects at the interface between the sea water and fluid mud layer and the lower frequency with around 30 kHz reflects at the interface between the fluid mud layer and consolidating bed (eg. van Leussen & van Velzen, 1989). In the present study, a sub-bottom profiler which operates at 4-24 kHz (System3100-G, EdgeTek) was used for monitoring the deposition of soft mud on the sea bed around the study site. Core samples of the bottom sediment were also taken as ground truth data for evaluations of the acoustic sounding images.

2.4.3 Measurement results and discussions

Relationship between thickness of fluidized mud categorized by the visual classification and the water depth of sampling locations are plotted in Figure 2.12, showing that the fluid mud exists only when the water depth is over 10 m and the maximum thickness is 30 cm. Spatial distribution or contour of the fluid mud thickness around the sampling area at the Tama River mouth is shown in Figure 2.13. The monitoring site include shallow area inside the Tama River with the water depth of less than 5 m, which connected to the deeper offshore through a fore set slope with the depth between 5 and 10 m at the river mouth. The contours of the fluid mud thickness correspond to the topography and the thicker fluid mud over 10 cm distribute at the offshore of the river mouth with the water depth of 20

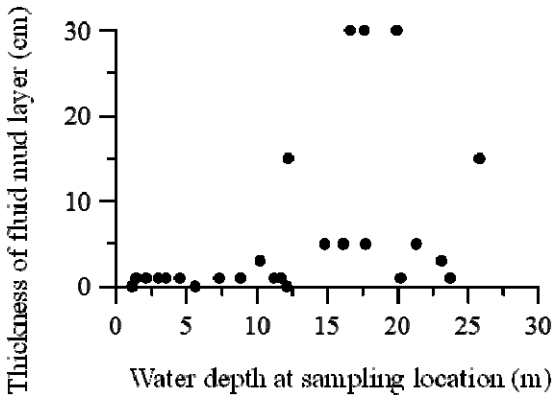

Figure 2.12 Relationship between results of visual classification of fluid or consolidated mud and their water content

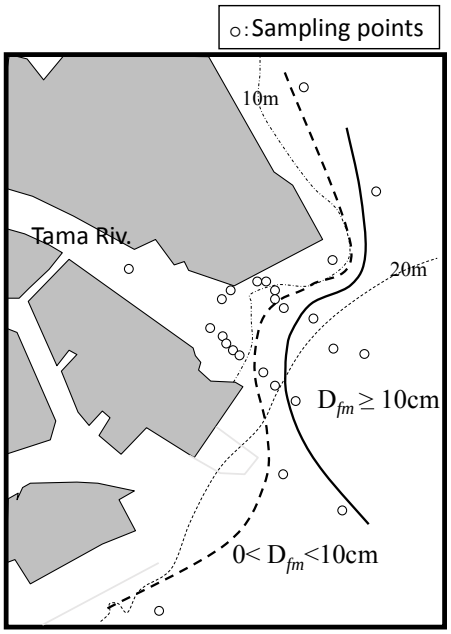

Figure 2.13 Spatial distribution of fluid mud thickness (Dfm) according to visual classification of sediment core samples

m. In other survey result of sediment core sampling, soft mud with the high water content of 300 to 400 % is observed in the offshore and deeper area of the present study site (Gomyo, 2001), indicating the soft mud distribute in the deeper area.

The results of classification as fluidized or non-fluidized mud are compared with the water content analysis for the same samples in Figure 2.14. The figure shows that the mud with the water content over 350 %

does not exist as consolidated mud and all of them are classified as fluid mud. There are several samples that are classified as fluid mud, though their water contents are less than 350 %. When the thickness of slicing sample is over 10 cm, some sediments collapse itself by self-weight, which is not able to keep the shape and are classified as fluid mud. Therefore, in order to make this visualizing classification more general method, the thickness of the sediment slice should be unified as 1 cm for example.

Measurements of the handy vane torque meter are compared with water content in Figure.2.15. The result shows that mud with water content of over 350 % has quite weak shear strength and the shear strength become the larger with the decrease of water content less than around 350 %. This characteristics correspond to the fact that critical water content for the existence of fluid mud is also around 350 % as mentioned above. Assuming dry density of sediment particle as 2.6 g/cm^3, bulk density is about 1.2 g/cm^3 for mud with water content of 300%. The value of bulk density, 1.2 g/cm^3, is often applied to determine the navigable depth or nautical depth for port and harbor operation in muddy environment (PIANC, 2008).

In the survey with sub-bottom profiler for taking acoustic data, a research boat equipped with the transducer was running on a survey line and was moored at several monitoring points also. An acoustic image taken on a survey line from the river mouth through the offshore is shown in Figure 2.16, and the

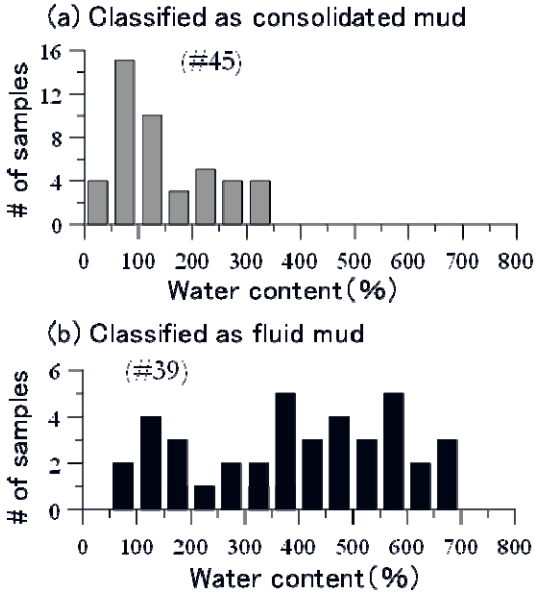

Figure 2.14 Histograms of fluid mud and non-fluid mud over water content

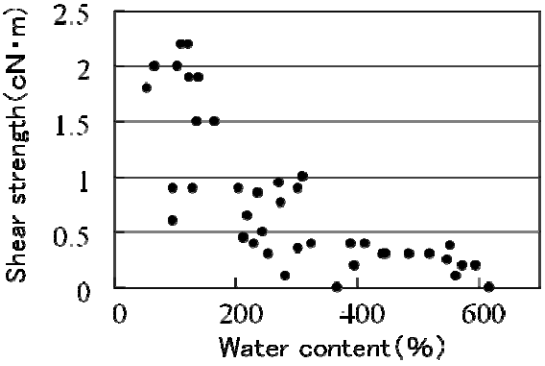

Figure 2.15 Comparison between water content and shear strength measured by handy vane torquemeter

lines indicates monitoring points Stn. A1 and Stn.A2.

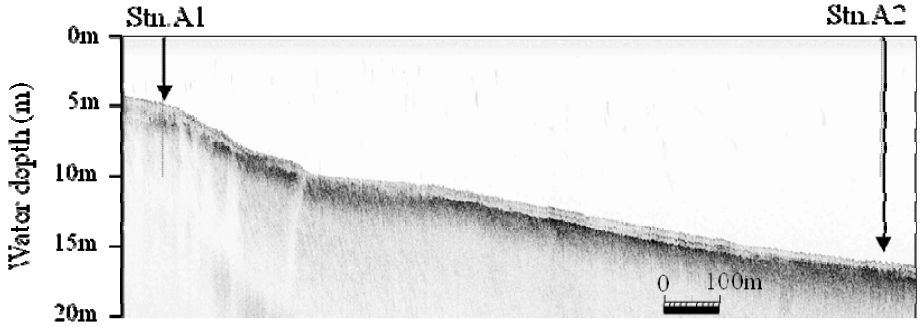

Figure 2.16 Acoustic image of sub-bottom profiler on survey line from river mouth to off shore.

Grey scale of the acoustic image is depend on the extent of back scatter intensity of acoustic signal and it becomes dark when the high intensity signal received from sediment layer with the relatively higher density condition. Around the slope of foreset, the acoustic image shows relatively higher reflection from bottom surface. On the other hand, the image shows 2 layer structure with the lower intensity near the surface and higher intensity layer appears beneath the low intensity layer at the offshore area.

In order to examine the spatial distribution of acoustic image, the acoustic profile image was compared with the analyzed data of sliced sediment core samples taken from Stn.A1 and Stn.A2. Acoustic profile images at Stn.A1 and Stn.A2 are shown in Figure 2.17, indicating that higher intensity layer appears at the surface layer in case of Stn.A1. In case of Stn.A2, low intensity layer covers on higher intensity layer and thickness of the lower intensity layer reads around 70 cm. Sedimentary profiles analyzed from core samples taken from these stations are represented by the parameter of bulk density and water content in Figure 2.18. The profile of bulk density at Stn.A1 shows slight increase into the depth over 1.4 g/cm^3 and water content is almost uniform around 100 % through the depth. In the data of Stn.A2, the bulk density start with 1.2 g/cm^3 at the surface and gradual increase into the depth and corresponding profile of the water content shows high water content 300 % near the surface, indicating existence of fluid mud at the surface layer. Under the depth of 60 cm at Stn.A2 the bulk densities are over 1.4 g/cm^3 with the decrease of water content down to around 110 %, showing consolidating state in the depth. These differences of vertical profiles correlates with the sediment type constituent and the

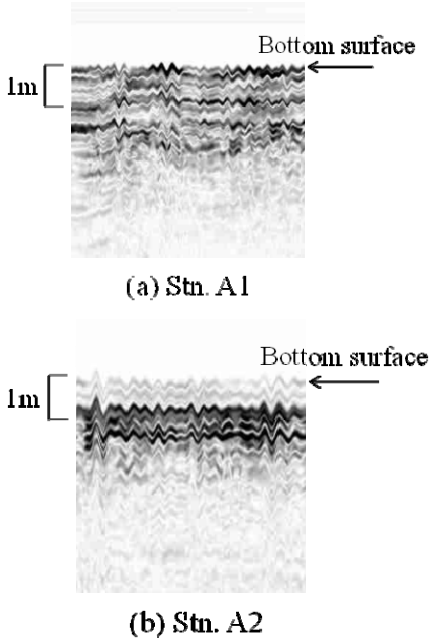

Figure 2.17 Acoustic image of sub-bottom profiler at (a) Stn.A1 and (b) A2.

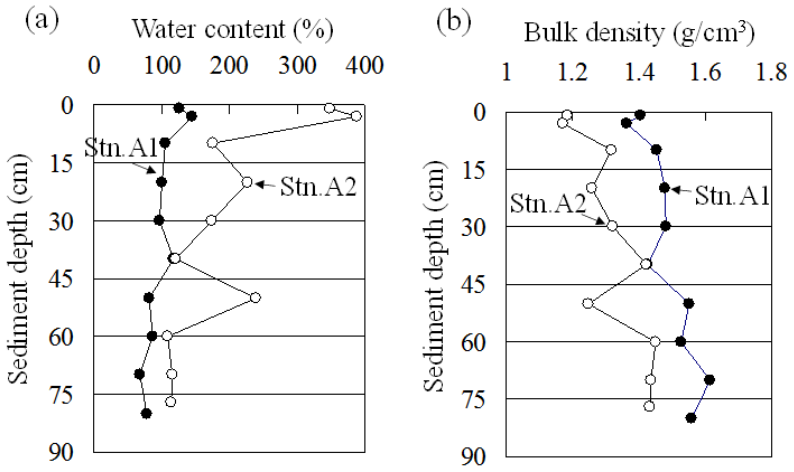

Figure 2.18 Vertical profiles of (a) water content and (b) Bulk density in the mud layers at Stn. A1 and Stn. A2.

sediment at Stn.A1 include 10 % of sand while the sediment at Stn.A2 consists of mud with 98 % of silt and clay. Acoustic intensity images at the stations correspond to the differences of sediment type and sedimentary structure. The high intensity reflection from the surface layer at Stn.A1 represent the sediment of sand mud mixture with low water content and the low intensity near the surface layer in the acoustic result of Stn.A2 corresponds to the mud layer with fluid mud on the surface.

For dynamics of muddy sediment transport, the vertical profile of bulk density or water content as represented in Figure 2.18 has a key role since the yield strength depends on the water content. In other additional surveys, core samples were taken at Stn. B1, B2 and B3 and analyzed for water content profiles as shown in Figure 2.19. Both of the off shore points at Stn. B2 and B3 shows high water content over 300 % in the surface layer and thickness of fluid mud layer exceeds 20 cm at Stn. B3. These characteristic of vertical structure is incorporated to derive the transport formula of the fluid mud in the chapter 4.

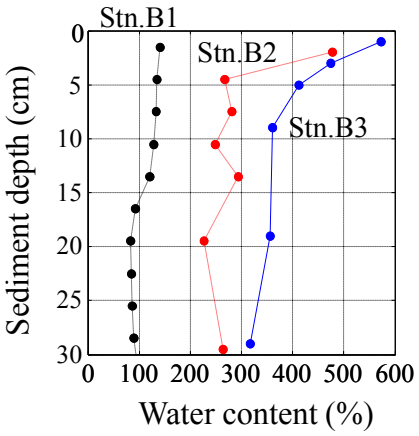

Figure 2.19 Vertical profiles of water content at Stn. B1, B2 and B3.

2.5 Conclusions

In order to reveal sedimentary structures near bed surface in typical muddy environments in Japan, the field surveys were conducted to measure vertical profiles of sediment properties in the Ariake Bay and the Tokyo Bay. In the present study, core samples were taken and sliced sediment were analyzed for representing vertical profiles such as bulk density and water content, which were compared with measurement results by other devices to examine muddy sediment characteristics including existence of fluid mud in the fields. Especially in case of high water content of muddy bed environments, the top surface of mud bed structure may not be captured by any conventional approach with grab type samplers with the destruction of near surface soft mud layer. By applying the several techniques in the present study, the vertical profiles and thickness of fluid mud layer and their spatial distribution in the field were newly obtained and shown quantitatively as followings.

At the study around the Kumamoto Port in the Ariake Bay, a tuning folk type of in-situ device for bulk density measurement was also applied in addition to taking core samples and thin fluid mud layers were observed on the bottom surface at the deeper stations with the water depth of 7 to 8 m. The relatively thicker fluid mud is formed in the navigation channel with the thickness of around 10 cm, indicating accumulation of fine sediment into the dredged deeper channel from surrounding shallow and inter tidal mud flat area.

At the Tokyo Bay site, formation of fluid mud layer is more apparently in the offshore area with the water depth over 10 m. According to visual classification of sediment core samples for fluid mud or consolidated mud, the muds with the water content over 350 % are classified as fluid mud and these soft mud have only weak strength based on the measurement results with a handy vane torque-meter. Thickness of fluid mud layer is relatively higher in the offshore from the river mouth area with the thickness of over 20 cm. The properties of vertical structure observed in the field studies should be considered in modeling of mud transport dynamics

discussed in Chapter 4.

References for Chapter 2

Gomyo, M., E. Yauchi and T. Ohtsuki (1990): Sedimentary characteristics of mud in Tokyo Bay, Proc. of Coastal Engineering, JSCE, Vol. 37, pp.848-852. (in Japanese)

Kineke, G.C., R. W. Sternberg, J. H. Trowbridge and W.R. Geyer, (1996): Fluid-mud processes on the Amazon continental shelf, Continental Shelf Research, Vol.16, Issues5-6, pp.667-696.

Kodama, K. and T. Horiguchi, (2011): Effects of hypoxia on benthic organisms in Tokyo Bay, Japan: A review, Marine Pollution Bulletin, Vol. 63. Pp.215-220.

Nichols, M. M., (1985): Fluid mud accumulation processes in an estuary, Geo-Marine Letters, Vol. 4, pp.171-176.

PIANC (2008): Minimizing harbor siltation, World association for waterborne transport infrastructures, Report No. 102, 75p.

Ross, M. A. and A. J. Mehta, (1989): On the mechanics of lutoclines and fluid mud, Journal of Coastal Research, SI. 5, pp51-61.

Sanford, L.P. and J. P.-Y. Maa (2001): A unified erosion formulation for fine sediments, Marine Geology, Vol.179, pp.9-23.

Sassa, S. and Y. Watabe (2007): Role of suction dynamics in evolution of intertidal sandy flats: Field evidence, experiments, and theoretical model, Journal of Geophysical Research, Earth surface, Vol. 112, F01003, DOI: 10.1029/2006JF000575

Traykovski, P., W. R. Geyer, J. D. Irish and J. ZF. Lynch (2000): The role of wave-induced density-driven fluid mud flows for cross-shelf transport on the Eel River continental shelf, Continental Shelf Research, Vol. 20. pp. 2113-2140.

van Leussen, W. and E. van Velzen (1989): High concentration suspensions: Their origin and importance in Dutch estuaries and coastal waters, Journal of Coastal Research, Vol.SI-5, pp.1-22.

Whitehouse, R., R. Soulsby, W. Roberts and H. Mitchener (2000): Dynamics of esutuarine muds, Thomas Telford Publications, 210 p.

Winterwerp, H., (1999): On the dynamics of high-concentrated mud suspension, PhD Thesis published as Report No.99-3, Communications on hydraulic and geotechnical engineering. Delft University of Technology, Faculty of Civil Engineering and Geosciences, 172p.

3 FINE SEDIMENT DYNAMICS UNDER TIDE-DOMINATED CONDITION

3.1 Introduction

Modelling of fine sediment movement is not straight forward because it involves several parameters describing the physical characteristics of sediment properties such as erosion and deposition rate. To obtain such parameters, many laboratory studies (e.g. Mehta, 1988, Kusuda et al. 1989) and field tests with in-situ erosion devices (e.g. Maa et al., 1993) have been made on specific sediments. The dynamics of muddy sediment transport process extensively depend on the site specific conditions both of sediment parameters and forcing conditions. Therefore, instead of the deployment of laboratory or field experimental instruments for directly measuring sediment parameters, there is another possible approach whereby the sediment parameters are obtained indirectly from analysis of time series data of suspended sediment concentration (SSC) measured in the field (Sanford and Halka, 1993, Hill et al. 2003, and Vinzon and Mehta, 2003).

The Ariake Bay, where is the study site in this chapter, experience relatively high tide with the maximum tidal range at spring tide of around 6 m in the upper bay as mentioned in the previous chapter. Dynamics of suspended fine sediment driven by strong tidal current in the bay is considered to play a key role not only in the topographical change but also in the ecosystem evolutions in the bay. High turbid water with suspended fine sediments may control the sun light penetration into the water column affecting the primary production and distribution of fine sediment has high correlation with habitat of benthic species. Several research works have been carried out for assessing the environment of the bay area. Although several field experiments for elucidating sediment transport characteristics were carried out in the Ariake Bay

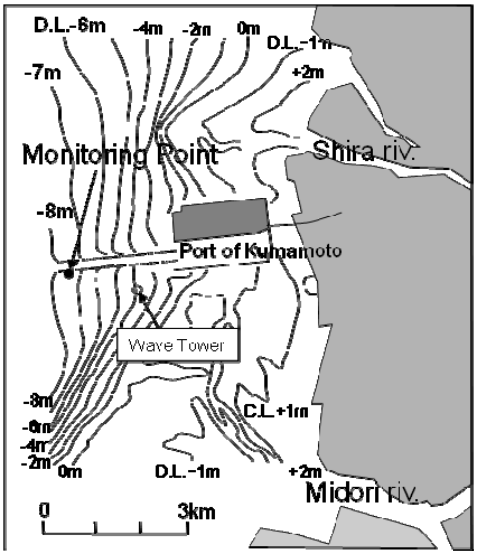

Figure 3.1 Location map of monitoring point off the Kumamoto Port. (The location is 32.45'23''N/ 130.33'03''E in WGS82 system)

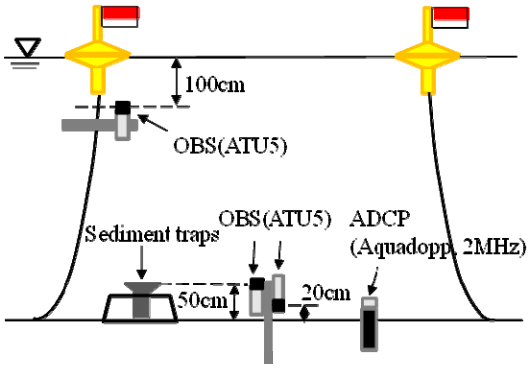

Figure 3.2 Schematic of instrumentations with bottom mounted sensors and moored system.

(Seguchi, et al. 1989, Kondo et al. 1996), the durations of their observations are restricted only to a one tidal cycle and there are few observations for the variation of the phenomena between spring and neap tidal cycle.

This chapter describes resuspension and settling dynamics of fine sediments under tidal current based on a half month deployment of field monitoring in the field. In the analysis of the monitoring data, acoustic backscatter intensity data of an acoustic Doppler current profiler, ADCP, is applied to obtain temporal variations of SSC profiles. From the time difference of

total suspended load (TSL), the erosion and deposition parameters can be estimated.

3.2 Field observation

The field data presented in this section were collected at a monitoring point off the Kumamoto port in south west of the Ariake Bay (Figure 2.3). The monitoring site is indicated in Figure 3.1 located approximately 5 km off the coastal line with the bottom level of -7.5 m from the local datum line (D.L.). Instruments layout is illustrated in Figure 3.2, which consists of bottom-mounted sensors and moored system, and the monitoring has been deployed for one month from mid-October through mid-November in 2001. Wave data were measured at a monitoring tower near the study site where the bottom level is -5 m from the D.L. which is operated by the Kumamoto port office, Ministry of Land, Infrastructure, Transport and Tourism. The wave data during the deployment period of the present study were provided by the port office as significant wave height and period every 2 hours.

An bottom mounted ADCP (Aquadopp 2MHz, Nortek) measured velocity with 30 cm bins of the water column from 40 cm above the bottom through approximately 1 m below the surface. The sample interval was 30 minutes and recorded 2 minutes averaged velocity. Optical backscatter sensors (ATU5, JFE Advantec Co. Ltd.), OBS, were deployed to estimate suspended sediment concentration, SSC, and two sensors fixed at 20 cm and 50cm above the bottom and another sensor was moored at 100cm below the surface. The data of the OBS sensors were collected every 5 minutes and converted to SSC in the unit of mg/l by applying calibrations using sediment samples taken from the monitoring site.

During the monitoring campaign, sea bed sediment and suspended sediment were taken for particle size distribution analysis. In order to take samples of suspended sediments in the water column, sediment traps were mounted on the bottom so that the top of the sampler was located at 50 cm above the sea bottom. Based on the bottom sediment analysis, silt and clay particles are dominant as indicated by solid line in Figure 3.3 and particle size distribution of suspended particles is plotted by dots, showing almost same cumulative curves between them.

3.3 Estimation of suspended sediment concentration profiles with ADCP's backscatter data

3.3.1 Relationship between SSC and backscatter intensity

The use of acoustic backscatter intensity for the estimation of SSC profiles has become popular (e.g. Hill et al., 2003, Gartner, 2004) and the application of this technique is powerful tool for suspended sediment transport studies. In the present study, measured ADCP backscatter intensity was calibrated to SSC using the estimated SSC from the OBS data measured at the several levels. The relationship between the backscatter intensity of suspended particles at distance of D from the ADCP transducers and SSC (in the unit of mg/l) is assumed to be given by Eq. (3.1),

$$A\log SSC = I - B + k\log D + 2\alpha D \qquad (3.1)$$

where I: measured back scatter intensity by ADCP (in the unit of count) and B: back ground intensity. The last two terms in the right hand side represent transmission

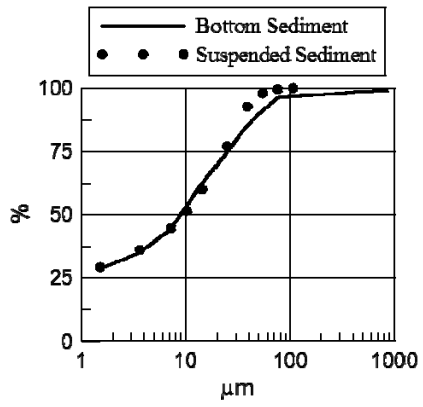

Figure 3.3 Size distributions of bottom sediment and suspended sediment at monitoring site

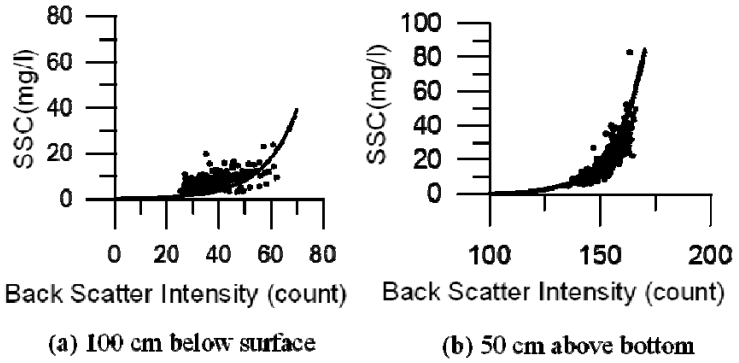

Figure 3.4 Comparison of SSC estimated with OBS and back scatter intensity of ADCP.

loss of sound and k is attenuation coefficients by diffusion and α is by absorption, respectively.

The coefficient for attenuation by absorption, α, depends on frequency of acoustic device used for the measurement and is set as 2.8 count/m in the present study, considering the study by Suetsugu et al. (2002) where the same type of ADCP was applied for the SSC measurement. The parameters, B, k, and A are calibrated so that Eq. (3.1) can well fit the relationship between the recorded intensity, I, and SSC estimated with OBS. In the present study, the parameters are set as A=30, B=95 count and k=31, respectively.

Comparisons between the OBS-derived SSC and the backscatter intensities of ADCP at 100 cm below the surface and at 50 cm above the bottom are shown in Figures 3.4. The SSC measured near the water surface are relatively low and the backscatter intensity is ranging from 20 to 60 count only. In case of the near-bottom measurement, SSC show more changeable with higher value and the backscatter intensity is ranging from 130 to 170 counts. The fitted curves by Eq. (3.1) with the calibrated parameters mentioned above are also shown in Figure 3.4 and it is showing that they reasonably fit the data, especially near-bottom data.

3.3.2 Estimated result of SSC by ADCP backscatter data

The time series of SSC estimated by Eq. (3.1)

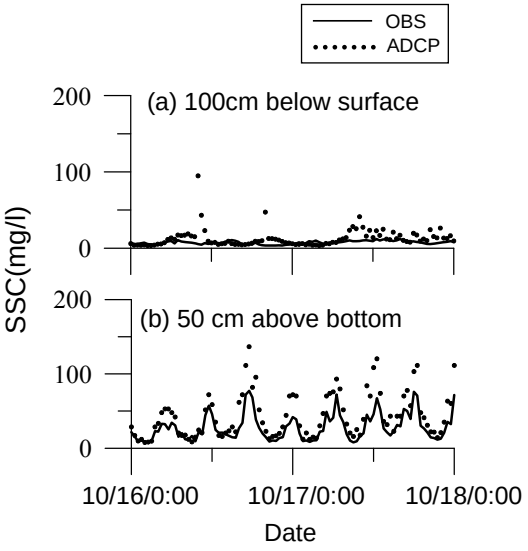

Figure 3.5 Time series of estimated SSC with ADCP comparing with OBS during spring tide.

during spring tide period are shown in Figure 3.5 comparing with OBS-derived SSC. The results show the estimates by ADCP data slightly over-estimate the OBS-derived SSC but the temporal variation of suspended sediment due to tidal force can be reasonably reproduced by the method with ADCP. The discrepancies in the time series result near the surface in Figure 3.5 (a) can be explained due to other sources of suspend ed matters near the surface including phytoplankton etc. and air bubble during higher wave condition with wave breaking, which affect response of acoustic signals differently from the suspended sediments near the bottom.

With the calibrated SSC from the back scatter data

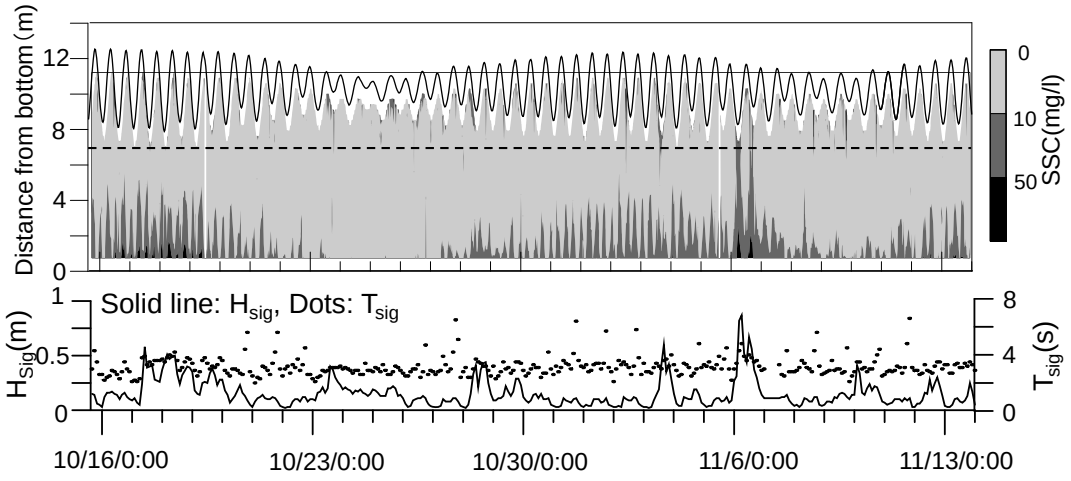

Figure 3.6 Estimated SSC profiles with ADCP (contour in the upper figure) during the whole monitoring period compering with wave conditions (the lower figure) monitored at wave tower.

of ADCP, temporal change in the vertical profile of SSC at the site are shown in Figure 3.6 during the whole monitoring period of one month. The figure also shows significant wave height and period that were observed at the monitoring tower. It is apparent in the figure that high concentration near the bottom occur during every spring tide period and higher suspension events are also indicated episodically according to the relatively rough wave condition as shown on November, 6, with the significant wave height of over 0.7 m.

As for the relationship between the temporal variation in near-bottom SSC and tidal current, the SSC increases during acceleration of flood and ebb current and decreases during deceleration and the minimum at slack water of high and low water at this coastal area (Nakagawa, 2002). The temporal change in the vertical distribution of SSC during the spring tide period is shown in Figure 3.7 and the higher concentration appears during the ebb tide, from the high tide down to the low tide, and the flood tide, from the low tide up to the high tide. Considering these response of SSC profile to the tidal force condition, the temporal change in the concentration of suspended sediment should be dominated by the tidal currents mainly by local resuspension around the monitoring site.

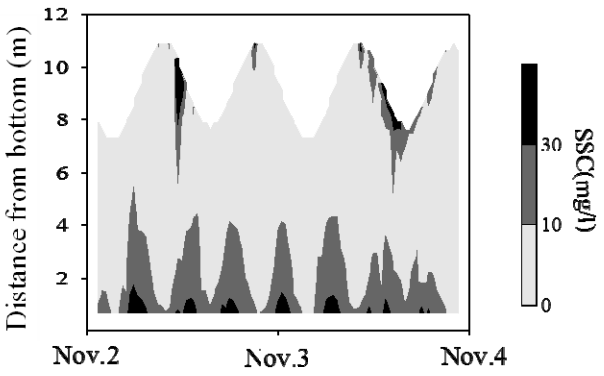

Figure 3.7 Estimated SSC profiles with ADCP during spring tide.

Snapshots of the vertical profiles of the SSC in the accelerating phases of ebb and flood current are shown in Figure 3.8. The highest concentrations are observed under the highest ebb current speed at 0:00 on Oct. 17 and under the highest flood current at 6:00 on Oct. 17, respectively, and these profiles are characterized by the higher concentration around 70 mg/l near the bottom and exponential decay in the upward direction. Furthermore, these concentration profiles indicate the higher concentration under the flood current condition rather than the ebb current condition and this asymmetry is caused by the stronger current condition during the flood period as is often observed around the monitoring site (Nakagawa et al. 2007).

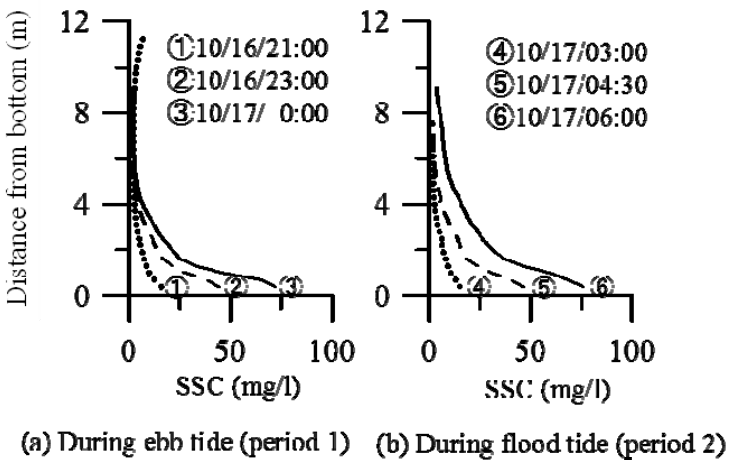

Figure 3.8 Change in the SSC profiles during accelerating period.

3.4 Estimation of erosion rate parameter from field data

3.4.1 Erosion rate formula for muddy bed

There are several key parameters for modeling of sediment dynamics and erosion speed and critical shear stress of bed material is crucial for estimation of sediment transport rate under forces such as waves and current. These parameters are site specific since they depends on sediment characteristics such as particle size, water content or bulk density as mentioned in the previous chapter. For cohesive sediments, the following equation (so called the Ariathurai-Partheniades formulation) is often used for estimation of erosion flux, E,

$$E = M(\frac{\tau_c}{\tau_e} - 1) \qquad (3.2)$$

where M is erosion rate parameter, τ_e is critical shear stress for erosion, τ_c is bottom shear stress by currents and waves. Although there are other types of formula for erosion rate estimation including a power low relationship between erosion rate and shear stress (e.g. Futawatari and Kusuda, 1993) and an exponential form (e.g Mehta, 1988), Eq. (3.2) has been widely applied to numerical models for simplicity of the form.

Typical values for M is usually taken constant typically as 0.06 mg/cm^2/min < M < 3 mg/cm^2/min and τ_e is ranging from 0.1 to 5 Pa (Winterwerp et al. 2004). Because these variation of parameters depends on site specific sediment characteristics, they should be taken as values which corresponds to sediment characteristics of target site in field for appropriate numerical simulations. In the present study, these parameters were evaluated with the field data of SSC estimated in the previous section.

3.4.2 Parameter acquisition procedure

Several studies have been worked on the examination of erosion parameters from field measured data set of SSC profiles such as Sanford and Halka (1993), Clarke and Elliott (1998) and Vinzon and Mehta (2003). The parameters of M and τ_e are, in the present study, estimated from the temporal variation of total suspended sediment load (*TSL*), which is obtained as total weight of the SSC estimated with ADCP data through the water column. The *TSL* is calculated here as total weight of suspended sediment from the bottom up to the level of 7 m from the bottom, considering the other sources of suspended matter such as phytoplankton near the surface.

As forcing parameter that is driving the temporal variation of the *TSL*, bottom shear stress due to tidal

current is considered here. The bottom shear stress is estimated with the following quadratic law,

$$\tau_c = \rho_w C_f \overline{U}^2 \tag{3.3}$$

where ρ_w is the density of sea water, C_f is drag coefficient and $\overline{U}$ is current speed. The value of the drag coefficient is the order of 10^{-3} for steady current (e.g. Soulsby, 1990) and ranging from 0.0016 to 0.0061 depend on the roughness of the bed. For this study, though the current is unsteady and tidally oscillate flow, the shear stress is simply estimated with a constant value of the drag coefficient as 0.0026 and $\overline{U}$ was taken to be the current speed measured at 40 cm above the bed.

The rate of change in the *TSL* was calculated by the difference of the values every 30 minutes and they were compared with the bottom shear stress estimated as mentioned above. Examples of the relationship between the rate of the *TSL* changes and corresponding bottom shear stress are shown in Figure 3.10, which represents the relationship during the same acceleration period of the ebb and flood current examined in Figure 3.8. The figure shows linear relationship between the bottom shear stress and the increasing rate of the total suspended sediment load and regression equations are indicated in the figure.

Considering the same analysis of erosion parameters for other acceleration periods (17 cases in total), the averaged erosion parameters are obtained as M=0.033 mg/cm^2/min. and τ_e=0.025 Pa, respectively. The values of both parameters M and τ_e are smaller than the minimum of the ranges of the parameters mentioned above. Since the observed maximum bottom shear stress is around 0.15 Pa, settled mud bed were not eroded considering the ordinal values as mentioned above. Therefore, it is conceivable that the suspended sediments are resuspended or picked up from fluff layer with high water content just above the consolidated mud bed and it makes the erosion rate and the critical shear stress so small values.

3.5 Simulation of temporal variation of total suspended load

3.5.1 A one-point TSL model

In general, the changes in SSC profile are affected by advection and diffusive transport and local resuspension-deposition processes. However, the data collected at the monitoring station of the present study, as shown in Figure 3.7 and 3.8, indicates the higher SSC events near the bed appear during ebb and flood peak current for a spring tide period. The data suggests that the change in SSC profiles is strongly dominated by resuspension and deposition due to the tidal current. This may simplify the phenomena and the temporal change of the total suspended load was examined with a simple 1D-model in the present study.

Assuming the homogeneity of the field and neglecting the horizontal advection and diffusion terms, SSin=SSout in Figure 3.9, temporal change in the total suspended load (*TSL*) through the water column can be simply expressed as balance between erosion rate, E, and deposition rate, D, at the bottom boundary.

$$\frac{d(TSL)}{dt} = E - D \tag{3.4}$$

For erosion rate, E, is estimated by Eq. (3.2) in the present study and the values of parameters in Eq. (3.2) are set as 0.033 mg/cm^2/min. for E and as 0.025 Pa for τ_e which are estimated in the previous section. On the other term in the right hand side, deposition rate, D, is determined with the following expression,

$$D = w_s C_b p \tag{3.5}$$

where w_s is settling velocity, C_b is the concentration of suspended sediments near the bed, respectively. The probability function, p, is sometimes formulated as a function of bottom shear stress with a parameter of critical stress for deposition, τ_d. (e.g. Krone, 1993).

$$p = \left(1 - \frac{\tau_c}{\tau_d}\right) \qquad (3.6)$$

Use of the probability term for deposition is not able to simulate the observed concentration of suspended sediment (Sanford and Halka, 1993) and they applied a continuous deposition formula (p=1) to reproduce observed concentration change.

3.5.2 Simulation of temporal variation of total suspended load

Based on Eq. (3.4), the time variation of the *TSL* was simulated considering Eq. (3.2), Eq. (3.3) and Eq. (3.5). The probability term is not included here but the result is compared with that with Eq. (3.6) later. The settling velocity was calibrated so that the observed *TSL* variation can be best fitted visually and the calibrated settling velocity, w_s', in the simulation is defined as following.

$$D = w_s' \overline{C} \qquad (3.7)$$

where $\overline{C}$ is depth averaged suspended sediment concentration.

The estimated result of *TSL* variation with w_s'= 0.18 cm/s is plotted in Figure 3.11 and compared with observed *TSL* data. For the simulation, the concentration during neap tide was considered as

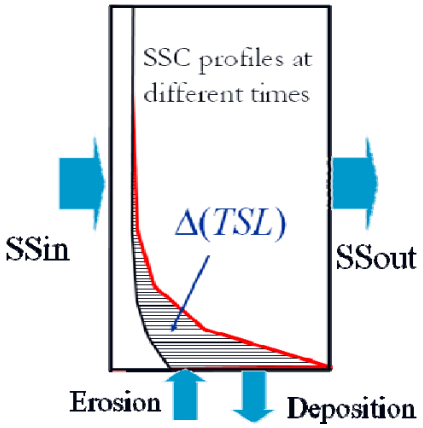

Figure 3.9 Sediment budget in water column for temporal variation of total suspended load (*TSL*)

background concentration. The figure shows that the observed *TSL* variation dominated by tidal current is reasonably well simulated by the model with the calibrated settling velocity and the continuous deposition formula. Since the model does not incorporate the wave induced bottom shear stress, there are discrepancies between the model result and observed *TSL* during the high wave event on Nov. 6, 2001. The good agreement of the numerical result means that the temporal variation of the *TSL* is dominated by the local resuspension around the monitoring site driven by the tidal current and these parameters can be applied to 3-D simulation for sediment transport.

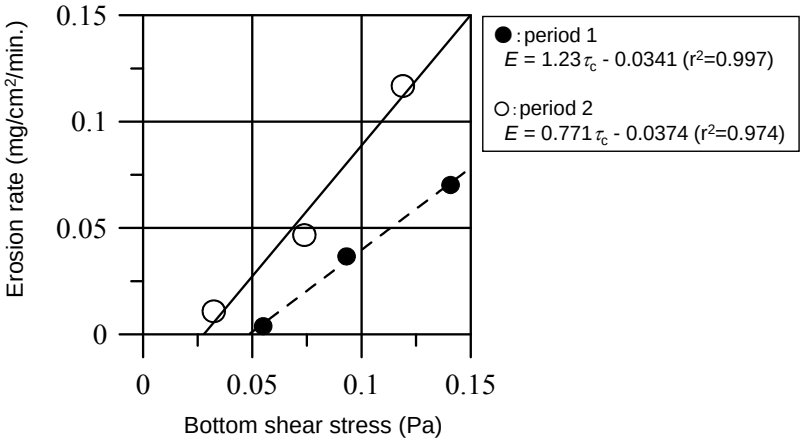

Figure 3.10 Relationship between erosion rates and bottom shear stress for the monitoring site

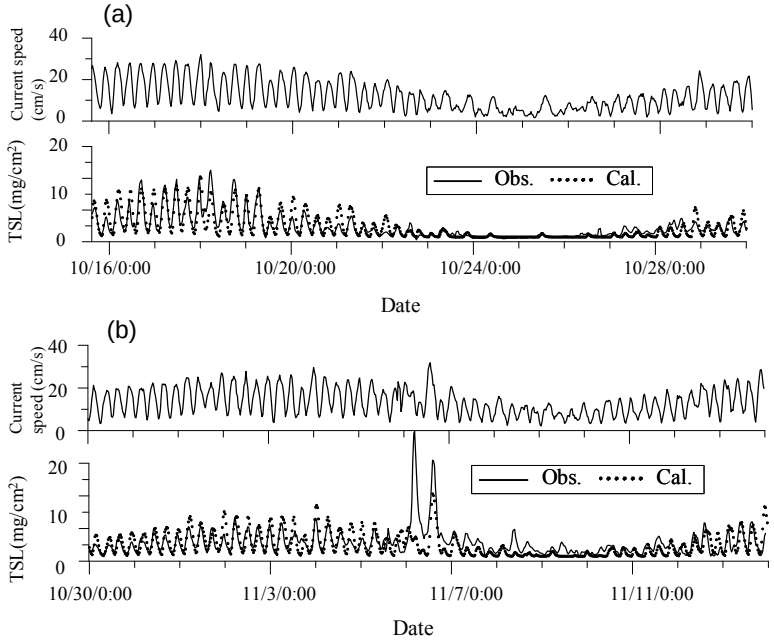

Figure 3.11 Comparison between observed (indicated as "Obs.") and simulated (indicated as "Cal.") total suspended load. ((a) Period from Oct. 16, 2001 through Oct. 29 , (b) Period from Oct. 30, 2001 through Nov. 13)

In order to check the effect of the probability term expressed with Eq. 3.6, another calculation was carried out for the *TSL* estimation, where τ_d was set as $\tau_d = \tau_e$ here. The computed result of *TSL* with Eq. (3.6) is compared with the observed and the computed result with the continuous deposition (p=1) in Figure 3.12. According to the comparison, the result with Eq. (3.6) shows that deposition does not occur until $\tau_c < \tau_d$ and the estimated result overestimate the *TSL* in the observed decreasing phase, while the continuous model is able to simulate well the pattern of TSL variation.

3.6 Conclusions

Monitoring campaign was deployed for measurement of current and turbidity for one month off the Kumamoto Port in the Ariake Bay. Sediment dynamics under the tidal dominated force condition were examined through analysis of the field measured data. Transformation technique of ADCP acoustic backscatter intensity into SSC has been applied through the calibration with OBS derived SSC data. The observed time series of SSC profiles indicates that local erosion and deposition processes are responsible for suspended sediment dynamics at the monitoring site.

Considering time series of total suspended sediment load (*TSL*) calculated from the estimated SSC profiles, erosion rate parameter, *M*, and critical shear stress for erosion, τ_e, are obtained as M=0.033 mg/cm^2/min. and τ_e=0.025 Pa, respectively. The values of both parameters M and τ_e are smaller than values in literatures and it is conceivable that the suspended sediments are resuspended or picked up from fluff layer with high water content just above the consolidated mud bed around the monitoring site. These parameters may be applied for practical numerical simulations of suspended sediment dynamics in the bay.

The temporal variation of the observed *TSL* is highly influenced by the tidal current and is in phase with the tidal current speed. The estimated *TSL* with observed suspended sediment concentration can be simulated well by a simple 1-DV model with the calibrated settling velocity as w_s'= 0.18 cm/s. The model with the continuous deposition concept shows quite good performance to simulate the temporal variation of observed *TSL*, while the model with probability function is not able to simulate the decrease

of the TSL during the decelerating current period. These result supports for the indications by Sanford and Halka (1993) and Winterwerp and van Keseren (2004) that the continuous deposition model is more reasonable than the model with probability function for deposition. The parameters obtained through the present study can be applied to 3-D simulation for sediment transport dynamics.

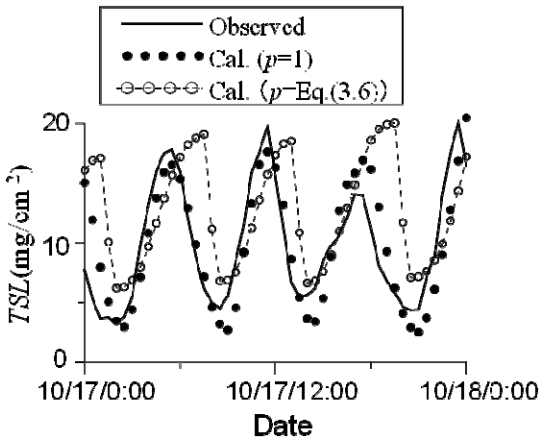

Figure 3.12 Reproducibility of estimated TSL with continuous deposition formula (p=1) and Krone's formula with Eq.(3.6).

References for Chpter3

Clarke, S. and Elliott, A. J., (1998): Modelling suspended sediment concentrations in the Firth of Forth, Estuarine, Coastal and Shelf Science, Vol.47, pp.235-250.

Futawatari, T. and T. Kusuda (1993): Modeling of suspended sediment transport in a tidal river. In: Mehta, A.J. (Ed.), Nearshore and estuarine cohesive sediment transport, Coastal estuarine studies, American Geophysical Union, Washington, DC. Pp.504-519.

Gartner, J. W., (2004): Estimating suspended solids concentrations from backscatter intensity measured by acoustic Doppler current profiler in San Francisco Bay, California, Marine Geology, Vol.211, pp.169-187.

Hill, D.C., Jones S.E. and Prandle, D., (2003): Derivation of sediment resuspension rates from acoustic backscatter time-series in tidal waters, Continental Shelf Research, Vol.23, pp.19-40.

Kondo, M., Y. Tohara, K. Hiramatsu, S. Shikasho and K. Mori (1996): Characteristics of Erosion on cohesive sedimentary materials by tidal current, Trans. of Japanease Society of Irrigation, Drainage and Rural Engineering (JSIDRE), No. 182, pp.109-115. (in Japanease)

Krone, R. B., (1993): Sedimentation revisited, In Mehta A. J.(Ed.) Nearshore and estuarine cohesive sediment transport, American geophysical union, Coastal and estuarine studies, pp.108-125.

Kusuda, T., H. Yamanishi, H. Yoshimi and R. Futawatari (1989): Experimental study on resuspension characteristics of disturbed and undisturbed muddy sediments, Proc. of Coastal Engineering, JSCE, Vol. 36, pp.314-318. (in Japanease)

Maa, J.P.Y, L. D. Wright, C. H. Lee and T. W. Shannon, (1993): Vims sea carousel – a field instrument for studying sediment transport. Marine Geology, Vol.115 (3-4), pp.271-287.

Mehta, A. J., (1988): Laboratory studies on cohesive sediment deposition and erosion, In Dronkers, J. and W. van Leussen (Eds.) Physical processes in estuaries, Springer-Verlag, pp.427-445.

Nakagawa, Y., S. Imabayashi and K. Suetsugu (2002): Field data analysis of fine sediment transport process in Ariake Bay, Proc. of Coastal Engineering, JSCE, Vol. 49, pp.556-570. (in Japanease)

Nakagawa, Y., H. Yoshida, K. Tanaka and M. Oh-hata (2007): Field observation on resuspension of fine sediments and turbulence structures in bottom boundary layer, Proc of Coastal Engineering, JSCE, Vol. 54, pp.445-450. (in Japanease)

Sanford, L. P. and J. P. Halka, (1993): Assessing the

paradigm of mutually exclusive erosion and deposition of mud, with examples from Chesapeake Bay, Marine Geology, Vol. 114, pp.37-57.

Seguchi, M., K. Watanabe and O. Katoh (1989): Near-bottom current and turbidity in shallow coast of eastern-shore of Ariake Bay, Proc. of Coastal Engineering, JSCE, pp.819-823. (in Japanease)

Suetsugu, T., K. Fujita, Y. Suwa and K. Yamamoto (2002): Influence of sediment transport on topography and bed material change at river mouth estuary, Technical Note of National Institute for Land and Infrastructure Management, No.32, 169p.

Soulsby, R. L., (1990): Tidal-current boundary layers, The Sea, Part2, pp.523-565.

Vinzon, S. B. and Mehta, A. J., (2003): Lutoclines in high concentration estuaries: Some observations at the mouth of the Amazon, Journal of Coastal Research, Vol.19, No.2, pp.243-253.

Winterwerp JC, van Kesteren W (2004): Introduction to the physics of cohesive sediment in the marine environment, Elsevier, 466p.

4 DATA ANALYSIS AND MODELING OF MUD TRANSPORT DURING STORM EVENT IN TOKYO BAY

4.1 Introduction

Sediment transport process at river mouths is highly dynamic system including dispersion of sediment particles by waves and currents. Although there are several field measurement works which have figured out sediment dispersal at river mouths during flood events, understanding of sediment transport mechanism is only limited because of difficulty of making long term measurements to capture such highly intermittent event. Since fine sediment transport process at river mouth has a key role on variations in surrounding water quality and ecological systems, better understanding of the mechanism is critical to maintain and restore estuarine and coastal environments in the area.

Study site of the present study is off the mouth of the Tama River in Tokyo Bay, Japan, where a new runway has been developed and just opened in the fall of 2010 as a part of the Tokyo international airport. In order to grasp any effects of the runway construction on the surrounding environment of the water area, comprehensive monitoring has been carried out since before the construction work started in 2007. This paper discuss observations of fine sediment transport process at the river mouth using measured data during the extreme storm and flood event by a passage of a typhoon in September 2007.

4.2 Site description

The study site is located at the Tama River mouth in the Tokyo Bay, Japan (Figure 4.1). The surface area of the bay is approximately 1,500 km^2 and averaged depth is around 15 m experiencing semi-diurnal, meso-tidal condition with a maximum spring tidal range of around 2 m in the upper bay area. Several rivers, including the Tama River, flow into the north western part of the bay

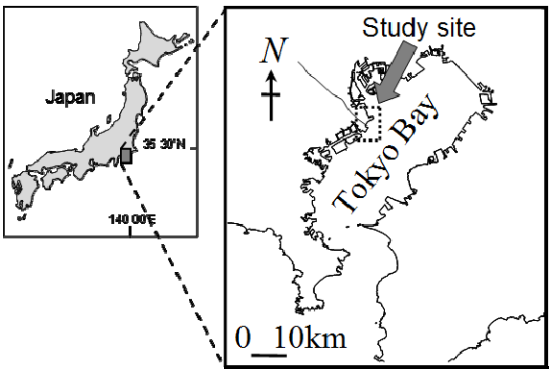

Figure 4.1 Location of Tokyo Bay and the Tama River

Figure. 4.2 Fluid mud on surface layer

with the total drainage basin area of 6,000 km^2. The Tama River has basin area of 1,240 km^2 (the second largest of the bay) and carries around 20 m^3 /s at typical background flow rates and 200-1,000 m^3 /s during flood events. The topography of the river mouth area has been highly developed artificially for industrial uses and a runway for the Tokyo International Airport has been newly extended in the water area for recent years. The monitoring point of the present study is located off the river mouth with the mean water depth of about 25 m. Bottom sediment is characterized by very soft mud (more than 99 percent of silt and clay) with high water content over 300% according to the sediment analysis of samples of bottom sediment as shown in Figure 4.2. Some examples of the vertical profiles of water content are represented in Figure 4.3, indicating also the sampling locations of the samples.

4.3 Instrumentation

Several acoustic and optical sensors were deployed

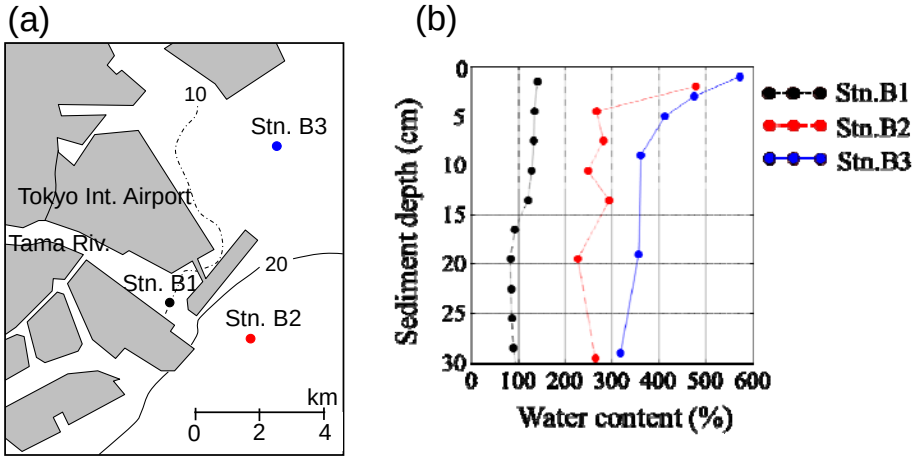

Figure. 4.3 Monitoring sites of bottom sediments (a) and water content profiles of samples (b). The contour lines represent the water depth in the map. (same figures as in Figure 2.13 and 2.19)

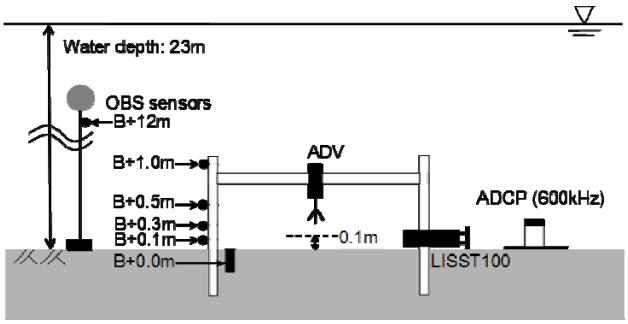

Figure. 4.4 Instrumentation layout for bottom boundary measurement

for the present study as shown in Figure 4.4. A Nortek Vector acoustic Doppler velocimeter (ADV) measured three dimensional velocities at 10 cm above the bottom every half hour at 8 Hz in about 2 minutes burst (1024 data per burst). For the measurement of vertical structure of water velocity, an upward looking 600 kHz Workhorse ADCP of Teledyne RD Instruments was used to record averages for 2 minutes every 10 minutes with 30 cm range bins starting 1.62 m above the bed. Optical back scatter sensors (OBS), using Compact-CLW of JFE Advantech Co., were moored at several levels near the bottom for the measurement of suspended sediment concentration (SSC) profiles. Measured optical backscatter intensity was calibrated using sediment samples taken from the site into SSC with the unit of mg/l. Particle size distribution of suspended sediment was measured with a LISST 100 (laser in situ scattering and transmissometry) developed by Sequoia Scientific Inc. and the measurement level was 10 cm above the bed.

4.4 Data analysis

4.4.1 Estimation of bed shear stresses

Bed shear stress was calculated with a bottom boundary model by Soulsby (1993) in the present study. Mean current ($\overline{U} = \left(\overline{u}^2 + \overline{v}^2\right)^{1/2}$) and representative wave velocity ($\tilde{U}_{br}$) were calculated from the ADV measuring three dimensional velocities at 10 cm above the bottom. The mean current stress is expressed as the following equation,

$$\tau_c = \rho_w C_f \overline{U}^2 \tag{4.1}$$

where ρ_w is the water density. The friction factor for mean current, C_f, is set as 0.0041 referenced to the measurement height (= 0.1 m) above the bed.

Wave stress is given by

$$\tau_w = \frac{1}{2}\rho_w f_w \tilde{U}_{br}^2 \tag{4.2}$$

with the following wave friction factor, f_w (Soulsby, 1997)

$$f_w = 1.39(A/z_0)^{-0.52} \quad (4.3)$$

where the wave orbital amplitude, $A=u_bT/2\pi$ and T is the wave period. The bottom roughness length, z_0, is assumed as 0.2 mm considering the bottom sediment properties. The value of the wave friction factor f_w varies between 0.003 and 0.05 under the present analysis. The representative wave velocity, $\tilde{U}_{br}$, is defined as (e.g. Madsen, 1994),

$$\tilde{U}_{br} = \sqrt{2\left(\tilde{u}^2{}_{rms} + \tilde{v}^2{}_{rms}\right)} \quad (4.4)$$

where the root mean square velocities, $\tilde{u}_{rms}$ and $\tilde{v}_{rms}$ are calculated with wave band variation, $\tilde{u}$ and $\tilde{v}$, of the ADV data over frequencies from 0.03 to 0.25 Hz.

The non-linear combined wave-current stress was calculated by the following equations as the maximum stress, τ_{max}, and the mean stress, τ_m (Soulsby, 1997)

$$\tau_{max} = \left[\left(\tau_m + \tau_w \cos\phi\right)^2 + \left(\tau_w \sin\phi\right)^2\right]^{0.5} \quad (4.5)$$

$$\tau_m = \tau_c\left[1 + 1.2\left(\frac{\tau_w}{\tau_c + \tau_w}\right)^{3.2}\right] \quad (4.6)$$

where ϕ is the angle between the mean current and dominant wave direction.

4.4.2 Erosion flux and bed elevation measurements

The ADV system can be used to estimate the suspended sediment concentration using the acoustic backscatter signal (e.g., Hay and Sheng 1992, Kawanishi and Yokoshi 1997, Fugate and Friedrichs 2002). In the present study, backscatter intensity was calibrated with SSC data obtained by the OBS at the same elevation in the vicinity of the ADV sensor. The relationship between the measured SSC and the mean acoustic backscatter intensity per burst is shown in Figure 4.5. Based on the correlation, acoustic backscatter measured by the ADV was calibrated to the SSC. The backscatter data of the ADV was recorded at the same sampling rate as the velocity measurement with the frequency of 8 Hz during each 2-minute burst every 30 minutes. The data can be used to estimate the vertical turbulent diffusion of suspended sediment as the Reynolds flux

$$F_z = \overline{c'w'} \quad (4.7)$$

where c' and w' represent fluctuating components of the suspended sediment concentration and the vertical velocity measured by the ADV, respectively. These fluctuations are defined as the deviation from the mean- and wave-band variations. In the results section of this paper, temporal variation of the flux is used to validate the proposed formulation to estimate the resuspension flux.

Acoustic devices were used to measure bed

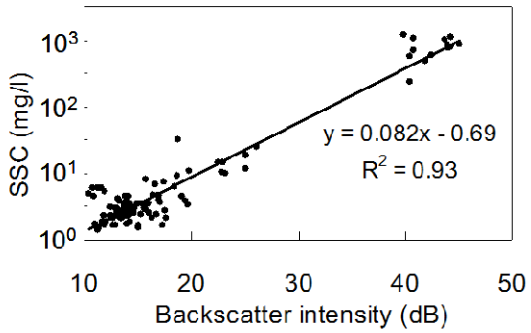

Figure. 4.5 Comparison of suspended sediment concentration estimated OBS with ADV backscatter

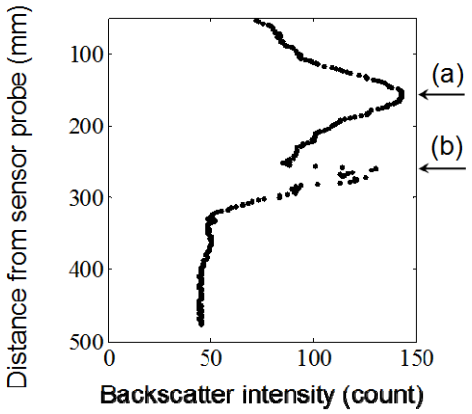

Figure. 4.6 Typical example of backscatter intensity profile obtained by the ADV measurement with (a) echo from velocity measurement layer and (b) echo from the bottom

elevation in several previous works (e.g. Andersen et al. 2006, Verney et al. 2007); acoustic backscatter records obtained by the ADV were used for this purpose in the present study. The instrument receives and records the backscatter signal not only from the velocity measurement range but also from other surrounding ranges (Nortek 2004) as shown in Figure 4.6. The distance from the sensor to the bottom boundary can be clearly detected in the profile of the backscatter data.

4.5 Observed data in the storm and flood event

While the instrument was deployed from August to September 2007, Tokyo Bay experienced an extreme storm and flood event due to the passage of a typhoon in early September. With strong southeasterly winds reaching 25 m/s, the significant wave height exceeded 2.5 m and the wave period was over 5 s at the time of closest passage of the typhoon (Figure 4.7 (a), (d), (e)). According to statistics based on the long-term wave records from 1983 to 1992 at a monitoring station in the Bay (Japan Weather Association 1994), the recurrence probability of the wave event is less than 1% and the waves were the highest in the last 10 years.

Coinciding with the wave event, there was also a prominent discharge of fresh water from the Tama River, peaking at over 3,500 m^3/s (Figure 4.7 (b)) and recording the largest flood since 1982. The wind data were measured by the Automated Meteorological Data Acquisition System (AMeDAS) at the Haneda station, operated by the Japanese Meteorological Agency. The wave gauge is located at the Tokyo Bay Light House station (35°33′58″N, 139°49′41″E) near Stn. C in Figure 4.3 where the water depth is about 14 m, some 6 km north from the long-term measurement site.

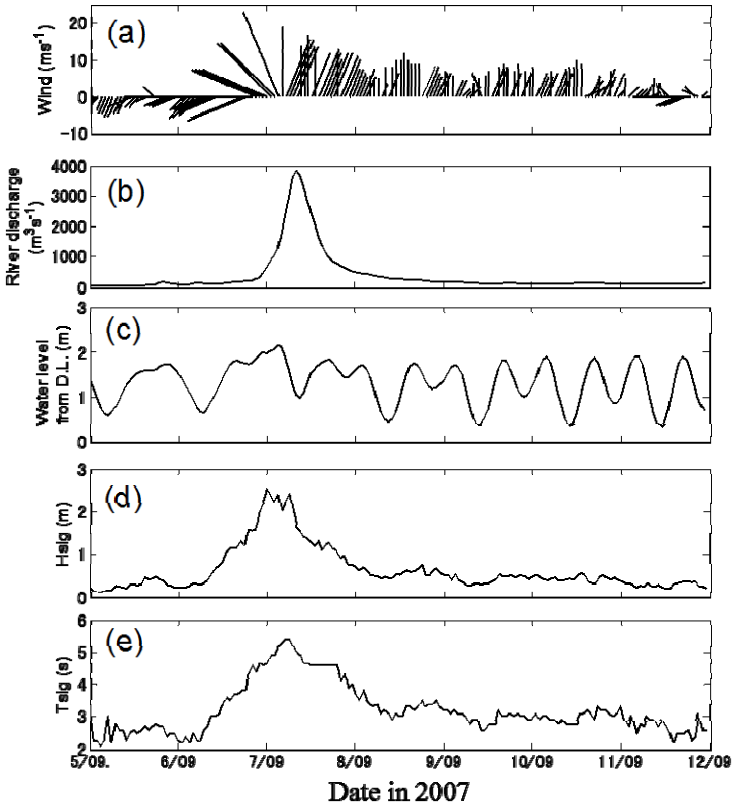

Figure. 4.7 Time series of (a) wind, (b) fresh water discharge of Tama River, (c) tide, and (d) significant wave height and (e) period

Temporal variations of SSC, turbulent diffusion flux and bed level are shown in Figure 4.8 compared with the force condition during the extreme storm and flood event between September 5 and 12. During the period of high shear stress caused by waves and currents on September 7, the near-bed SSC rapidly increased with a high concentration of 2,000 mg/l just above the bottom (B + 0.0 m), 1,000 mg/l at 10 cm, and 100 mg/l at 50 cm. During the high near-bed SSC event, the turbulent diffusion flux of sediments calculated by Eq. (4.7) also showed higher values in the upward direction during the period. At the same time, the sea floor underwent slight erosion of 20 mm according to acoustic measurements of the bed elevation.

The data shows a deposition of 50 mm following the erosion event, where the combined shear stress decreased to 0.3 Pa. During this deposition period, the SSC at the lowest layer, B + 0.0 m, experienced an extremely high concentration of over 30,000 mg/l indicating the existence of fluid mud near the bed. In spite of the continuous deposition during the period, the SSC at B + 0.0 m decreased, which was probably due to the limitation of the sensor range.

4.6 Estimation of near-bed sediment fluxes

The sediment concentration or density profile is characterized as shown in Figure 4.9, considering the observed near-bed structures around the study site. There is a clear gap between the sea water and the top of the thin fluid mud layer over the consolidated mud. Key processes that should be estimated to model this muddy sediment environment include vertical transport rate expressed as upward flux (F_z) and downward flux (F_D). It is also necessary to model the advection process of the sediment in the mud layer in horizontal directions. This paper examines methods of estimating these processes.

4.6.1 Vertical fluxes

The settling flux, based on the simultaneous erosion and deposition concept (e.g. Winterwerp and van Kesteren 2004), is given by:

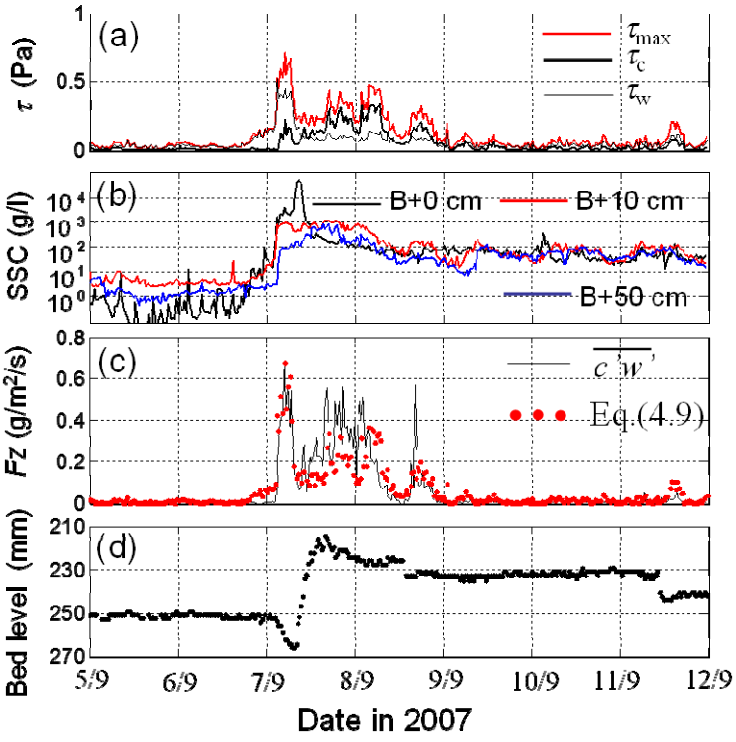

Figure. 4.8 Observed data during storm and flood event of (a) bottom shear stresses, (b) SSC, (c) erosion flux, and (d) bed elevation change

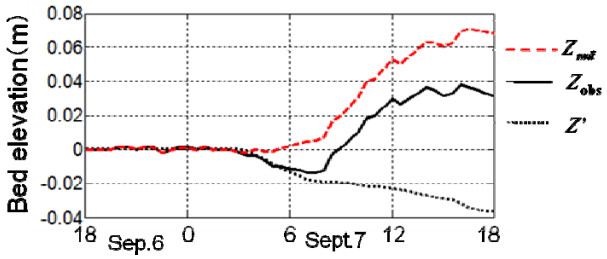

Figure. 4.9 Estimated contribution of sediment fluxes on bed level change calculated by sediment budget analysis near the bottom layer. (Zobs: Observed bed level change, Z': Bed level change by vertical fluxes, Zrsd: Residual bed level change estimated as contribution of horizontal flux in the present study.)

$$F_d = w_s C_b \tag{4.8}$$

where w_s is the settling velocity of the suspended sediment and C_b is the concentration. For the upward flux in the water column, the following diffusion flux formulation (e.g. Ross and Mehta 1989) can be applied:

$$F_z = -K_z \frac{\partial C}{\partial z} \tag{4.9}$$

where K_z is diffusivity, which can be modeled using the gradient Richardson number, Ri, and the diffusivity in the neutral condition without stratification, K_0:

$$K_z = K_0 (1 + \beta Ri)^{-\alpha} \tag{4.10}$$

The parameters α and β in the equation are set at 3.33 and 1.5, respectively, as proposed by Munk and Andersen (1948). The gradient Richardson number, Ri, is the ratio of potential to kinetic energy gradients and is expressed in the following form,

$$Ri = -\frac{g}{\rho} \frac{(\partial \rho / \partial z)}{(\partial u / \partial z)^2} \tag{4.11}$$

where g is the acceleration due to gravity, ρ is the local fluid bulk density, and u is the current speed in the horizontal direction. The bulk density is related to the sediment concentration, C, in the fluid as:

$$\rho = \rho_w + C[(\rho_s - \rho_w)/\rho_s] \tag{4.12}$$

where ρ_w is the density of water and ρ_s is the density of sediment particles.

In the present study, Eq. (4.9) was used to estimate the upward flux between the fluid mud layer and the upper water column. The estimation was carried out for the observed forcing and suspended sediment conditions during the storm event as described in section 4.5.

4.6.2 Fluid mud flow

For estimating the advection flux in the fluid mud layer, an analytical solution for the velocity profile in the mud layer was derived by assuming non-Newtonian fluid behavior in the layer. Many previous works dealt with mud flow as a non-Newtonian fluid (e.g. Liu and Mei 1989, Huang and Garcia 1999, Knoch and Malcherek 2011). Here, the Bingham fluid model is used in which the relationship between stress and strain is expressed as:

$$\tau = \tau_y \operatorname{sgn} \frac{\partial u_m}{\partial z} + \mu \frac{\partial u_m}{\partial z} \quad , \quad \text{if} \quad |\tau| \geq \tau_y \tag{4.13.a}$$

$$\mu \frac{\partial u_m}{\partial z} = 0 \quad , \quad \text{if} \quad |\tau| < \tau_y \tag{4.13.b}$$

where μ is the kinematic viscosity and τ_y the yield stress of the fluid mud. These parameters depend on the bulk density and mineralogy. Analytical solutions for the vertical profiles of the horizontal current speed, u_m, in the fluid mud layer are derived from an integral form of Eq. (4.13):

$$u_m(z) = \frac{1}{\mu} \int_{-h_y}^{z} [\tau(z) - \tau_y(z)] dz \tag{4.14}$$

The lower limit of the integration interval, $-h_y$, is the yield surface level at which the external force, $\tau(z)$, is equal to the yield shear stress, $\tau_y(z)$, in the mud layer.

The shear stress distribution in the mud layer can be derived from momentum-balance equations.

Under a simplified condition with a flat bed and equilibrium state in space and time, external shear stress in the mud layer becomes a constant and indicated as τ_b. The external stress represents the shear stress at the boundary between the upper water column and the mud layer. The kinematic viscosity is treated as constant through the depth considering the mud concentration as 0.5 Pa.s in the present study. On the other hand, non-uniformity of yield shear stress in the mud layer is taken into account in the present analysis. The distribution profile was determined by considering the observed density profiles in the mud layers as described precisely in the results section.

4.7 Results

4.7.1 Erosion flux estimation

The erosion flux during the observed storm period was estimated with Eq. (4.9) by using the field measurements of forcing and suspended sediment conditions described in section 4.4. For calculating the diffusivity in Eq. (4.10), the modified Richardson number *Ri*' is introduced:

$$Ri' = -\frac{g\Delta h(\rho_{10} - \rho_b)}{\tau_{b\_\max}} \tag{4.15}$$

where Δh is the distance between the bottom and the ADV measurement point (10 cm), ρ_{10} is the bulk density of sea water with suspended sediment at 10 cm above the bed, and ρ_b is that at the surface of the fluid mud layer. The bottom shear stress, τ_{b_max}, is evaluated by the velocity measurement data as non-linear combined wave-current stress as described in section 4.4.

By substituting Eq. (4.15) into Eq. (4.10), the vertical flux was calculated with Eq. (4.9) for the period of the storm event in September 2007 shown in Figure 4.8. The results estimated by Eq. (4.9) are plotted in Figure 4.8 (c) compared with the directly measured resuspension flux calculated as Reynolds flux. The estimation delivers quite reliable results, except the slight overestimates of resuspension during the early period of the storm event around September 7. This can be improved in practice by introducing a critical *Ri*' for erosion. This result implies that Eq. (4.9) is applicable to the bottom boundary condition of the resuspension flux in the case of an unconsolidated loose muddy bottom.

For the estimation by Eq. (4.9), the parameter K_0 is calibrated and set at a constant value of 0.0044 m^2/s for the result in Figure 4.8, considering the time series of the directly measured flux or Reynolds flux by Eq. (4.7). Note that the modified Richardson number *Ri*' (Eq. (4.15)) is not the same as the expression of flux Richardson number; non-dimensional friction factors for current and waves are included in the bottom shear stress term in Eq. (4.15). Therefore, the calibrated value of the parameter K_0 above is not equivalent to the diffusivity in the neutral condition. However, it is remarkable that the diffusive flux expression dependent on the Richardson number and vertical gradient of the mean concentration can reliably reproduce the temporal variation of the measured Reynolds flux after the adequate calibration of the coefficient.

4.7.2 Sediment budget analysis near bed surface

Considering the estimation results of vertical sediment fluxes near the bed, sediment budget can be analyzed with the following sediment weight balance equation.

$$-\rho_d \frac{dZ(t)}{dt} = F_z + F_d + F_r \tag{4.16}$$

where ρ_d is dry density of sediment and $Z(t)$ is the observed bed level detected by the ADV's backscatter signal. The sediment density was assumed as 1,300 kg/m^3, which is equivalent to mud concentration of 300 kg/m^3, and it is relatively high concentration of fluid

mud concentration range. In case that the mud condition is assumed as consolidating mud with the concentration of 500 kg/m^3, the mud thickness becomes 60 % of the present results. F_z and F_d are upward and downward sediment fluxes and they are calculated with Eq.(4.7) and Eq.(4.8), respectively. The settling velocity was assumed as 0.1 mm/s considering the sediment particle size. F_r is residual term in the analysis and it deserves as the sediment flux that is contributed by horizontal flux in the layer under the ADV measurement height at 10 cm from the original bed level.

The result of the analysis is shown in Figure 4.9 for the duration of 24 hours under the storm event condition. The solid line in the figure is the temporal change in the bed level, which is already shown in Figure 4.8 (d). Dashed black line is bed level change calculated as the contribution of net vertical flux of F_z and F_d, and Red line is residual terms. Based on the assumptions mentioned above, the bed level change by the residual contribution becomes 6 cm of deposition through the storm event. The result means that this deposition should be compensated by the horizontal flux and the horizontal transport should be taken into account for near bed sediment transport dynamics as shown in Figure 4.10.

In order to estimate the horizontal mud flux, estimation formula is newly derived in the following section.

4.7.3 Derivation of fluid mud flux formula

Considering the observed near-bed structure of the muddy sediments, we propose a method for estimating horizontal sediment transport flux in the mud layer. By integrating Eq. (4.14), we can obtain a vertical velocity profile in the fluid mud layer. In order to make the integration of Eq. (4.14) possible, we introduce the following relationship between the yield shear stress, τ_y, and the sediment concentration, C_m, proposed by van

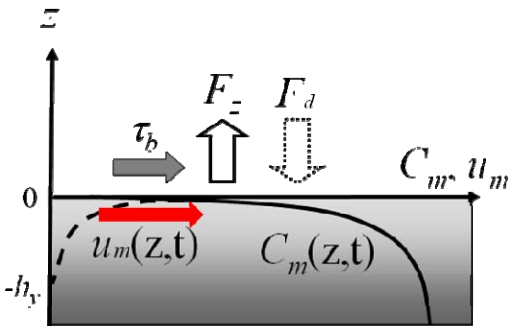

Figure. 4.10 Schematic diagram of the transport process of mud bed with thin fluid mud layer

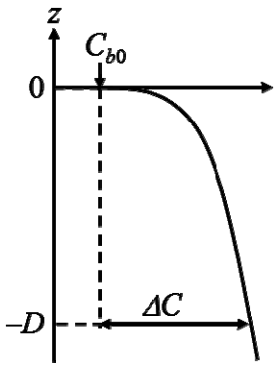

Figure. 4.11 Definition of parameters for sediment concentration profile

Kessel and Kranenburg (1996),

$$\tau_y(z) = c_1\left[\frac{C_m(z)}{\rho_s}\right]^{c_2} \tag{4.17}$$

where the empirical parameters c_1 and c_2 are set at 1,000 N/m^2 and 3 respectively and ρ_s represents the density of sediment particles (= 2.6 g/cm^3). For the sediment concentration profile of $C_m(z)$, the following function (e.g. Foda et al. 1993) is introduced:

$$C_m(z) = C_0 + \Delta C\left(-z/D\right)^{0.25} \tag{4.18}$$

In Eq. (4.18), C_0 is the concentration at the top of the fluid mud layer and ΔC represents an increase in the concentration at the depth of $-D$ from the surface of the mud layer as shown in Figure 4.11. These parameters are chosen so that the approximate function, Eq. (4.18), closely fits the field data of sediment concentrations as shown in Figure 4.12 (a). Substituting the distribution

function of the yield shear stress, Eq. (4.17), into Eq. (4.14) allows us to derive a formulation of the velocity profile in the mud layer under the shear stress on the surface of the mud layer, τ_b, as

$$u_m(z) = \frac{1}{\mu}[(\tau_b - \alpha_0)(z + h_y) + \alpha_0\alpha_1 \frac{4}{5} D\left(\frac{(-z)^{5/4} - h_y{}^{5/4}}{D^{5/4}}\right) + \alpha_0\alpha_2 \frac{2}{3} D\left(\frac{(-z)^{3/2} - h_y{}^{3/2}}{D^{3/2}}\right) + \alpha_0\alpha_3 \frac{4}{7} D\left(\frac{(-z)^{7/4} - h_y{}^{7/4}}{D^{7/4}}\right)] \tag{4.19}$$

where

$$\alpha_0 = c_1(\frac{C_0}{\rho_s})^3, \alpha_1 = 3\frac{\Delta C}{C_0}, \alpha_2 = 3(\frac{\Delta C}{C_0})^2, \alpha_3 = (\frac{\Delta C}{C_0})^3 \quad .$$

The height of the yield surface, h_y, is defined by the relations between external shear stress and internal yield shear stress. The results of computing velocity profiles using Eq. (4.19) are indicated in Figure 4.12 (c) in the two cases of τ_b = 1.0 and 1.5 Pa, as examples. The parameters in the model used in the present study are indicated in the figure. In both shear stress cases, the shear flows appear at the near surface of the mud layer under the effect of the shear stress exerted by the current of the upper water layer. The mobility layers are limited up to the yield surface level.

Furthermore, by considering the velocity profile in the fluid mud layer and the fitted concentration profile, the horizontal sediment transport rate can be formulated as

$$\mathbf{q}_m(x,y,z,t) = \int_{-h_y}^{h_b(x,y,t)} C_m(x,y,z,t)\mathbf{u}_m(x,y,z,t)dz$$

$$= \frac{D^2}{\mu}\left[(\tau_b - \alpha_0)\left(\frac{1}{2}C_0 h_y'^2 + \frac{16}{45}\Delta C h_y'^{\frac{9}{4}}\right) - \alpha_0\alpha_1\left(\frac{4}{9}C_0 h_y'^{\frac{9}{4}} + \frac{8}{25}\Delta C h_y'^{\frac{5}{2}}\right)\right]$$

$$+ \frac{D^2}{\mu}\left[-\alpha_0\alpha_2\left(\frac{2}{5}C_0 h_y'^{\frac{5}{2}} + \frac{16}{55}\Delta C h_y'^{\frac{11}{4}}\right) - \alpha_0\alpha_3\left(\frac{4}{11}C_0 h_y'^{\frac{11}{4}} + \frac{4}{15}\Delta C h_y'^{3}\right)\right] \tag{4.20}$$

where

$$h_y{}' = \frac{h_y}{D} = \left(\frac{C_0}{\Delta C}\right)^4 \left\{\left(\frac{\tau_b}{c_1}\right)^{1/3} \frac{\rho_s}{C_0} - 1\right\} \tag{4.21}$$

By using the above equation, horizontal sediment mass transport rate in the fluid mud layer can be estimated as a function of the external force or the bottom shear stress on the surface of the mud layer as demonstrated in Figure 4.13. After appropriate validations of the results, the method could be applied for spatial mud transport simulations.

4.8 Conclusions

The present study examined the transport characteristics of a mud bed with a thin fluid mud layer observed in Tokyo Bay, where muddy sediments with high water content appear at the bed surface. Field measurements captured a near-bed process with erosion and deposition of the muddy sediments during a storm and flood event. As a preliminary work for modeling

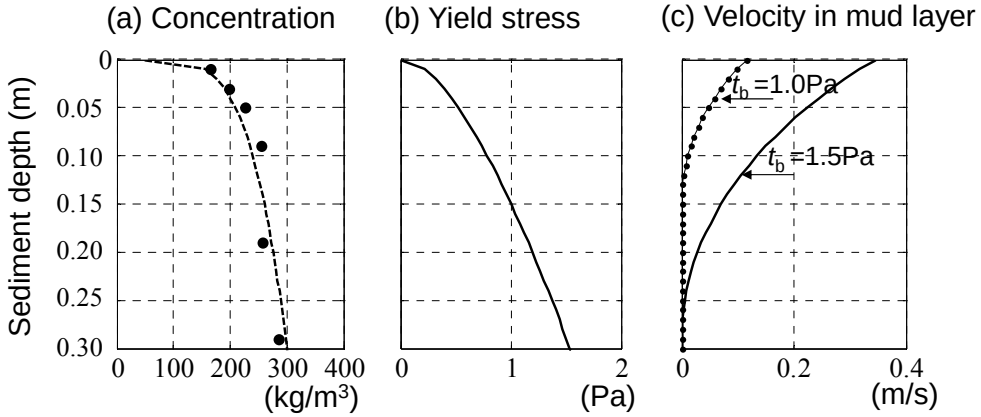

Figure. 4.12 Profiles of modeled sediment properties: (a) concentration, (b) yield shear stress, and (c) estimated current speed in mud layer (C_{b0} = 50 kg/m^3, ΔC = 250 kg/m^3, D = 0.3 m, μ = 0.47 Pa s)

the entire muddy sediment transport process in Tokyo Bay, estimation methods were examined for the key processes.

A diffusion flux model was calibrated and used for estimating the temporal variation of the vertical flux of resuspended sediment near the bed. For the calibration, field measurements of current and suspended sediment concentrations during a storm and flood event in Tokyo Bay were used. The estimated result showed reliable performance, implying that the diffusion flux type of formula can be applied for the bottom boundary condition of the erosion flux from an unconsolidated loose muddy bed.

The study also examined an estimation of total horizontal transport rate in the mud layer driven by external shear stress. Flow velocity profiles in the mud layer were derived from a set of basic equations, where the fluid mud layer was assumed to be a Bingham fluid. We also considered the observed vertical structure of the sediments in the study site and incorporated a distribution function, which fits the sediment concentration profile, in the model. Analytical solutions for flow velocity in the fluid mud layer were derived under an arbitrary shear stress condition assuming an equilibrium state in space and time. The total advection flux in the mud layer can be estimated as a function of external force by the proposed model.

For the estimated horizontal sediment flux, there is no available data for validating the dynamics in the fluid mud layer. Therefore, the result is confined to a derivation of the analytical formula in the study; the method remains to be validated appropriately in future. Mathematically, the proposed methods in the present study could be easily applied for mud transport simulations by coupling with 3D hydrodynamic models. Interaction between the sea water and mud behavior is neglected in the present study because the thickness of the fluid mud layer is relatively small as the order of few decimeter compared with water depth of 20 to 30 m.

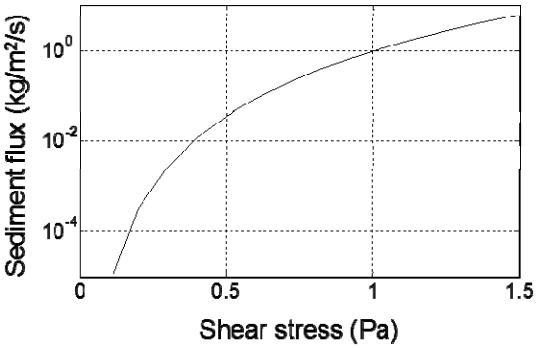

Figure. 4.13 Calculated sediment flux in mud layer under shear stress by overlying water current

For application to more dynamic environment with thick fluid mud layer often observed in the river mouth area, the interaction should be considered in the momentum equations or damping effect on the hydrodynamics of water above the fluid mud layer.

References for Chapter4

Andersen TJ, Pejrup M, Nielsen AA (2006): Long-term and high-resolution measurements of bed level changes in a temperate, microtidal coastal lagoon. Marine Geology 226, pp 115–125.

Ariji R, Yagi H, Nadaoka K, Nakagawa Y, Ogawa H, Shimosako K, Shirai K (2011): Temporal and spatial variations of bottom sediment characteristics around the Tama River mouth in Tokyo Bay, Japan. The 21st International Offshore (Ocean) and Polar Engineering Conference, June 22, 2011.

Fan S, Swift DJP, Traykovski P, Bentley S, Borgeld JC, Reed CW, Niedoroda W (2004): River flooding, storm resuspension, and event stratigraphy on the northern California shelf: observations compared with simulations. Marine Geology 210, pp 17–41.

Foda MA, Hunt JR, Chou H-T (1993): A nonlinear model for the fluidization of marine mud by waves. Journal of Geographical Research Vol. 98, No. C4, pp 7039–7047.

Fugate DC, Friedrichs CT (2002): Determining concentration and fall velocity of estuarine particle

populations using ADV, OBS and LISST. Continental Shelf Research 22, pp. 1867–1886.

Harris CK, Traykovski PA, Geyer ER (2005): Flood dispersal and deposition by near-bed gravitational sediment flows and oceanographic transport: A numerical modeling study of the Eel River Shelf, northern California. Journal of Geophysical Research Vol. 110, 110, C09025, doi:10.1029/2004JC002727.

Hay AE, Sheng J (1992): Vertical profiles of suspended sand concentration and size from multifrequency acoustic backscatter. Journal of Geophysical Research Vol. 97, No. C10, pp. 15,661–15,677.

Hsu T-J, Ozdermir CE, Traykovski PA (2009): High-resolution numerical modeling of wave-supported gravity-driven mudflows. Journal of Geophysical Research Vol. 114, C05014, doi:10.1029/2008JCO005006.

Huang X, Garcia MH (1999): Modeling of non-hydroplaning mudflows on continental slopes, Marine Geology Vol. 154, pp. 131–142.

Japan Weather Association (1994): Bulletin of Meteorological and Oceanographic Condition in Tokyo Bay, 420p.

Kawanishi K, Yokoshi S (1997): Characteristics of suspended sediment and turbulence in a tidal boundary layer. Continental Shelf Research Vol. 17, No. 8, pp. 859–875.

Knoch D, Malcherek A (2011): A numerical model for simulation of fluid mud with different rheological behaviors. Ocean Dynamics Vol. 61, pp. 245–256.

Kodama K, Horiguchi T (2010): Effects of hypoxia on benthic organisms in Tokyo Bay, Japan: A review. Marine Pollution Bulletin Vol. 63, pp. 215–220.

Liu KF, Mei CC (1989): Spreading of thin sheet of fluid mud on an incline. Journal of Coastal Research, SI No. 5, pp. 139–149.

Madsen, O.S., (1994): “Spectral wave-current bottom boundary layer flows,” Coastal Engineering 1994: Proceedings, 24th International Conference, ASCE, pp. 384–398.

Munk W, Andersen ER (1948): Notes on a theory of the thermocline. Journal of Marine Research Vol. 7, No. 3, pp. 276–295.

Nakagawa Y, Ariji R, Nadaoka K, Yagi H, Shimosako K, Shirai K (2011): Field measurement of erosion and deposition processes of muddy bed sediment during storm event in Tokyo Bay. Proc. of Coastal Sediments, ASCE, pp. 2403–2414.

Nobre AM, Ferreira JG, Nunes JP, Yan X, Bricker S, Corner R, Groom S, Gu H, Hawkins AJS, Hutson R, Lan D, Lencart e Silva JD, Pascoe P, Telfer T, Zhang X, Zhu M (2010): Assessment of coastal management options by means of multilayered ecosystem models. Estuarine, Coastal and Shelf Science Vol. 87, pp. 43–62.

Nortek (2004): Vector current meter user manual, 84p.

Odd NVM, Cooper AJ (1989): A two-dimensional model of the movement of fluid mud in a high energy turbid estuary. Journal of Coastal Research, SI No. 5, pp. 185–193.

Ross MA, Mehata AJ (1989): On the mechanics of lutoclines and fluid mud. Journal of Coastal Research, SI No. 5, pp. 51–61.

Sohma A, Sekiguchi Y, Kuwae T, Nakamura Y (2008): A benthic-pelagic coupled ecosystem model to estimate the hypoxic estuary including tidal flat – Model description and validation of seasonal/daily dynamics. Ecological Modeling Vol. 215, pp. 10–39.

Soulsby RL (1997): Dynamics of marine sands, Thomas Telford Publications, 249p.

Traykovski P, Wiberg PL, Geyer WR (2007): Observations and modeling of wave-supported sediment gravity flows on the Po prodelta and comparison to prior observations from the Eel shelf. Continental Shelf Research Vol. 27, pp. 375–399.

van Kessel T, Kranenburg C (1996): Gravity current of fluid mud on sloping bed. Journal of Hydraulic

Engineering Vol. 122, No. 12, pp. 710–717.

Verney R, Deloffre J, Brun-Cottan J-C, Lafite R (2007): The effect of wave-induced turbulence on intertidal mudflats: Impact of boat traffic and wind. Continental Shelf Research 27, pp. 594–612.

Winterwerp JC, van Kesteren W (2004): Introduction to the physics of cohesive sediment in the marine environment, Elsevier, 466p.

5 EFFECT OF WIND WAVE DISTURBANCE ON TEMPORAL VARIATION OF NEAR- BOTTOM DISSOLVED OXYGEN IN INNER TOKYO BAY

5.1 Introduction

In addition to the bottom sediment qualities, there are several water quality parameters that are crucial for the benthic ecosystem biodiversity and they may be affected by physical conditions by waves and current. Among them, dissolved oxygen near the bed is quite important indicator for estuaries and inner bays where hypoxic state have often occur. Tokyo Bay also has chronic occurrence of hypoxia or anoxia especially in the inner bay area in summer season and the mechanisms of variation in space and time have been studied in the previous studies (e.g. Fujiwara et al., 2000). From the hydro dynamical viewpoints, the importance of meteorological condition including wind and fresh water discharge has been pointed out on the movement of hypoxic water in the lower layer around the inner bay (Ueno et al, 1993, Nakayama et al. 2007, Yagi et al., 2008). Although the wind waves also may have an important role on the variation of the spatial distribution of dissolved oxygen through the vertical mixing, the waves are not inferred in the previous literatures.

In the present chapter, the field observations of water quality in the summer of 2010 reveal that the wind wave is one of key factors for temporary recovery of near bed dissolved oxygen (DO) concentration from hypoxic state in the inner Tokyo bay. The observation was a part of monitoring campaign to elucidate the behavior of the hypoxic water in the area. Basic parameters of water quality such as dissolved oxygen, salinity, temperature and turbidity were measured by a mooring system for 3 month from July through September in 2010. Physical parameters were also obtained for current profile by a bottom mounted ADCPs and for wind waves by an ultrasonic wave gauge respectively. DO concentration measured at 50 cm above the bottom intermittently increased especially after relatively higher wave events. The data also shows that the DO concentration near the bed is highly correlated with suspended sediment concentrations.

5.2 Monitoring site and instrumentations

The data analyzed in the present chapter was obtained through the monitoring campaign at the site in the north east of the Tama River mouth shown in Figure 5.1 for 3 month from July through September in 2010. As shown in Figure 5.2, surface mooring for the measurement of water quality at several depths and bottom mounted instrumentation for current and wave measurements were deployed at the monitoring station.

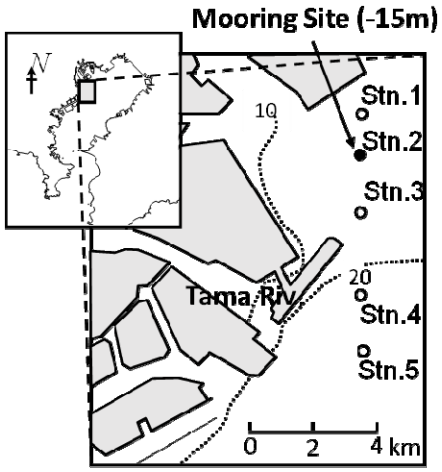

Figure. 5.1 Location of monitoring site

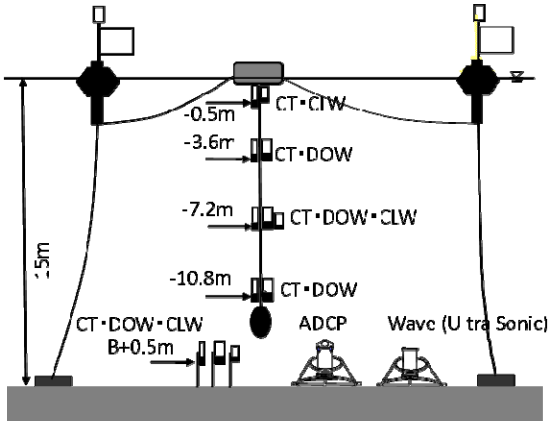

Fig. 5.2 Instrument set up for monitoring of wave, current and water qualities.

Measurement items of water quality includes dissolved oxygen concentration, salinity, temperature and turbidity with Compact-CT, Compact-DOW and Compact-CLW of JFE Advantech Co. Ltd., which recorded the data every 10 minutes. These sensors were located at the 4 depths of 0.5 m, 3.6 m, 7.2 m and 10.8 m from the sea surface and were recovered on a boat for checking and cleaning the sensors to prevent from biofouling twice a week during the monitoring period. Checking operation of the bottom mounted instruments for current measurement by ADCP and wave measurement by Wave Hunter (IO Technic) were carried out by scuba divers once a week during the whole monitoring period. Besides the mooring and bottom mounted instrumentations, vertical profile data of water quality were measured by hanging a water quality profiler (AAQ-1183 of JFE Advantech Co. Ltd.) every 4 or 5 days at the monitoring stations as shown in Figure 5.1.

5.3 Measurement results and discussion

5.3.1 Salinity, temperature and DO concentration variations in summer of 2010

Temporal variation of the vertical profiles of water temperature, salinity and density expressed by σ_t are shown in Figure 5.3, which are monitored under the depth of 3.6 m from the water surface. The water near the bottom experienced hypoxic condition from July through early September with density gap developed. After that, the density gap was cleared and it is found increasing of water density and recovery of the dissolved oxygen in the end of September. It is noted that even during the hypoxic state period from July through early September, there are several temporary recoveries of dissolved oxygen concentration as indicated triangles in Figure 5.3. This chapter focuses on the temporal recovery of near-bottom DO concentration and relationship between the event and physical conditions such as wind waves and currents.

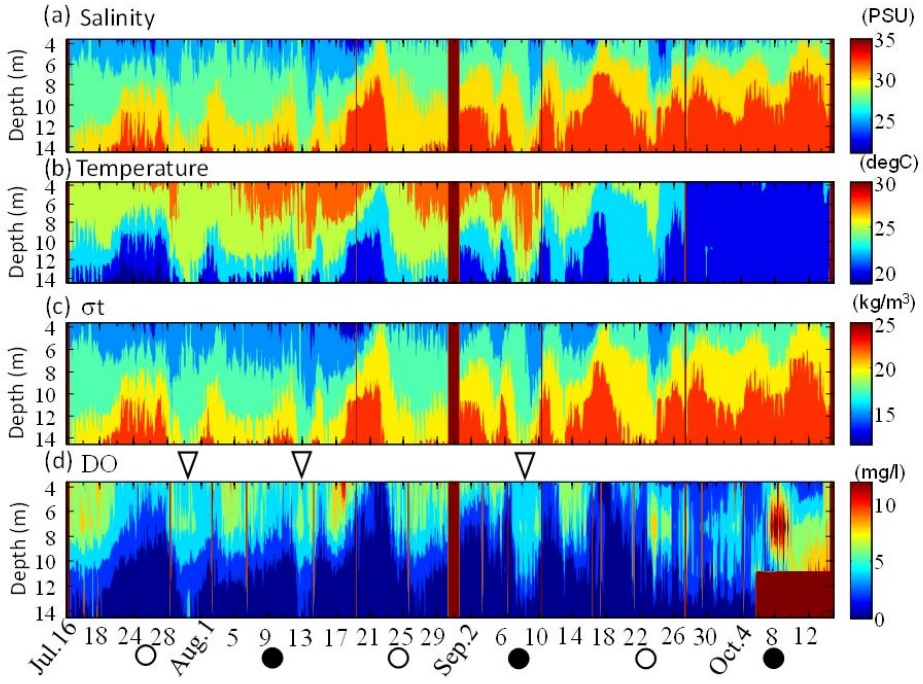

Figure 5.3 Temporal variations of (a) Salinity, (b) Water temperature, (c) density (σt) and (d) concentration of dissolved oxygen during whole monitoring period. Triangles in (d) indicate typical recovery events of near bed dissolved oxygen concentrations.

During the monitoring period, there were only slight precipitation with the maximum of 30 mm/hour on Sept. 8 and less than 10 mm/hour on Jul. 29 and Aug. 9.

5.3.2 DO concentration and wind events

The temporal variation of DO concentration in the inner Tokyo Bay is owing to dynamics of hypoxic water (e.g. Fujiwara et al. 2000, Nakayama et al. 2008). Yagi et al. (2008) indicated that the advection of hypoxic water is affected not only by intrusion of higher density water through the mouth of the bay but also by wind driven current with field measurements and numerical simulations. Sequential southerly wind blowing, which direction is from mouth of the bay to the upper bay, makes the density interface layer to be shifted downward by the effect of wind drift of the surface water.

Observed density variation in the water column is compared with wind velocity and DO in Figure 5.4, which shows also significant wave height, period and the depth of σt=20 as an indicator of density interface between upper light and lower dense water. It is found that downward shift of the density interface happen during southerly or northward wind conditions for a few days as indicated by the arrows, period-1, -2 and -3, in the figure. During the terms of these higher southerly wind periods, the DO concentrations are increased (Figure 5.4 (a)) and the concentration at 7.2 m from the surface, the half level of the total water depth, is raised up to almost the same concentration as the near surface layer at 3.6 m from the surface.

If wind is continuously blowing with the speed of

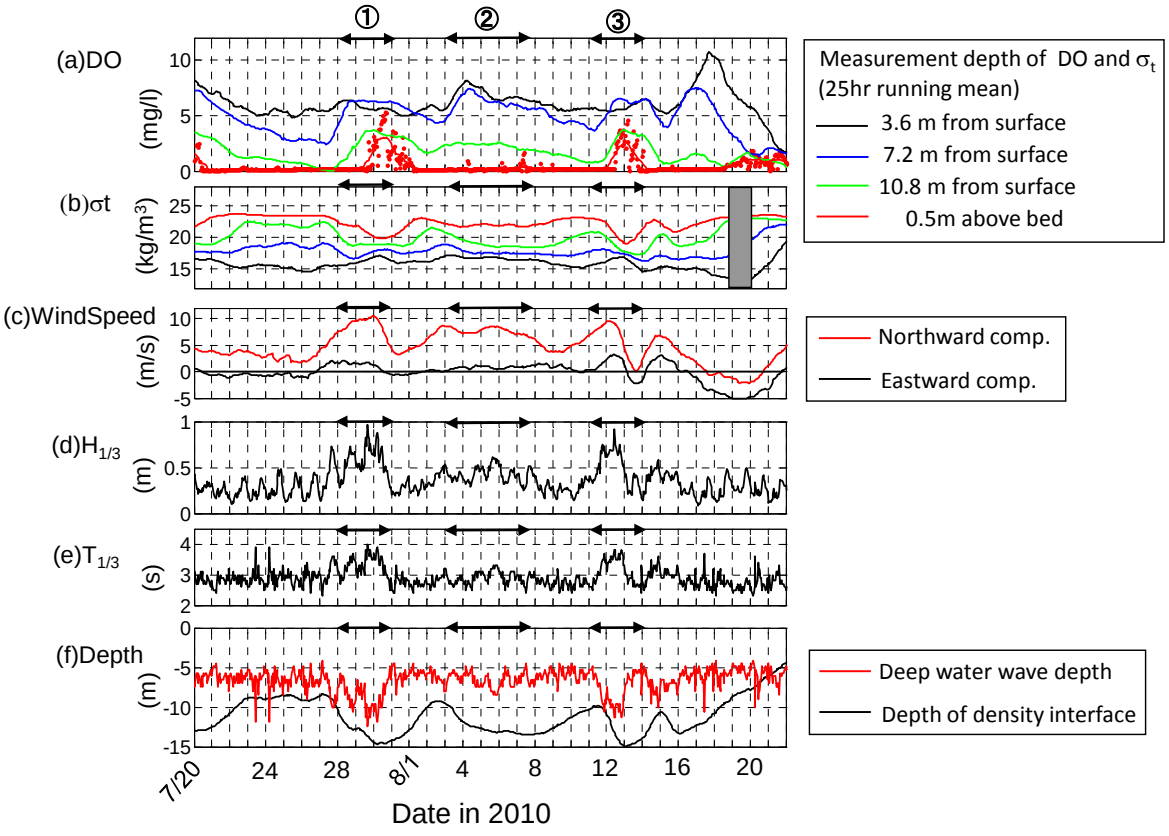

Figure 5.4 Temporal variations of DO (a), σ_t, (b), wind speed (c), significant wave height and period (d,e) and depths of deep water wave condition and density interface (f). Red dots in (a) means row (every 1 hour) data of DO measured at 0.5 m above bed.

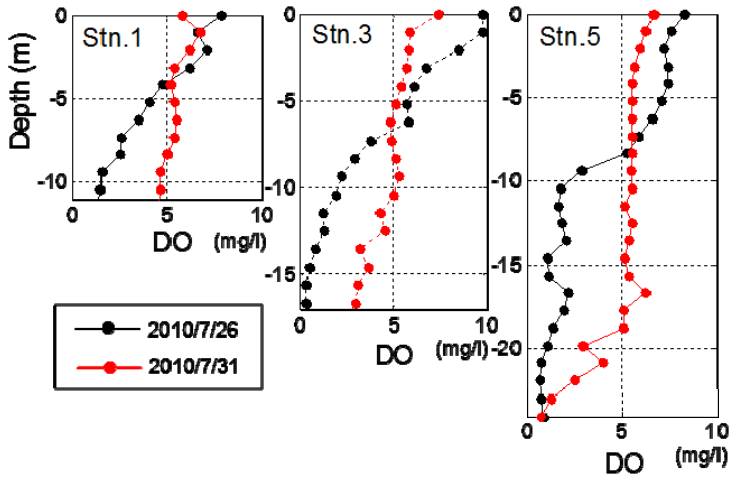

Figure 5.5 Vertical distributions of DO at Stn. 1, 2 and 3 during hypoxia state on Jul. 26, 2010 and recovery state on Jul. 31, 2010.

10 m/s on a water surface of two density layer system in a rectangular shaped embayment with the length of 40 km from an open end to another closed end, the depression of the density interface by wind drift of water body in the upper layer would be approximated as around 7 m. Based on the simple estimates, it is conceivable that the recovery of DO concentration at the middle layer at the inner bay is caused by the wind drift of the upper layer with relatively higher DO concentration.

DO concentration measured at the nearest height from the bottom or 0.5 mab shows temporary increases from the almost anoxia condition, which prominently occur corresponding to the higher southerly wind events of the period-1 and -3. Also at the surrounding stations at Stn.1, 3 and 4, for example, comparison of the vertical profiles of DO concentration measured before the period-1 on Jul.26, 2010, and during the period on Jul. 31, 2010, clearly shows the increase in the DO concentrations in the lower layer as shown in Figure 5.5. During both these periods where the rapid increase of the DO concentrations near the bottom occur, by the effect of the higher southerly wind, the wind waves are also developed with the longer wave period at the inner bay area presented in Figure 5.4 (d) and (e), respectively. It is pointed out also by Sato et al. (2012) that the sudden recovery of near-bottom DO concentrations from hypoxic state in summer season of the Tokyo Bay correlates with events of strong wind from the south with the speed of over 10 m/s. They discuss the effect of wind event on the circulation of the water body at inner bay. In the present study, in addition to the circulation by the wind stress, effect of vertical mixing by the wind wave disturbance on the near-bottom DO concentrations is also discussed in the followings.

5.3.3 DO concentration and wind waves

While the downward shift of the density interface occur during the period-1 and -3 where sudden recovery of the near-bottom DO concentration occur, vertical density gradient in the water column is decreased by mixing of waters between upper and lower layers as shown in Figure 5.4 (b). In order to evaluate the extent of the mixing of water, we can introduce the parameter as the relative density between the upper and lower layer as indicated by the following equation.

$$\varepsilon = (\rho_2 - \rho_1)/\rho_2 \qquad (5.1)$$

In the present study, for the upper layer density, ρ_1,

and the lower layer density, ρ_2, the water density at the depth of 3.6 m from the surface and 0.5 m above the bottom, respectively. The density was calculated considering the temperature and salinity measured at each depths. The relative density difference clearly shows negative correlation with the wind speed during the period-1 as shown in Figure 5.6 (a) and the relative density rapidly decrease when the wind speed is over 10 m/s. This wind condition coincides with the stochastic analysis on the relationship between the wind condition and recovery of the DO concentration inner Tokyo Bay by Nakayama et al. (2010), where wind speed exceeding 10 m/s contribute the recovery of the near bed DO.

On the other hand, considering the deep water wave condition of the linear wave theory, penetration depth of the wave motion from the surface, h', is estimated with the following equation,

$$h' = 0.5gT_{1/3}^2/(2\pi) \tag{5.2}$$

where $T_{1/3}$ is significant wave period, g is the gravity acceleration. With the longer wave period almost of 4 s during the period-1 and -3, the penetration depth becomes larger than 10 m as shown in Figure 5.4 (f). The comparison of penetration depth, h', and the wind speed during the period-1 is presented by Figure 5.6 (b) which shows the sudden increase of the penetration depth under the condition of wind speed of over 10 m/s. Both dependencies of the density difference and the penetration depth on the wind speed are very similar as shown in Figure 5.6 and it indicates that the wave disturbance works for vertical mixing of the water or decreasing of density difference. The penetration depth depends on the wave period and orbital excursion of sea water depends on the wave height also. The dependency of these parameters on the wind speed are also shown in Figure 5.6 (c) and (d), respectively. It can be seen that both of these parameters also increased rapidly after the wind speed of around 10 m/s. As the mechanism of enhancement of vertical mixing due to surface wave propagations, several processes may develop turbulence such as breaking waves at the

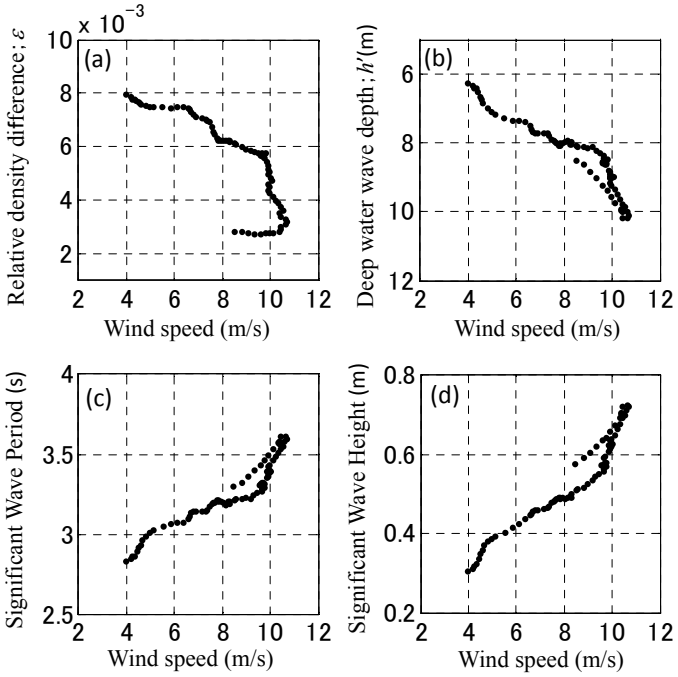

Figure 5.6 Dependency of relative density difference between upper and lower layer (a), deep water depth (b), significant wave period (c), and significant wave height (d) on wind speed.

surface, bottom shear stress and wave induced vertical diffusion (Qiao et al. 2004, Mori et al. 2010). In the following chapter, the wave induced disturbance near the bottom is focused on and the effect of it on the recovery of DO concentration during hypoxic condition is discussed comparing measured wave induced orbital velocities and the temporal variation of the DO concentration.

5.3.4 Near-bed processes of wave induced disturbance and DO concentration

Measured wave orbital velocity of eastward and northward components are shown in Figure 5.7(a) and the data were measured at the height of 0.5 m above the bed with the sampling frequency of 2 Hz. The data apparently detects wave orbital velocity due to surface wind wave propagation with the peak frequency of 0.2 Hz or wave period of 5 s as indicated in the power spectrum of these velocity time series presented in Figure 5.7(b). From these data set measured with 20 minutes bursts at 60 minutes interval, intensity of the wave orbital motion during each burst is estimated as representative wave velocity amplitude, considering the frequency domain, by the following equations.

$$U_w = \sqrt{u_{rms}^2 + v_{rms}^2} \tag{5.3}$$

where

$$u_{rms} = \sqrt{\overline{u^2}} = \sqrt{\int_{f_1}^{f_2} S_{uu}(f)df} \quad ,$$

$$v_{rms} = \sqrt{\overline{v^2}} = \sqrt{\int_{f_1}^{f_2} S_{vv}(f)df} \quad . \tag{5.4}$$

In the analysis, the velocity amplitudes were analyzed for the higher frequency components with the wave period of 3 to 8 s, which represents mainly wind wave induced velocity, and for the lower frequency components with the period of 30 to 300 s representing the effect of infra gravity waves.

Temporal variation of the wave velocity amplitudes of the wind wave component and the longer wave component during the period-1 are shown in Figure 5.8, comparing with variation of DO concentration near the bottom. According to the comparison between them, the DO concentration recovered from the hypoxic state just after the peak of the wave velocity amplitude of the wind wave component. This time lag between the peak of wave velocity amplitude and the recovery of the DO concentration is observed also in the event during the period-3. The reason of this time lag is considered to be related with the consumption of dissolved oxygen near the muddy bed. Even if the oxygen is supplied from the upper layer, it may be consumed in the near-bed hypoxic water and DO may not rise up for a while under the wave disturbance.

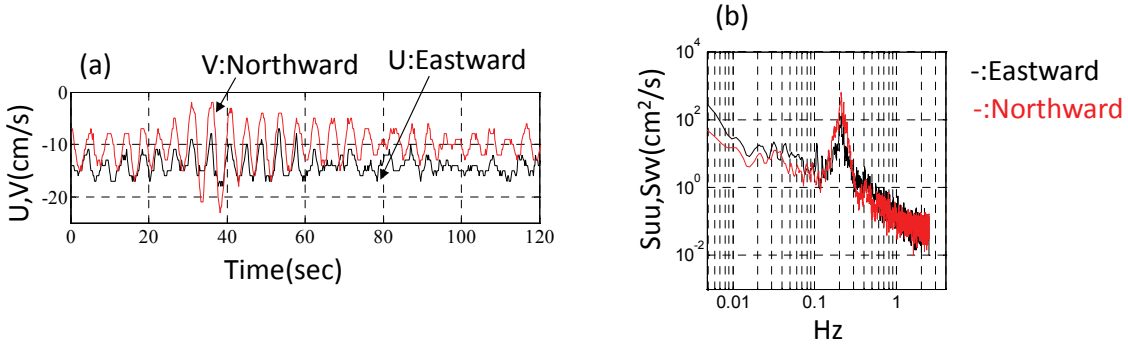

Figure 5.7 Measured near-bed current speeds (U: Eastward component, V: Northward component) and their power spectra (Suu and Svv) during rough wave condition at 4pm on Jul. 29, 2010.

The characteristic of the near-bed water can be characterized by the water temperature, T, and salinity, S, as shown in T-S diagram of Figure 5.9 where colors of plots means the measurement depths and the red plots are the data at 0.5 m above the bed. The data with DO concentration of less than 2 mg/l plotted by circle in the figure, the T-S relationships apparently differ from other water in the above layers. However, the T-S relationship of the near-bottom water, when the DO is over 2 mg/l, is almost consistent with the above layer and it is considered to represent the dependency of the rising of near-bottom DO concentration on the vertical mixing process.

On the other hand, during the temporal recovery of the near-bottom DO concentration, sudden drop of the concentration as indicated by the arrows in Figure 5.8

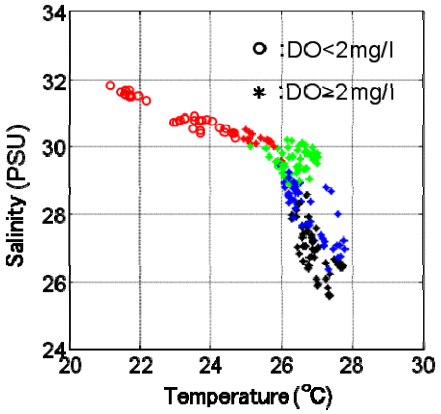

Figure 5.9 Relationship between salinity and temperature considering dissolved oxygen concentration (Black dots: data taken at 3.6 m below water surface, Blue: at 7.2 below water surface, Green: at 10.6 m below water surface and Red: at 0.5 m above bed)

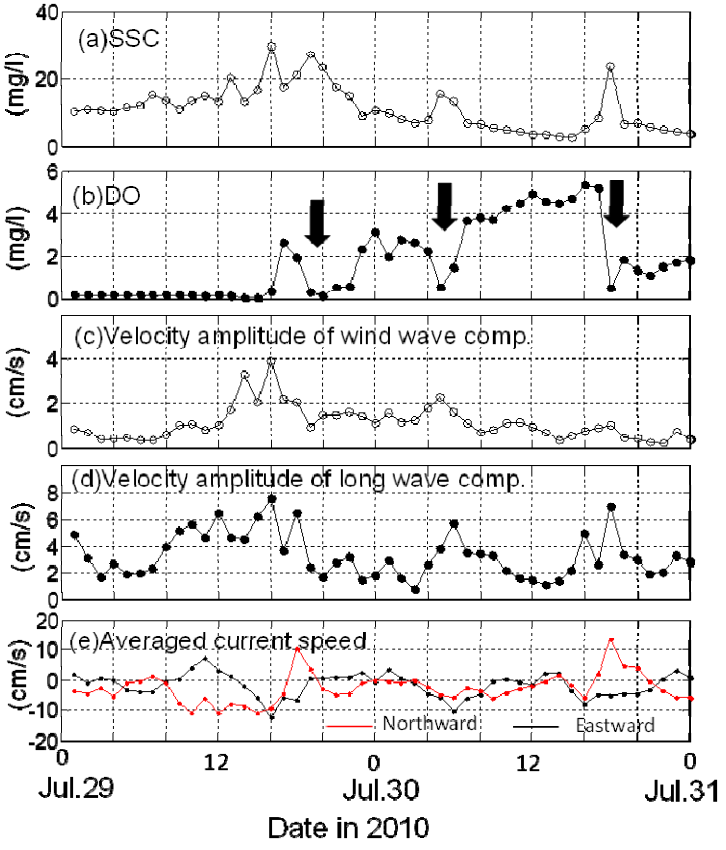

Figure 5.8 Temporal variations of SSC (a), DO (b), orbital velocity amplitudes of wind wave component (c) and long wave component (d) and averaged current speed (d) measured at 50 cm above the bed

(b). These falls of DO concentration correspond to the increase of the orbital velocity amplitude of the lower

frequency component and suspended sediment concentration too. It is conceivable that the resuspended sediment by the longer wave disturbance consume dissolved oxygen.

5.4 Conclusions

In order to elucidate the roles of wave induced disturbance on the near-bottom environment, field monitoring was carried out at inner Tokyo Bay in the summer of 2010 under hypoxic condition in the near-bottom layer. The monitoring consists of a mooring system of instruments for water quality measurements including salinity, Temperature, DO, and SS concentrations at several depths and also a set of bottom mounted current and wave measurement devices. Measurement results shows that the temporal change in vertical profiles of water density clearly responds to the wind event from the south with downward shift of density interface in the water column, which provides the vertical mixing and recovery of DO concentrations in the lower layers. Furthermore, the effect of wave disturbance on the water quality near the bottom has been revealed by comparison of temporal change in the near-bottom DO with wave orbital velocities amplitudes analyzed from measured data with high time resolution. The wind wave disturbance on the bottom has a key role as a trigger of recovery of the near-bottom DO concentration from hypoxic condition.

References for Chapter 5

Qiao,F. , Y. Yuan, Y. Yang, Q. Zheng and C. Xia (2004): Wave-induced mixing in the upper ocean: Distribution and application to a global ocean circulation model, Geophys. Res. Lett., 31, L11303, doi: 10.1029/2004GL019824

Fujiwara, T., T. Takahashi, Y. Yamada and A. Kaneko (2000): Response of hypoxic water mass in Tokyo Bay to the variation in hydrographic condition outside of the bay, Oceanography in Japan, The oceanographic society of Japan, pp.303-310. (in Japanese)

Mori, N., T. Suzuki and N. Kihara (2010): A study on air-sea mixing due to wind and wave under strong wind condition, Journal of Japanese Society of Civil Engineers, B2(Coastal Engineering), Vol.66, No.1, pp.311-315. (in Japanese)

Nakayama, K., M. Sivapalan, C. Sato and K. Furukawa (2010): Stochastic characterization of the onset of and recovery from hypoxia in Tokyo Bay, Japan: Derived distribution analysis based on “strong wind” events, Water resource research, Vol.46, W12532, doi: 10.1029/2009 WR 008900.

Ueno, S., K. Nadaoka, H. Katsui and H. Ohtani (1993): Field observation of sudden change in density, current and water quality field and internal wave under stratified condition in Tokyo Bay, Proc. of Coastal Engineering in Japan, Vol. 40, pp.246-250.

Yagi, H., T. Pokavanich, S. Yasui, K. Nadaoka, R. Ariji, S. Matsuzaka, N. Suzuki, K. Morohoshi, R. Oda and Y. Nihei (2008): Temporal and spatial variations of hypoxic water mass in Tokyo bay governed by the coastal upwelling at bay mouth and wind-driven current, Proc. of Coastal Engineering in Japan, JSCE, Vol.55, pp.1081-1085.(in Japanese)

6 APPLICATION OF FLUID MUD MODEL WITH STOCHASTIC APROACH OF BOTTOM SHEAR STRESS ESTIMATION TO STORM EVENT SIMULATION

6.1 Introduction

Numerical simulations of sediment transport in coastal and estuarine area by process-based approach are generally used for understanding of sediment dynamics and morphological evolution of study site (e.g. Harris et al. 2008). Process-based model consists of several modules which represent relevant processes to sediment transport dynamics, including hydrodynamic module for determining force conditions in current and wave fields and sediment transport module in which transport rates for vertical and horizontal directions are calculated considering sediment properties such as sediment size and cohesiveness (e.g. Amoudry and Souza, 2011).

For cohesive sediment or muddy environment on which the present study focus, the processes are more complicated than non-cohesive or sandy case and key parameters for determining critical condition of initiation of movement include not only sediment particle size but also water content or bulk density of moisture mud (e.g. Whitehouse et al. 2000). Because bottom boundary condition for sediment movement depends on sediment properties as mentioned above, it is crucial to consider information on spatial distribution of sediment properties in target field for getting reasonable simulation result. Another characteristic feature that should be taken into account in numerical simulations of muddy environment is formation and transport process of fluid mud layer above underlying consolidating mud layer. Due to lack of information on the fluid mud process in detail, dynamics of the layer is often simplified by 2-layer approach in practical models (e.g. Tsuruya et al. 1994, Deltares, 2014), where the density of the fluid mud layer is assumed as constant in vertical. As represented in Chapter 4, however, the vertical profiles of sediment concentration taken from the sediment cores shows rapid increases in the sediment concentration toward the deeper layer especially in the fluid mud layer near the bottom surface with the thickness of a few decimeters and these vertical structure is considered in the present study for the derivation of the equations to estimate horizontal fluid mud transport rate.

Another critical issue for providing reliable estimates of sediment transport rates in numerical simulations is computation of the bottom shear stress due to waves and currents. Wave induced bottom shear stress is often evaluated by representative bottom orbital velocities, which can be estimated by the statistic parameters of surface waves, such as representative wave height and period. Since the influence of wave propagation on the sediment dynamics depends on the characteristics of wave frequency, near-bottom orbital velocities can be obtained more accurately considering surface wave spectra for relatively deeper water condition (e.g. Wiberg & Sherwood, 2008). Furthermore, sediment dynamics beneath waves involves strongly nonlinear phenomena including critical stresses for the initial movement of sediments and importance of wave groups or fluctuation of wave amplitude in the movement of sediment has previously been confirmed from field observations (e.g. Williams et al. 2002, Kularatne & Pattiaratchi, 2008). Although time averaged bottom shear stress is generally calculated with representative wave parameters such as orbital velocity amplitude in sediment transport modeling, the use of time averaged stress may underestimate transport rate because of the above mentioned reasons.

The aim of this chapter is to apply the derived formula of fluid mud transport rate in Chapter 4 to numerical simulation of sediment dynamics during the observed storm event in the Tokyo Bay by coupling

with a 3-D circulation and wind wave models, incorporating the irregularity of wave induced bottom shear stress. Before the numerical simulation, a stochastic approach for evaluating bottom shear stress due to irregular waves is proposed, where probability distribution of bottom shear stress is derived through a stochastic characterization of field measured data of wave induced instantaneous velocities. These numerical results are compared with those calculated by conventional estimations of time averaged bottom shear stresses.

6.2 Stochastic approach for estimation of wave induced bottom shear stress

6.2.1 Characterization of wave induced instantaneous velocity

The field measured data used in this study were obtained at the same location at Stn.B in Figure 4.3 in Chapter 4 during the storm event in September 2007. A bottom-mounted acoustic wave gauge with an electromagnetic current meter was installed for a month at the station as shown in Figure 4.4. The surface elevation and near-bed (30 cm above the bed) current speed were recorded with the sampling rate of 5 Hz for a 20-minute burst every hour. There are errors in wave height measurements by acoustic device during the storm caused by air bubble generated with wave breaking near surface but near-bottom current speed data are recovered without error during the storm period.

The temporal variations in the representative wave orbital velocity amplitude, $\widetilde{U}_{br}$, and mean velocity, $\overline{U} = \sqrt{\overline{u}^2 + \overline{v}^2}$, for each burst are shown in Figure 6.1. The representative wave orbital velocity is defined with the following form (e.g. Madsen, 1994),

$$\widetilde{U}_{br} = \sqrt{2\left(\widetilde{u}^2{}_{rms} + \widetilde{v}^2{}_{rms}\right)} = \sqrt{2}\widetilde{U}_{rms} \quad , \qquad (6.1)$$

where $\widetilde{u}_{rms}$ and $\widetilde{v}_{rms}$ are the RMS values of the instantaneous wave orbital velocity components, $\left(\widetilde{u}(t), \widetilde{v}(t)\right)$, that are determined as deviations from the mean velocity of each component,

$$\left(\widetilde{u}(t), \widetilde{v}(t)\right) = \left(u(t) - \overline{u}, v(t) - \overline{v}\right) \quad . \qquad (6.2)$$

These procedures are the same as Eq. (4.4) described in Chapter 4.

During the period indicated in Figure 6.1, the maximum velocity of the representative wave orbital velocity is 0.2 m/s at 5:00 am on Sep. 7, while the maximum mean current speed is 0.3 m/s at 6:00 am on Sep. 7. During this event, the maximum significant wave height and period were observed at the Tokyo Bay Light House Station as 2.5 m and 5 s, respectively as represented in Figure 4.7. The wave event was caused by the passage of a near-by typhoon, whereas the high current speeds were mainly caused by fresh water influx during the storm from rivers flowing into the

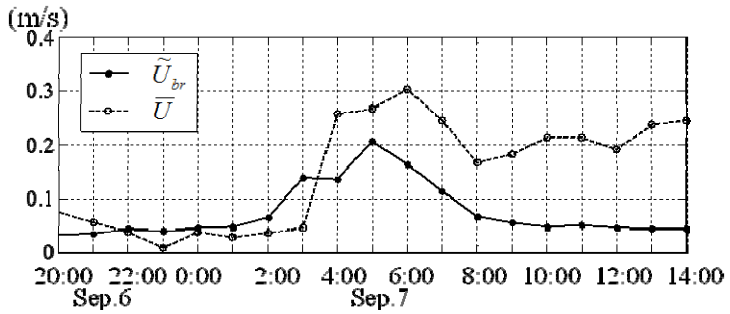

Figure 6.1 Measured $\widetilde{U}_{br}$ and $\overline{U}$ during the storm event

inner bay. The main direction of the averaged current was south west ward direction at the monitoring station (Nakagawa et al. 2009).

6.2.2 PDFs of instantaneous orbital velocity and bottom shear stress

The components of the instantaneous wave orbital velocity in the mean current direction, $\tilde{U}'$, were computed and resulting histograms for each burst during the high wave event are shown in Figure 6.2. All of these distributions are characterized by the shape with a peak that indicates the averaged current over each burst sampling and symmetrical distribution of wave induced fluctuations around the peak. Histograms of instantaneous orbital velocities are often assumed as the Gaussian distribution (e.g. You, 2009) and probability density function (PDF) of the instantaneous velocities observed in the present study can be also represented by the normalized Gaussian distribution as shown in Figure 6.3, where the instantaneous orbital velocity is normalized by the RMS value of $\tilde{U}'$. The normalized robability function, $P(x)$, is expressed in the form,

$$P(x) = (2\pi)^{-\frac{1}{2}} \exp\left(-\frac{x^2}{2}\right), \qquad (6.3)$$

where

$$x = \frac{\tilde{U}'}{\tilde{U}'_{rms}} \quad . \qquad (6.4)$$

If we can obtain the relationship between the instantaneous current speed and corresponding bottom shear stress, the PDF of the instantaneous orbital velocity can be transformed into the PDF of bottom shear stress. For example, Tanaka and Samad (2002) derived a formulation for transformation from instantaneous orbital velocity into bottom shear stress for irregular waves by the following equation,

$$\tau(t) = \frac{\rho}{2} 0.035(\omega\nu)^{0.16} \tilde{U}'(t)\left|\tilde{U}'(t)\right|^{0.68}, \qquad (6.5)$$

where ω is the representative angular frequency, and ρ and ν are the density and viscosity of the sea water. By using Eq. (6.5), the probability density function of τ can be obtained from the probability distribution of the instantaneous velocity.

However, their model consider only wave fluctuation of velocity field without uniform current

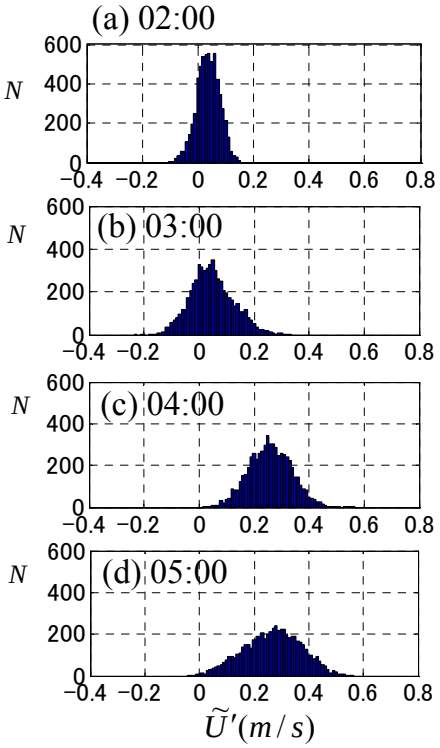

Figure 6.2 Histograms of instantaneous velocity, $\tilde{U}'$, in the mean current direction during the storm event of 7 September 2007.

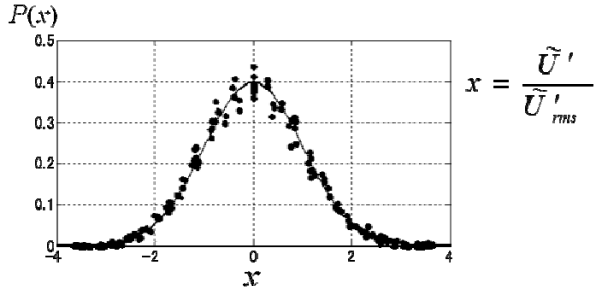

Figure 6.3 Probability density function of the instantaneous orbital velocity assumed by a Gaussian distribution (solid line) and measured data (dots) from 22:00 on 6 September to 09:00 on 7 September 2007.

and the friction coefficients used in Eq. (6.5) are the numbers for smooth turbulent conditions as mentioned by the authors, while the bed current observed in the field is basically under rough turbulent condition. Therefore, in the present study, the transformation of instantaneous bottom shear stress from orbital velocity considering uniform current as the following equation,

$$\tau_{cw}(t) = (1-\gamma)\tau_c(t) + \gamma\tau_w(t) \tag{6.6}$$

where γ is introduced to combine the shear stresses by current, τ_c, and waves, τ_w, in order to incorporate the non-linear effect considering the instantaneous velocity, $U'(t) = \overline{U} + \tilde{U}'(t)$. The parameter, γ is expressed as the following equation.

$$\gamma = \left(\frac{\tilde{U}'_{rms}}{\overline{U} + \tilde{U}'_{rms}} \right)^2 \tag{6.7}$$

This parameter indicates relative strength of the wave disturbance to the averaged current. If wave disturbance is relatively weak with small value of the root mean square of wave orbital velocity, $\tilde{U}'_{rms}$, the parameter γ becomes zero and the bottom shear stress is expressed only by the stress due to current effect.

The bottom shear stress due to current is the same expression as Eq.(4.1) and the velocity term is replaced with the instantaneous velocity here.

$$\tau_c = \rho_w C_f U'(t)^2 \tag{6.8}$$

The friction factor for mean current, C_f, is set as 0.003 referenced to the measurement height (= 0.2 m) above the bed in this case. The bed shear stress due to waves is expressed in the same form of Eq. (4.2) in Chapter 4 and the velocity terms are replaced with the instantaneous velocity here also.

$$\tau_w(t) = \frac{\rho}{2} f_w U'(t)|U'(t)| \tag{6.9}$$

For the friction coefficient, f_w, the same form as Eq. (4.3) in Chapter 4 and was modified here, considering wave orbital velocity, $\tilde{U}'_{rms}(t)$, as expressed by the following,

$$f_w(t) = 1.39\,(A(t)/z_0)^{-0.52} = 1.39\left(\frac{\tilde{U}'_{rms}(t)}{\omega z_0} \right)^{-0.52} \tag{6.10}$$

where $\omega = T/2\pi$ and T is the wave period and representative period was used in the analysis.

An example of the transformation of the PDF of the wave orbital velocity into the bottom shear stress with Eq. (6.6) is shown in Figure 6.4. The probability distribution of bottom shear stresses has a peak at the bottom shear stress of the uniform current and asymmetrically decreases in both sides of the peak. This is caused by the linear combination of current and wave induced bottom shear stress expressed with Eq. (6.6). There is nonlinear interaction between waves and current and the PDF of bottom shear stress combined waves and current may distorted around the peak, but reasonable way of transformation of instantaneous velocity does not exist for co-existence condition of

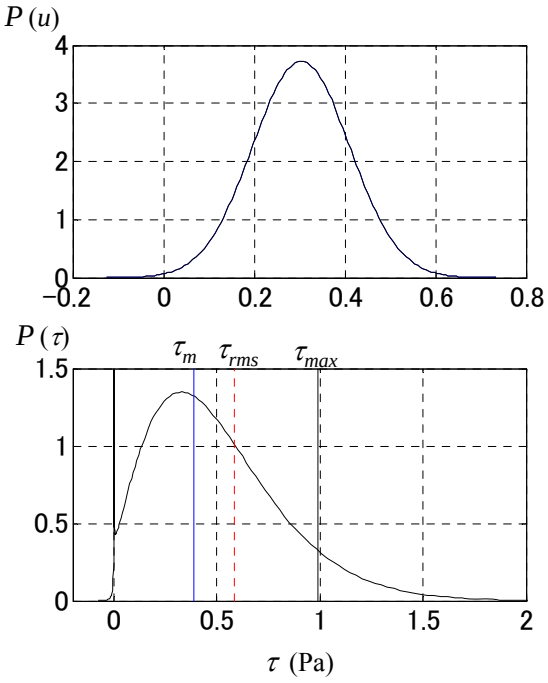

Figure 6.4 Probability Density Functions of the instantaneous velocity in the direction of the mean current (upper figure) and the converted bottom shear stress (lower figure). The wave and mean current conditions are $\overline{U}$ =0.3 m/s and $\tilde{U}_{br}$ =0.15 m/s.

current and wave. Therefore, the simplified expression is introduced in the present study to obtain the probability distributions and they are considered to estimate sediment transport rate in the following sections. The time averaged bottom shear stress considering the wave-current interaction calculated by the method of Soulsby (1997) is also indicated in the figure as τ_m, with the root mean square value (τ_{rms}) and the maximum (τ_{max}) values of the combined wave and current bottom shear stress. The rms value is defined as $\tau_{rms}=(\tau_m^2+0.5\tau_w^2)^{0.5}$ and the maximum value is defined as Eq. (4.5).

6.3 Stochastic formula for sediment transport rate

For sediment transport phenomena, critical conditions are often assumed for the initial movement of sediment particles and these can be represented by the yield stress in case of cohesive sediments. Based on this assumption, sediment would move only when the bottom shear stress exceeds the yield stress, as indicated in Figure 6.5. If we introduce a probability density function for the bottom shear stress, considering a sediment transport rate that is modeled as the function of the bottom shear stress, $q_m(\tau_{cw})$, the total sediment transport rate, $Q(\tau_{cw})$, may be estimated with the form,

$$Q(\tau)=\int_{\tau_{yield}}^{\infty}P(\tau)q_m(\tau)d\tau+\int_{-\infty}^{-\tau_{yield}}P(\tau)q_m(\tau)d\tau \quad .(6.11)$$

The equation (6.11) itself shows universal form and any type of sediment transport model that is expressed as a function of bottom shear stress. Same concept has been applied for estimating sediment bed load by Tsujimoto (1990) and effect of surface wave is also considered. But the wave effect is incorporated merely as the fluctuation of the uniform current in his model and the fluctuation by the surface waves is not incorporated as shear stress due to waves. In the present study, the bottom shear stresses due to current and waves are separately evaluated as described in the previous section and the probability density function is obtained considering both contribution of them.

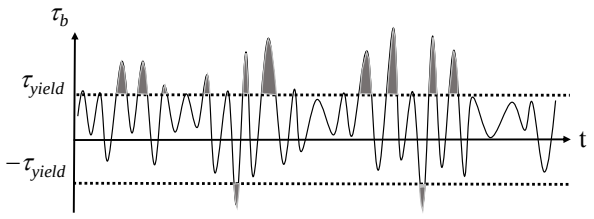

Figure 6.5 Schematic diagram of the relationship between fluctuating bottom shear stress and yield stress. (Sediment movement occurs only when the bottom shear stress exceeds the yield stress indicated in grey.)

For the sediment transport rate function, $q_m(\tau)$, in Eq. (6.11), arbitrary model can be substituted into the equation. In the present study, the newly derived fluid mud transport model described in the Chapter 4 is used for computation of fluid mud transport rate in the field.

6.3.1 Excess bottom shear stress

For estimation of sediment transport rate under bottom shear stress, excess shear stress is generally introduced for cohesive bed materials as an indicator of strength of muddy sediments. In order to represent the fundamental characteristics of the stochastic model introduced in the present study, the excess shear stresses were calculated. For the stochastic model, the excess shear stress was calculated by the following equation,

$$\tau_{ex\_present}=\int_{\tau_{yield}}^{\infty}P(\tau)(\tau-\tau_{yield})d\tau+\int_{-\infty}^{-\tau_{yield}}P(\tau)(\tau-\tau_{yield})d\tau \quad (6.12)$$

The results was compared with the other excess shear stress that is obtained with the conventional constant shear stress, which is calculated as,

$$\tau'_{excess}=\tau_m-\tau_{yield}\,. \quad (6.13)$$

Assuming that the wave and current conditions are parameterized with a representative wave orbital velocity and a mean current, the excess shear stresses can be computed as in Figure 6.6, where the results for the case of $\overline{U}$ =0.3 m/s and $\tilde{U}'_{br}$ =0.15 m/s are indicated.

The horizontal axis in the figure corresponds to the yield stress of the muddy sediment and the curves show the excess shear stress over the yield stress computed with Eqs. (6.12) and (6.12). The probability density function for τ in Eq. (6.12) is obtained by the procedures outlined in the previous section, considering the bottom shear stress estimated by the instantaneous velocity and the Gaussian distribution for the instantaneous velocity. For the time averaged constant bottom shear stress due to waves and currents in Eq. (6.13), and the time averaged form, τ_m, is expressed with Eq. (4.6) formulated by Soulsby (1997).

Calculated excess shear stress results with these equations are shown in Figure 6.6, showing the dependency of the excess shear stress on the yield shear stress, which is indicated in the horizontal axis in the figure. In the case of the constant stress model with the time averaged shear stress, the excess shear stress linearly decreases to zero when $\tau_m=\tau_{yield}$. This means there is no movement of sediment under conditions where $\tau_m<\tau_{yield}$. In contrast, the curves for the stochastic approach decreases relatively slower than the case for the constant model and the value of excess shear stress is not zero even when $\tau_{yield} > \tau_m$. For the same yield shear stress condition, the excess shear stress estimated with the stochastic model is larger than the value of the time averaged constant shear stress model and this corresponds to the under estimate of the sediment transport rate by the time averaged model.

For reference, the excess shear stress estimated by the root mean square and maximum values are also indicated in Figure 6.6 and these values are higher than the stochastic model in the case of smaller value of τ_{yield},

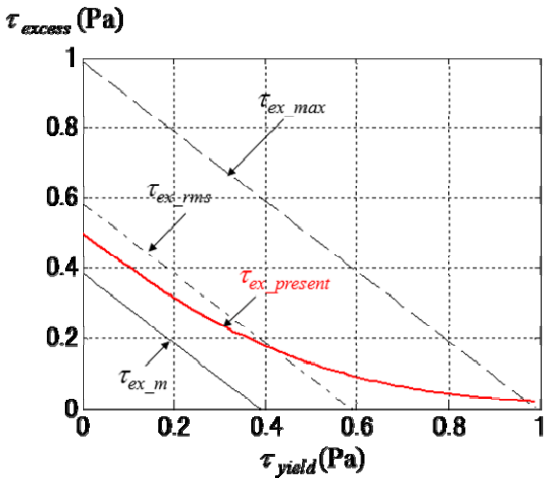

Figure 6.6 Comparison of excess shear stresses computed with the stochastic model (Eq. (6.7)) and the constant shear stress model (Eq. (6.8)). Case for $\overline{U}$ =0.3 m/s and $\tilde{U}'_{br}$ =0.15 m/s.

but the excess shear stress by the stochastic approach is between the values estimated by the root mean square and the maximum from around τ_{yield}=0.4 Pa through τ_{yield}=1.0 Pa. The difference between the estimation results between the stochastic model and the time averaged constant model also depends on the extent of wave orbital velocity. Their dependency on the variation of wave orbital velocity conditions are indicated in Figure 6.7. The figure shows estimated results of excess bottom shear stress and the rms values of wave orbital velocities, $\tilde{U}_{rms}$, are set as 0.01 m/s (Case1), 0.05 m/s (Case2) and 0.1 m/s (Case3) with the same current condition ($\overline{U}$ =0.3 m/s). The effect of wave velocity variation is already prominent from Case2, where the rms value of wave velocity is about 15 % of the current speed.

6.3.2 Estimation of fluid mud transport rates

Applying the fluid mud transport formulation derived in Chapter 4, sediment transport rate was computed following the stochastic approach of Eq. (6.11), considering the wave and current parameters,

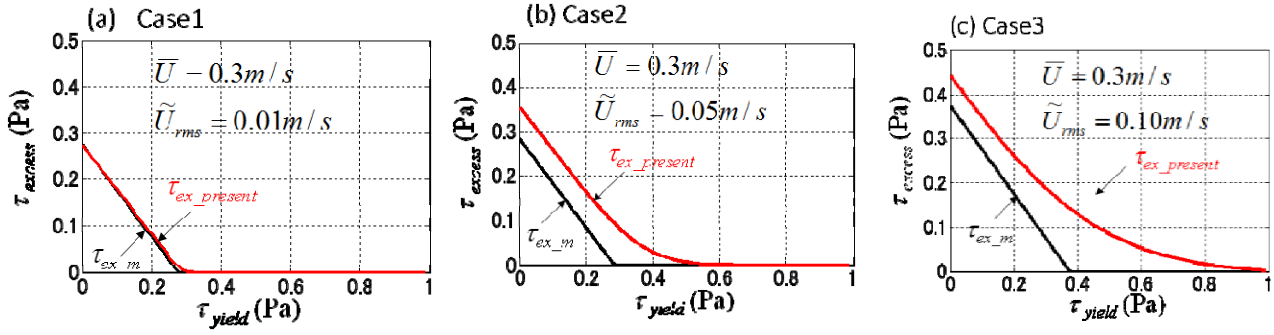

Figure 6.7 Relative differences of estimated excess shear stress by the stochastic model ($\tau_{ex\_present}$) and the constant shear stress model (τ_{ex_m}) depending on variation of wave orbital velocity.

$\widetilde{U}_{br}$ and $\overline{U}$, observed during the wave event as shown in Figure 6.1. Computation of the fluid mud transport rate by Eq. (4.20), with a constant bottom shear stress, was also undertaken and compared with the stochastic model result. For the constant stress case, the bottom shear stress due to waves and currents, τ_m, is estimated by Soulsby's formulation with the $\widetilde{U}_{br}$ and $\overline{U}$, as shown in Figure 6.1.

In figure 6.8 (a), calculated bottom shear stresses considering the observed current and wave parameters of $\overline{U}$ and $\widetilde{U}_{br}$ are indicated as τ_m, τ_{rms} and τ_{max}, respectively. The temporal variation of the time averaged bottom shear stress, τ_m, is basically coincide with the variation pattern of the current speed and it experiences maximum value of around 0.4 Pa at 6:00 am on Sep. 7. Other constant bottom shear stresses have much higher values than the time averaged and the maximum values of τ_{rms} and τ_{max} are 0.7 Pa and 1.0 Pa, respectively.

Computed results of the sediment transport rates using these constant bottom shear stresses are shown in Figure 6.8 (b), comparing with the results of the stochastic model. The estimation of the constant stress model with the time averaged shear stress is extremely low value and the result with stochastic model is close to the estimation by the constant shear stress model

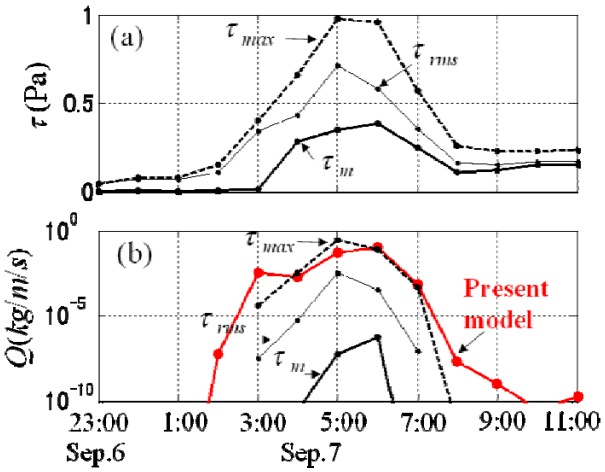

Figure 6.8 Force condition during the observed storm event (a) and Simulation of fluid mud transport rates by the stochastic model and the constant shear stress model (b).

with the τ_{max}. In the simulation, the yield stress of muddy sediment is assumed to be 0.24 Pa and the transport rate estimated by the constant stress model become zero when the estimated shear stress is less than the yield shear stress, which means that there is no movement of fluid mud. On the other hand, even under force conditions where τ_m is less than τ_{yield}, the transport rate can be calculated as non-zero value with the stochastic approach by the contribution of the bottom shear stress over the yield stress in the probability distribution. The amount of the transport rate in the stochastic approach is strongly owing to the sediment transport model, $q_m(\tau)$.

For the constant stress model, the use of other parameters representing the force conditions such as the maximum shear stress, τ_{max}, instead of the time averaged one, τ_m, provide closer result with the stochastic model in the present case. In the case of a relatively narrow distribution of bottom shear stresses, any representative constant shear stress could result in a reasonable approximation. However, as indicated in the previous section, larger wave orbital velocities or $\tilde{U}_{br}$ correspond to larger $\tilde{U}_{rms}$, and result in a wider distribution of instantaneous orbital velocities and bottom shear stresses. Therefore, the stochastic model is considered to be a more reasonable approach for sediment transport modeling in storm conditions.

6.4 Application of the model to simulation of observed storm event

6.4.1 Simulation of current and wave field during storm event

In order to reproduce the sediment dynamics process during the storm event observed in the Tokyo Bay, a numerical simulation was carried out with the newly derived fluid mud transport model and the stochastic wave force model as represented in the previous section. Current and wave field was simulated with an integrated model of a circulation model and a wave model, which is specially developed for assessing the environmental impacts by a topographical developments around Tama river mouth in the Tokyo Bay (Nadaoka et al. 2015). In the integrated model, the Princeton Ocean Model, POM, (Mellor, 2004) is applied for the circulation and the SWAN model (SWAN team, 2006) for wave field simulation, respectively. Calculated results of horizontal velocities at the nearest layer to the bottom boundary and significant wave height and period of surface waves at

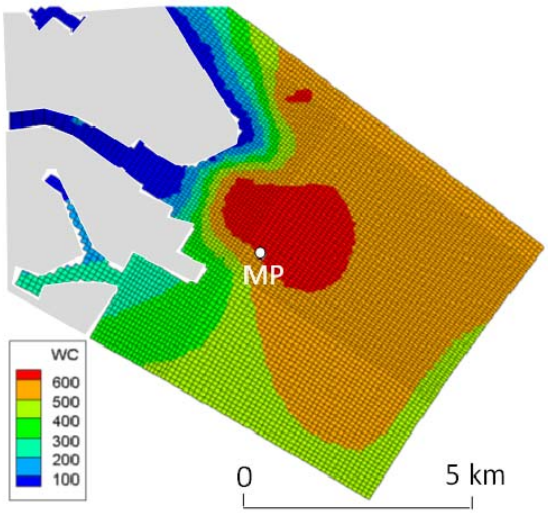

Figure 6.9 Computational domain and distribution of water content (WC) of mud (%). "MP" is monitoring point of field observation during storm event.

every one hour are utilized for the simulation of the fluid mud transport in the present study. Computation domain of the present study is shown in Figure 6.9 and the spatial resolution is 20 to 100 m. Considering the numerical results of current and wave parameters on the grids of the computation domains, fluid mud transport rate on the grids are calculated with Eqs (4.10) and (6.11). The spatial distribution of water content observed in the field was applied to estimate yield shear stress distribution in space, though it is assumed as constant in time in the present simulation. The target of the simulation is to explain the residual sediment influx by transport of fluid mud flow in the fluid mud layer. The monitoring point in the field is indicated as "MP" in the figure and model result is validated comparing with the observed data at the monitoring point.

The present study proposed computation method with a stochastic approach of wave force estimation for simulation of sediment transport rate, which may reproduce more correctly than any conventional time averaged approach for bottom shear stress due to current and waves. In the present model, it is required that the wave parameters of wave induced velocity near the bottom are given through the numerical simulations

of wave field. Temporal variations of the computed results of near-bottom current and wave parameters are shown in Figure 6.10, comparing with field data observed at MP. In the observed data, there are some loss data of wave parameters during the high wave energy period, where air bubbles generated by breaking waves may influence acoustic measurements, though near-bottom velocity data is collected without errors all through the monitoring period including the extreme storm period. Simulated significant wave height reasonably agree with the observed data before and after the missing data of high wave energy period but there are slightly difference in the result of significant wave peod, where the calculated period is relatively longer before the storm and relatively shorter after the storm event. Because of these discrepancies, calculated representative wave orbital velocity amplitude with the simulated wave height and period is slightly underestimated after the storm event.

Representative orbital velocity can be estimated reasonably from power spectrum of surface wave height, considering frequency dependence of the transfer characteristics of surface wave motion down to the bottom. The representative wave orbital velocity amplitudes were calculated from simulated wave frequency spectrum by the SWAN model and they are plotted in Figure 6.10 also. The estimates of velocity amplitude from surface wave spectrum are slightly larger than those estimated directly from the representative surface wave parameter of significant wave height and period. However, the calculated value from the wave spectrum are still underestimated the observed wave orbital velocities. It should be noted that the estimated results are significantly smaller than observed values during the storm event, which means the wave height and period are not correctly estimated by the wave model. This issue of wave model should be improved for getting more reliable wave field data as a future work. Therefore, the computed results of wave orbital velocities were corrected in the present study as described in the following section.

6.4.2 Simulation results of fluid mud transport

In the present study, representative wave orbital velocity amplitudes at all grids in the computational domain were corrected multiplying the numerical results by the factor of the ratio between of the observed and numerical values at the monitoring station of MP in Figure 6.9. Computational result of spatial distribution of fluid mud flux for the time step of 5:00

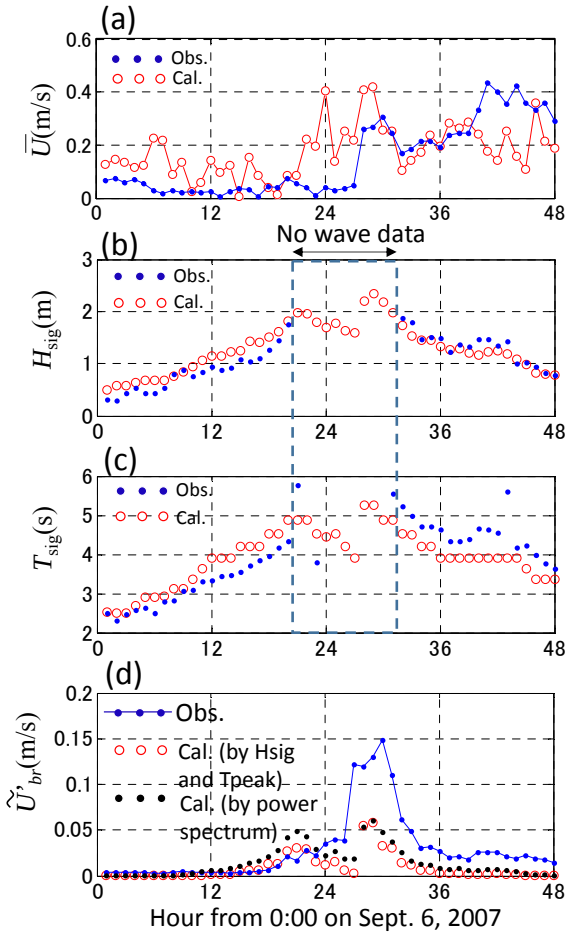

Figure 6.10 Comparison of calculated results and observed data for (a) Averaged current, $\overline{U}$, (b) Significant wave height, H_{sig}, (c) Significant wave period, T_{sig}, and (d) Representative wave orbital velocity ($\widetilde{U}'_{br}$). Numerical results are indicated as "Cal." and field data as "Obs.", respectively.

am on Sep. 7 during the storm event is shown in Figure 6.11 (a), representing horizontal movement of the fluid mud around off the Tama River mouth. Mud with higher water content distributes off the Tama River mouth area are forced to move by the current and waves. Another result obtained with the time averaged bottom shear stress, τ_m, is also shown in Figure 6.11 (b), indicating the area of fluid mud movement is apparently narrower than the result with the stochastic approach in Figure 6.11 (a) under the same force condition.

Temporal variations of the bed level at each grid were also calculated by a mass balance considering the computed results of sediment flux at every one hour. Spatial distribution of the bed level change due to fluid mud flow after 24 hour experiencing the storm event is in Figure 6.12, which represents the results with the stochastic approach and the conventional time averaged model, respectively. The both results show change in the bed level around the river mouth area with a spatial pattern of erosion at the near shore and deposition at the off shore area. The spatial distribution of the bed level change is due to the dominant or averaged current direction because the present model assume that fluid

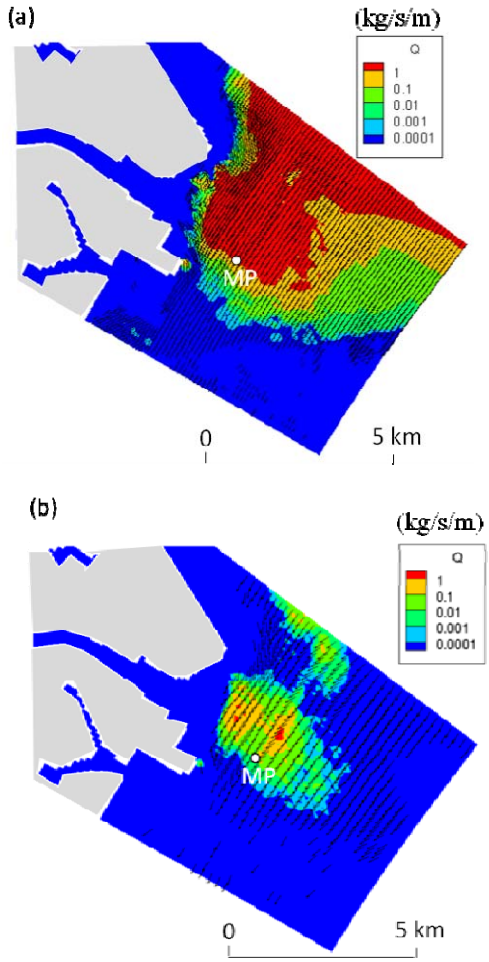

Figure 6.11 Computational results of spatial distribution of fluid mud transport rate for time step at 5:00 am on Sep. 7 by the stochastic model (a) and averaged shear stress model (b).

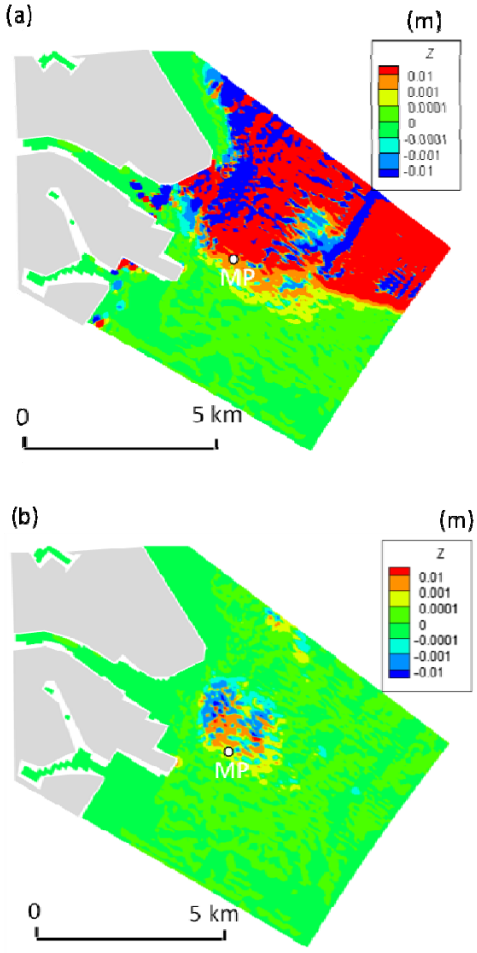

Figure 6.12 Distribution of bed level change due to fluid mud transport during the storm period by the stochastic model (a) and averaged shear stress model (b).

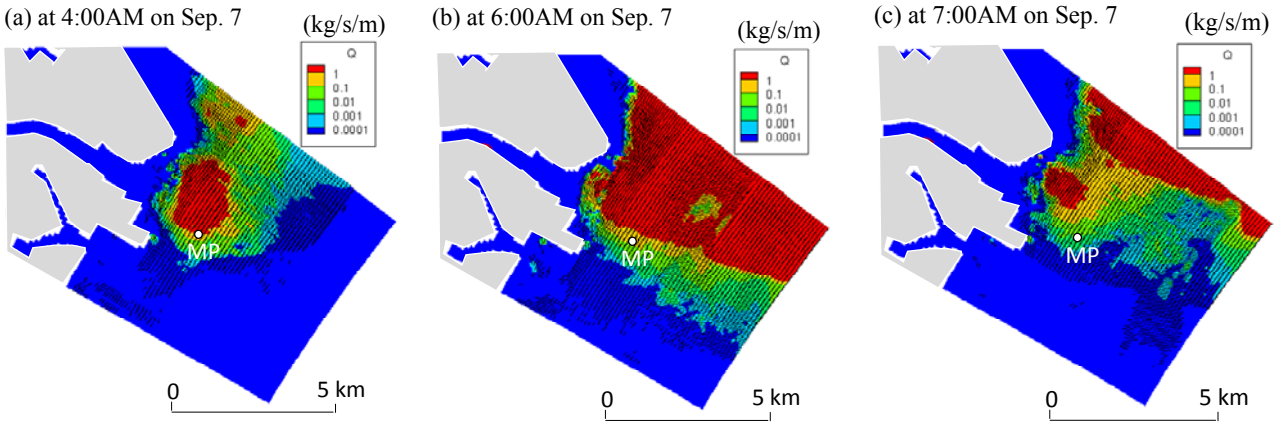

Figure 6.13 Computational results of spatial distribution of fluid mud transport rate with the stochastic model during the storm. (Result for time step at 5:00 am on Sep. 7 is in Figure 6.11(a))

mud is transported in the direction of dominant current, which is flowing southward through the storm event.

The results in Figure 6.12 show wider area of bed level change in the case of stochastic bottom shear stress model rather than the time averaged model in accordance with the result of the sediment flux distribution in Figure 6.11. Furthermore, change in the bed level during the storm event observed at the MP is deposition of around 4 cm and the contribution of the fluid mud transport to the bed level change is estimated as deposition of around 6 cm as discussed in Chapter 4. The present model considers only horizontal fluid mud transport and the numerical results with the stochastic model represent deposition of 5.5 cm in the vicinity of MP, though the simulation with the time averaged model results in deposition of only less than 0.1 cm. Although the number of monitoring point is restricted and the validation should not be enough with only one station, the present model reproduces more reasonably the observed bed level change than the conventional time averaged shear stress model. Spatial distributions of mud sediment fluxes computed with the stochastic model at several time steps are also indicated in Figure 6.13 and they shows that the distribution of calculated flux varies depending on the force conditions during the

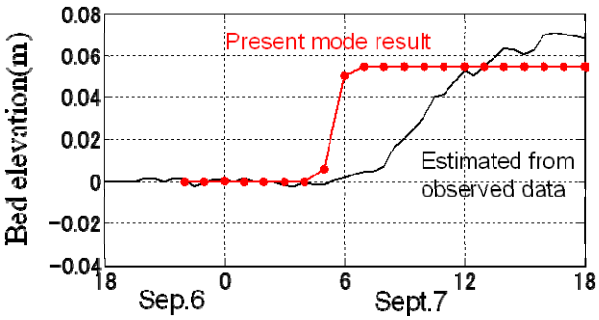

Figure 6.14 Temporal change in bed level due to fluid mud transport calculated with the present model compared with estimated bed level change from observed data at the monitoring point, MP.

storm event. Furthermore, the temporal variation of the bed level simulated by the present model is also compared with the bed level change estimated by the observed data as in Figure 6.14. There is slightly difference in the time evolution between the model result and observed data and it would owe the accuracy of force condition simulated with the numerical models. It means that there are still work to improve the reproducibility of force conditions for near bed dynamics in numerical modeling.

6.5 Conclusions

Numerical simulation was carried out to examine

fluid mud transport during the storm event observed in the Tokyo Bay. The newly derived formulations for fluid mud transport rate in Chapter 4 was applied for the numerical simulation. In the present study, furthermore, a stochastic approach was introduced for the estimation of wave induced bottom shear stress to incorporate the effect of irregularity in the wave forces acting on a bed.

For the formulation of the stochastic model for bottom shear stress, it was confirmed that the probability density function of instantaneous wave orbital velocities can be approximated well by a Gaussian distribution, where the distribution is parameterized with the representative wave orbital velocities or the standard deviations of the orbital velocities. The probability function of bottom shear stress is obtained using a formula that estimates the instantaneous bottom shear stress based on the instantaneous orbital velocity.

The present model was validated through a storm event simulation, where calculated results of current field by the POM and wave field by SWAN model were utilized as force condition for the sediment transport simulation. Comparison of simulated results for bed level change during the storm with the present model and those with a conventional time averaged bottom shear stress model shows an underestimation by the time averaged model, representing more reliable results by the present model based on the validation with the observed data.

Since the present model focused on the transport of fluid mud observed offshore of the river mouth and their modeling, it is considered as future works that the model incorporate another transport factors erosion and deposition, downward transport of fluid mud on the slope at the river mouth.

References for Chapter 6

Amoudry, L. O. and A. Souza (2011): Derterministic coastal mor-phological and sediment transport modeling: Areview and discussion, Reviews of Geophysics, 49, pp.RG2002-2011.

Deltares (2014): Delft3D-FLOW user manual, ver:3.15.34158, 684p.

Harris, C. K., C. R. Sherwood, R. P. Signell, A. J. Bever and J. C. Warner (2008): Sediment dispersal in the northwestern Adriatic sea, Journal of Geophysical Research, Vol. 113, CS11S03, doi: 10.1029/2006JC003868.

Kularatne, S. and Pattiaratchi, C., (2008): “Turbulent kinetic energy and sediment resuspension due to wave groups”, Continental Shelf Research, 28, pp. 726-736.

Madsen, O.S., (1994): “Spectral wave-current bottom boundary layer flows,” Coastal Engineering 1994: Proceedings, 24th International Conference, ASCE, pp. 384–398.

Meller, G. L. (2004): Users guide for a three-dimensional, primi-tive equation, numerical ocean model, Program on Atmos-pheric and Oceanic Sciences, Princeton University, Prince-ton, NJ 08544-0710.

Nadaoka, K., H. Yagi, Y. Nakagawa, Y. Nihei, R. Yamanaka, N. Uchikawa, K. Kawasaki and T. Mishima (2015): Development of integrated environmental impact assessment model and its application to Tama Rivr estuary around Haneda Airport, Journal of Japan Society of Civil Engineers, Ser. B2 (Coastal Engineering), Vol.71, No.1, (in Japanese), in press.

Nakagawa, Y., R. Ariji, S. Matsuzaka, K. Morohoshi, H. Yagi, K. Nadaoka and S. Tanaka (2009): Observations of fine sediment transport event during typhoon attack in Tokyo Bay, Proc. of 5th International Conference on Asian and Pacific Coasts (APAC’09), World Scientific, pp.8-15.

Soulsby, R. L. (1997): “Dynamics of marine sands,” Thomas Telford Publications, 249 p.

SWAN team (2006): SWAN user manual, SWAN Cycle III ver-sion40.51.

Tanaka, H., and Samad, M. A. (2006): “Prediction of instantaneous bottom shear stress for smooth turbulent bottom boundary layers under irregular waves,” Journal of Hydraulic Research, 44(1), pp. 94-106.

Tsujimoto, T. (1990): Stochastic analysis of bed-load fluctuation due to fluctuating bed shear stress, Journal of Japan Society of Civil Engineers, Vol.417/Ⅱ-13, pp.119-127. (in Japanese)

Tsuruya, H., K. Murakami, I. Irie, H. Sasajima and M. Itoi (1994): 3-D numerical model for siltation estimate considering fluid mud dynamics, Proc. of Coastal Engineering, Vol. 41, pp.1011-1015. (in Japanese)

Whitehouse, R., R. Soulsby, W. Roberts and H. Mitchener (2000): Dynamics of esutuarine muds, Thomas Telford Publications, 210 p.

Wiberg, P.L. and Sherwood, C. R., (2008): “Calculating wave-generated bottom orbital velocities from surface-wave parameters,” Computers and Geosciences, 34, pp. 1243-1262.

Williams, J.J., Rose, C.P., and Thorne, P. D., (2002): “Role of wave groups in resuspension of sandy sediments”, Marine Geology, 183, pp. 17-29.

You, Zai-Jin. (2009): “The statistical distribution of nearbed wave orbital velocity in intermediate coastal water depth”, Coastal Engineering, 56(8), pp. 844-852.

7 SUMMARY AND CONCLUSIONS

Muddy sediment transport in estuary and embayment is dynamical process under various forcing terms such as current and waves. Response of the muddy sediment to the forces depends on sediment properties and their vertical structure near the bottom. In the present study, field monitoring to grasp sedimentary characteristics were carried out in fields providing spatial distribution and vertical structures of muddy sediment. Sediment transport dynamics were also examined through implementations of monitoring campaigns to elucidate how tidal current and wave forces drive temporal variation of near-bottom environment including muddy sediment dynamics and water quality change. Based on the information obtained from the field data analysis, a formula for estimating fluid mud transport rate was newly derived and a stochastic model for evaluating bottom shear stress under irregular waves was also proposed in the present study. These methods were applied to numerical simulation of fluid mud dynamics during a storm event and verified with observed data. Summary and conclusions of each chapter is as followings.

In Chapter 2, sediment characteristics in the target field of the present study in the Ariake Bay and the Tokyo Bay were represented with the field monitored data. In the Ariake Bay, sediment core sampling and their analysis results were carried out and in-situ device for bulk density measurement was introduced in the field monitoring. The monitoring in the Tokyo Bay included extensive core sampling and fluid mud layer does stationary exist and the thickness of the fluid mud layer is around 10 cm.

In Chapter 3, characteristics of muddy sediment transport under tidal force was examined based on the field data obtained in the Ariake Bay where is categorized as meso-taidal estuary with maximum tide of around 5 m. By applying the acoustic Doppler velocity profiler to estimate total suspended sediment fluxes, the suspended sediment load under tidal current was formulated.

In Chapter 4, observed data of muddy dynamics under extreme storm event was demonstrated and their process was modeled. The observed data successfully captured the near-bottom process during high wave energy condition due to a typhoon event in the Tokyo Bay. A new formula for estimation of fluid mud transport rate was derived based on the Bingham model concept.

In Chapter 5, in order to elucidate the effect of wave disturbance on the other near-bottom environment than sediment transport process, observed temporal change in dissolved oxygen near the bottom was examined comparing wave force condition by using field monitored data monitored in summer at the inner Tokyo Bay. The data shows that the recovery of dissolved oxygen from hypoxic condition near the bottom apparently occur just after the peak of wind wave event.

In Chapter 6, the newly derived fluid mud model was applied to numerical simulation of sediment dynamics during the observed storm event in the Tokyo Bay. A stochastic approach was also developed for estimating bottom shear stress under irregular wave condition. From the field measured data of near-bottom velocity shows that probability function of instantaneous velocity induced wind waves are well approximated by the Gaussian distribution and the present study proposed transformation from the probability function of instantaneous velocity into the probability function of bottom shear stress. It is verified through comparison of numerical results and observed data that the present model can estimate the bed level change during the storm event well rather than a conventional time averaged bottom shear stress model.

Based on all the studies of this thesis, we can summarize as followings. 1) Practical methods are proposed to simulate muddy sediment transport process,

depending on the transport conditions of mud, including suspended state and fluid mud state, and new formula is provided for fluid mud transport rate estimation. 2) The study shows the wave has a key role on the near bed environment of the embayment and proposed new approach for evaluation of wave forces on the bottom as a stochastic model considering variation of instantaneous wave orbital velocity of irregular waves. This approach can be applied not only to fluid mud transport but also other near bed dynamic process such as pick up of sediments. 3) All knowledge obtained through the studies can be applied to improve the assessment works for sedimentary and near bed environments in embayment, which needs the more reliable simulation techniques.

As future works, the following aspects could be considered for extending the knowledge obtained through the present study. The model developed for simulating fluid mud dynamics in the present study can be coupled with other sediment transport process to establish over all sediment dynamics model. For application to more dynamic environment with thick fluid mud layer often observed in the river mouth area in the south east Asian countries, the interaction between the sea water and mud behavior should be considered in the momentum equations, although the interaction is neglected in the present study because the thickness of the fluid mud layer is relatively small as the order of few decimeter compared with water depth of 20 to 30 m. Another challenge with development of the present work is coupling the physical process such as resupension of muddy sediment and chemical processes to forecast the water quality change including near bed dissolved oxygen concentration, which is important parameter for evaluating the water environment.

(*Received on Jan 25, 2016*)

ACKNOWLEDGEMENTS

I would first like to express my deep appreciation to Dr. Kazuo Nadaoaka, Prof. of Tokyo Institute of Technology (TIT), for his valuable suggestions, guidance and continuous encouragements through the study. I am also thank Profs. Toshihiro Osaragi (TIT), Hiroshi Yagi (National Defense Academy), Shinjiro Kanae (TIT), Yasuo Nihei (Tokyo University of Science), Asso. Prof. Naoki Kagi (TIT) and Dr. Takashi Nakamura (TIT) for reviewing my dissertation and their valuable and helpful comments to improve the thesis.

I want to express my gratitude to Dr. Hiroich Tsuruya, who was the Head of Hydrodynamics Laboratory when I started to work for Port and Harbour Research Institute (PHRI), for his guidance to the interesting research world of muddy sediment dynamics. I also would like to thank Dr. Yoshiaki Kuriyama, Distinguished Researcher of Port and Airport Research Institute (PARI), for his continuous encouragements and valuable comments on my study works.

I would like also to thank the ports and harbours bureau and the both regional development bureaus for Kanto and Kyushu regions of the Ministry of Land, Infrastructure, Transport and Tourism (MLIT) for providing funding to carry out this research.

Furthermore, I would like to extend my gratitude to all of former and current colleagues of PHRI and PARI, including Profs. Tadashi Hibino (Univ. of Hiroshima), Hirofumi Hinata (Univ. of Ehime), Yusuke Uchiyama (Univ. of Kobe) and Dr. Tomohiro Kuwae (PARI), for their valuable and helpful comments and encouragements through many open discussions in the institute and personal discussions.

港湾空港技術研究所資料　No.1320

２０１６．６

編集兼発行人　国立研究開発法人海上・港湾・航空技術研究所

発　行　所　港湾空港技術研究所
横須賀市長瀬３丁目１番１号
TEL. 046(844)5040　URL. http://www.pari.go.jp/

印　刷　所　株式会社シーケン